

ABSOLUTE EMISSION INTENSITY STUDIES  
ON THE HALOGEN AFTERGLOWS  
AND EXCITED MOLECULAR OXYGEN

by

ROBERT JAMES BROWNE

B.Sc., University Of Western Ontario, 1963

A THESIS SUBMITTED IN PARTIAL FULFILMENT OF  
THE REQUIREMENTS FOR THE DEGREE OF  
DOCTOR OF PHILOSOPHY

in the Department of  
CHEMISTRY

We accept this thesis as conforming  
to the required standard

THE UNIVERSITY OF BRITISH COLUMBIA

June 1969

In presenting this thesis in partial fulfilment of the requirements for an advanced degree at the University of British Columbia, I agree that the Library will make it freely available for reference and study. I further agree that permission for extensive copying of this thesis for scholarly purposes may be granted by the Head of my Department or by his representatives. It is understood that copying or publication of this thesis for financial gain will not be allowed without my written permission.

Department of \_\_\_\_\_

The University Of British Columbia  
Vancouver 8, Canada

Date July 30/69

## TABLE OF CONTENTS

	page
Abstract	i
List of Tables	iii
List of Illustrations	iv
Acknowledgements	vi
 PART I: A STUDY OF THE HALOGEN AFTERGLOWS	
INTRODUCTION	1
Electronic States of the Halogens	3
Halogen Atom Recombination Studies	7
Rate Studies on Halogen Atom Recombination	9
Studies on the Luminescence from Halogen Atom Recombination	12
Purpose of this Investigation	18
 EXPERIMENTAL	
The Flow System	19
Materials	23
Production of the Excited Species	
(a) Chlorine and Bromine Atoms	24
(b) Production of Iodine Atoms in a Flow System	26
Atom Detection and Measurement	27
Spectroscopic Measurements	
(a) Equipment	34
(b) Measurement of Spectra	35
(c) Signal Detection	36
(d) Signal Amplification	38
(e) Calibration of Detectors for Absolute Emission Intensities	39
(f) Experimental Determination of the Transmission of the Optical System and Detector Sensitivity	44
 RESULTS	
The Bromine Afterglow Spectrum	46
Kinetics of the Bromine Afterglow	49
(a) Dependence of Emission Intensity on [Br]	50
(b) Pressure Dependence of the Emission Intensity	51
(c) Absolute Rate Constant Measurements	51
Emission from Iodine Atom Recombination	53
The Chlorine Afterglow Spectrum	54
Kinetics of the Chlorine Afterglow Emission	56
(a) Dependence of the Emission Intensity on [Cl]	57
(b) Dependence of the Emission Intensity on [Cl <sub>2</sub> ]	58
(c) Absolute Rate Constant Measurements	59
Estimation of Error in the Rate Constants	60

TABLE OF CONTENTS  
(Continued)

	page
DISCUSSION	61
Contribution of Two Body Radiative Recombination to the Halogen Afterglows	62
(a) Chlorine	63
(b) Bromine	66
The Iodine Afterglow	67
The Origin of the Bromine Afterglow	67
Kinetics of the Bromine Afterglow	73
Mechanism of the Emission Reaction	
(a) Formation of Excited States in the Br <sub>2</sub> Afterglow	75
(b) Relaxation Processes in the Excited States	78
Origin of the Chlorine Emission	81
Kinetics of the Chlorine Afterglow	
(a) Order of Emission Intensity with Respect to [Cl]	82
(b) Pressure Dependence of the Emission Intensity	84
Mechanism of the Emission Reaction in Chlorine	
(a) Formation of the Emitting State	85
(b) Relaxation of the $3\Pi_{O+u}$ State	88
(i) Vibrational Relaxation	89
(ii) Quenching by [Cl <sub>2</sub> ]	89
(iii) Quenching by Atoms	90
(c) Participation of Other Electronic States in the Cl <sub>2</sub> Afterglow	93
Suggestions for Further Study of Halogen Afterglows	94
PART II: STUDIES ON EXCITED MOLECULAR OXYGEN	
INTRODUCTION	
Electronic States of Molecular Oxygen	96
Studies on Excited Molecular Oxygen	99
Purpose of this Investigation	102
EXPERIMENTAL	
Production of O <sub>2</sub> ( $^1\Delta_g$ ) and O <sub>2</sub> ( $^1\Sigma_g^+$ ) Molecules	103
Measurement of Emission from the Cl <sub>2</sub> - H <sub>2</sub> O <sub>2</sub> System	104
RESULTS	
Estimation of [O <sub>2</sub> ( $^1\Sigma_g^+$ )] from Absolute Emission	106
Absolute Emission Intensity of the 6340A Band	108
The Chlorine-Hydrogen Peroxide System	109
DISCUSSION	
Radiative Lifetime of the (O <sub>2</sub> ) <sub>2</sub> Complex	113
Chemiluminescence from the Cl <sub>2</sub> -H <sub>2</sub> O <sub>2</sub> System	117
APPENDIX	122
BIBLIOGRAPHY	

ABSTRACT

The bromine afterglow emission was studied using the discharge-flow technique. The spectrum of discharged bromine was observed to extend from 6000Å to 22000Å and has been attributed to the  $\text{Br}_2(^3\Pi_{o+u} \rightarrow ^1\Sigma_g^+)$  and  $\text{Br}_2(^3\Pi_{1u} \rightarrow ^1\Sigma_g^+)$  transitions. The dependence of the emission intensity on atom concentration was observed to vary between  $I \propto [\text{Br}]^{2.0 \pm 0.1}$  at short wavelengths, and  $I \propto [\text{Br}]^{1.5 \pm 0.1}$  in the long wavelength region of the spectrum. In the pressure range studied (0.5 to 2 torr), the intensity was found to be independent of the molecular bromine concentration. By measuring the absolute emission intensity between 6000Å and 12000Å, values of the apparent rate constant, defined as

$$k_{\text{app}} = I/[\text{Br}]^2[\text{Br}_2],$$

were measured. These rate constants were found to depend on atom concentration and pressure and varied between  $k_{\text{app}} = 5.4 \times 10^{13}$  and  $1.3 \times 10^{15} \text{ cc}^2 \text{ mole}^{-2} \text{ sec}^{-1}$ . A mechanism of the emission reaction is discussed and it is suggested that as much as 15% of the total recombination of bromine atoms may be proceeding via excited states.

In a similar study of the chlorine afterglow, all of the emission was attributed to the  $\text{Cl}_2(^3\Pi_{o+u} \rightarrow ^1\Sigma_g^+)$  transition. A study of the emission intensity in narrow bands revealed that  $I \propto [\text{Cl}]^{2.0 \pm 0.1}$  at short wavelengths,

corresponding to low vibrational levels of the  ${}^3\Pi_{o+u}$  state, while  $I \propto [Cl]^{1.0 \pm 0.1}$  at long wavelengths and higher vibrational levels. Similarly, the pressure dependence of the intensity changed from  $I \propto [Cl_2]^{0.0 \pm 0.2}$  at long wavelengths to  $I \propto [Cl_2]^{0.5 \pm 0.2}$  at short wavelengths. Absolute emission intensity measurements were made in the region from  $5000\text{\AA}$  to  $12000\text{\AA}$  and the rate constants, defined by

$$k_{app} = I/[Cl]^2[Cl_2],$$

were found. Extrapolation of these values of  $k_{app}$  to zero atom concentration yields  $k_{app} = 1.8 \times 10^{14} \text{cc}^2 \text{mole}^{-2} \text{sec}^{-1}$ . A mechanism for the formation and relaxation of the excited state is discussed.

The study of absolute emission intensities was extended to measurements on excited oxygen molecules in a flow system. Observations on the  $7619\text{\AA}$  band of the  $O_2({}^1\Sigma_g^+ \rightarrow {}^3\Sigma_g^-)$  transition yielded  $[O_2({}^1\Sigma_g^+)] = 1.77 \times 10^{-9} \text{ moles l.}^{-1}$ , thereby confirming that this species is a minor constituent in the products of discharged oxygen. Absolute intensity studies on the  $6340\text{\AA}$  and  $7030\text{\AA}$  bands of the  $(O_2({}^1\Delta_g))_2 \rightarrow (O_2({}^3\Sigma_g^-))_2$  transition indicate that the halflife of the  $(O_2({}^1\Delta_g))_2$  collision complex is around 0.1 seconds.

The emission spectrum produced when  $Cl_2$  is reacted with  $H_2O_2$  in solution was observed to originate in various transitions involving excited molecular oxygen. A yield of  $O_2({}^1\Delta_g)$  of 10% from this reaction was estimated.

LIST OF TABLES

- Table 1 - Rate Of Recombination Of Iodine And Bromine Atoms At Room Temperature
- Table 2 - Measurement Of The Band Heads Of The  $\text{Br}_2$  Afterglow In The Region  $7000\text{\AA} - 8300\text{\AA}$
- Table 3 - Bands In The  $\text{Br}_2$  Afterglow Spectrum Recorded By The Hilger Monochromator
- Table 4 - The Dependence Of  $I_\lambda$  Upon  $[\text{Br}]$
- Table 5 - Values Of  $n$  In The Expression  $I_\lambda \propto [\text{Br}]^n$
- Table 6 - Values Of  $k_{\text{app}}$  For Emission Between  $6000\text{\AA}$  And  $12000\text{\AA}$  In The Bromine Afterglow
- Table 7 - Band Heads Recorded From The Chlorine Afterglow Spectrum
- Table 8 - Dependence Of  $I_\lambda$  Upon  $[\text{Cl}]$
- Table 9 - Values Of  $n$  In The Expression  $I_\lambda \propto [\text{Cl}]^n$
- Table 10 - Values Of  $m$  In The Expression  $I_\lambda \propto [\text{Cl}_2]^m$
- Table 11 - Values Of  $k_{\text{app}}$  For The Chlorine Afterglow Emission
- Table 12 - Bands Observed In The Spectrum Of The  $\text{Cl}_2 - \text{H}_2\text{O}_2$  System

LIST OF ILLUSTRATIONS

- Figure 1 - Chlorine potential energy diagram.
- Figure 2 - Bromine potential energy diagram.
- Figure 3 - Iodine potential energy diagram.
- Figure 4 - Schematic diagram of experimental apparatus.
- Figure 5 - Reaction tube used in bromine afterglow studies.
- Figure 6 - Circuit diagram of the detector bridge.
- Figure 7 - Relative response of the RCA 7265 photomultiplier.
- Figure 8 - Relative response of the RCA 7102 photomultiplier.
- Figure 9 - Relative response of PbS detector.
- Figure 10 - Recorder trace of the bromine afterglow spectrum.
- Figure 11 - Assignments to the  ${}^3\Pi_{o+u} \rightarrow {}^1\Sigma_g^+$  transition in the spectrum of discharged bromine.
- Figure 12 - Spectral distribution of the bromine afterglow spectrum obtained by PbS detector.
- Figure 13 - True spectral distribution of the bromine afterglow spectrum.
- Figure 14 - Plots of (a)  $\log I_\lambda$  vs.  $\log [\text{Br}]$  and (b)  $\log (\int I_\lambda d\lambda)$  vs.  $\log [\text{Br}]$ .
- Figure 15 - Plots of (a)  $\log I_\lambda$  vs.  $\log [\text{Br}]$  and (b)  $\log (\int I_\lambda d\lambda)$  vs.  $\log [\text{Br}]$  for a pressure of 1.82 torr.
- Figure 16 - The spectrum of discharged  $\text{I}_2$ .
- Figure 17 - Iodine afterglow spectrum produced by  $\text{ICl} + \text{Cl}$  reaction.
- Figure 18 - The change in the spectral distribution of the  $\text{Cl}_2$  afterglow with atom concentration.
- Figure 19 - The change in spectral distribution of the  $\text{Cl}_2$  afterglow spectrum with pressure.

LIST OF ILLUSTRATIONS  
(Continued)

- Figure 20 - True spectral distribution of the chlorine afterglow spectrum.
- Figure 21 - Plots of  $\log I_\lambda$  vs.  $\log [Cl]$  for a pressure of 1.70 torr.  
 (a)  
 (b) - Plot of  $\log (I_\lambda d\lambda)$  vs.  $\log [Cl]$  for a pressure of 1.70 torr.
- Figure 22 - Plots of  $\log I_\lambda$  vs.  $\log [Cl]$  for a pressure of 3.08 torr.  
 (a)  
 (b) - Plot of  $\log (I_\lambda d\lambda)$  vs.  $\log [Cl]$  for a pressure of 3.08 torr.
- Figure 23 - Plot of  $\log P$  vs.  $\log I_\lambda$  for bands centred at five wavelengths.
- Figure 24 - Plot of  $k_{app}$  vs.  $1/[Cl]$  for a pressure of 1.70 torr.
- Figure 25 - Plot of  $k_{app}$  vs.  $1/[Cl]$  for a pressure of 2.33 torr.
- Figure 26 - Plot of  $k_{app}^{TOTAL}$  vs.  $1/[Cl]$  for five pressures.
- Figure 27 - Plot of  $\Delta G'_{v+1/2}$  vs.  $v'$  for the  ${}^3\Pi_{1u}$  state of  $Br_2$ .
- Figure 28 - Plot of  $k_{app}$  vs.  $[Br]^2$  for a pressure of 0.92 torr.
- Figure 29 - Plots of  $1/k_{app}$  vs.  $[Br]$ .
- Figure 30 - Plot of  $k_{app}$  vs.  $[Cl]^2$  for a pressure of 1.70 torr.
- Figure 31 - Plots of  $k/k_{app}^{TOTAL}$  vs.  $[Cl]$  in the pressure range 0.83 to 3.08 torr.
- Figure 32 - Pressure dependence of the chlorine afterglow emission intensity.
- Figure 33 - Schematic diagram for proposed mechanism of Cl atom recombination.
- Figure 34 - Potential energy curves for the oxygen molecule.
- Figure 35 - Emission spectrum from the reaction of chlorine with hydrogen peroxide.
- Figure 36 - Effective potential energy curves for the Lennard-Jones (6-12) potential.

ACKNOWLEDGEMENTS

I would like to express my sincere appreciation to:

Dr. E. A. Ogryzlo at whose suggestion this investigation was undertaken and under whose encouragement and guidance this work was carried out,

Dr. A. V. Bree and Dr. N. Basco for helpful discussions and suggestions,

The National Research Council of Canada for a Bursary and Scholarships during the course of this research,

And finally, Mr. Norman Finlayson for his enthusiastic help in writing computer programs, and Miss Thea Alma for her patience in typing and proof-reading the manuscript.

To My Aunt Jessie

P A R T   O N E

A STUDY OF THE HALOGEN AFTERGLOWS

## INTRODUCTION

It is a surprising fact that one of the simplest conceivable reactions, the recombination of atoms to form diatomic molecules, is still poorly understood. Not only is the overall mechanism of recombination open to question, but the role played by electronically excited states is uncertain. It was in an attempt to shed some light on this latter problem that this research was undertaken. The question which we sought to answer was what part in the association process is played by collisions into electronically excited states. The technique which shows the greatest potential for this type of study is the "discharge-flow" method by which atoms and excited molecules can be produced at pressures at which the elementary processes can be observed. Prior to the development of the discharge-flow technique, a number of investigators undertook a study of these processes by discharging gases in static systems. The first report of this type of study was given by Bequerel (1) in 1859 who passed an electric current through oxygen. The development of the electrical discharge method by Wood (2) in 1923 and later by Bonhoeffer (3) made

possible a more satisfactory method of studying atom reactions, and a great deal of work on nitrogen atoms was done. Finally the advent of the electrodeless discharge, made possible by the development of high intensity microwave sources, provided the best source of excited species and this is the method most widely used today.

Until recently, the majority of experiments were performed on "active" nitrogen and oxygen and the results were highly qualitative in nature. However, the application of discharge-flow experiments to the study of the upper atmosphere (4) and to certain biophysical phenomena (5), has stimulated a renewed interest in the technique. Recent developments have made possible the study of halogen atoms (6) and also of excited oxygen molecules (7) in flow systems.

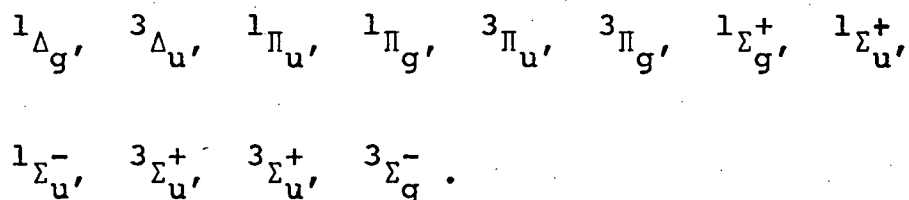
Many atom reactions have accompanying chemiluminescent emissions, as in the case of the reaction of oxygen atoms with nitric oxide (8), but until recently, most investigations of these emissions involved only a spectroscopic identification of the excited species. Today, however, the development of sensitive detectors in the visible and near infrared regions, together with the availability of a convenient standard for absolute emission intensity (9) has made possible a more detailed study of these emissions, and it is now possible to measure the absolute emission intensities from association reactions.

In the present work we have attempted such measurements on the discharge afterglow of oxygen and the halogens.

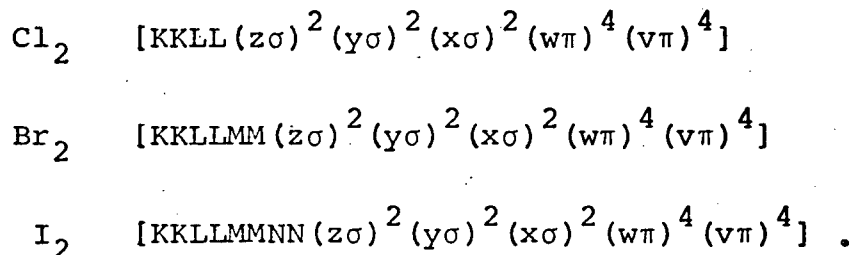
Before describing some of the previous work on recombination luminescence, however, we will review briefly our knowledge about the excited states of  $\text{Cl}_2$ ,  $\text{Br}_2$  and  $\text{I}_2$ .

### Electronic States Of The Halogens

Applying the Wigner-Witmer correlation rules (10), the following states can be shown to correlate with two  $^2\text{P}$  atoms:



Mulliken (11, 12) suggested that the lowest energy electron configurations of the halogens which lead to a  ${}^1\Sigma_g^+$  ground state are the following:

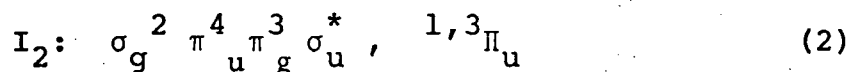


In order to understand the various electronic transitions which the halogens undergo, the coupling of the various angular momenta within the molecule must be

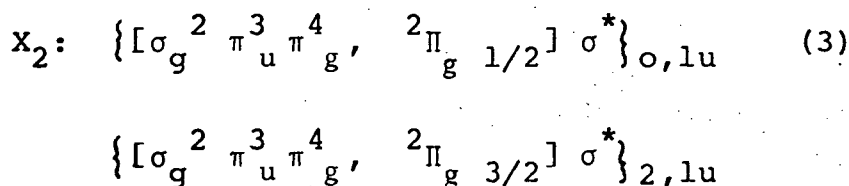
understood. The coupling in the halogens is not strictly Hund's case (a) or (c) but falls in between these two classifications. In the excited states, the tendency is more toward case (c) coupling, especially in the heavier atoms. Moreover, in the excited states of the halogen molecules the energies of dissociation are very small, ( $D = .55$  eV. for  $I_2$ ;  $.39$  eV. for  $Br_2$ ;  $.23$  eV. for  $Cl_2$ ) (13) and are roughly about equal to the doublet separations between the  $^2P_{3/2}$  and  $^2P_{1/2}$  sublevels. From these figures we conclude that, especially in the heavier halogens, the interaction between L and S is stronger than the interaction with the internuclear axis. Thus the quantum numbers of the individual atoms  $L_1, S_1, J_1$  and  $L_2, S_2, J_2$  retain their significance to a considerable extent in the molecule, and the quantum numbers  $\Lambda$  (the component of the electronic orbital angular momentum along the internuclear axis) and  $\Sigma$  for the molecule as a whole are no longer good quantum numbers. The only electronic quantum number which is significant is  $\Omega$  ( $\Omega = |M_1 + M_2|$  where  $M_1$  and  $M_2$  are projections of  $J_1$  and  $J_2$  on the internuclear axis). Nonetheless, these quantum numbers can be assigned to a state by imagining that the atoms are forced closer together creating a stronger field, breaking down the L,S coupling and thereby approaching Hund's case (a). The convention which has been adopted in naming the electronic states of the halogens

utilizes a mixture of case (a) and (c) nomenclature. For example the  ${}^3\Pi_{o+u}$  state would be named  $O_u^+$  if case (c) naming were strictly adhered to.

In predicting the possible excited states of the halogens, Mulliken (14) visualized a different type of coupling. Using his scheme, the excited states are obtained by adding one electron in an "excited orbital" to any of the various states of the ions  $X_2^+$ . Each excited orbital has an ionization potential which is smaller than that of any orbital present in the unexcited molecule. In the case of  $I_2$ , such an orbital is the anti-bonding  $5p\sigma^*$  orbital (referred to as  $\sigma_u^*$ ) which has an ionization potential of the same order of magnitude as the ordinary ionization potential of the molecule. Thus the lowest excited state is obtained by adding a  $\sigma_u^*$  electron to the normal state of  $I_2^+$ :



Transitions from the ground state of  $X_2$  to the  ${}^3\Pi_{o+}$  and  ${}^3\Pi_1$  levels of (2) give the well known visible and infra-red absorption bands of the halogens. If we write (2) in a slightly different form where the  $X_2^+$  core is separated, we get



In (3), we have a core with good quantum numbers  $S_c$ ,  $\Lambda_c$ ,  $\Sigma_c$ ,  $\Omega_c$  and an electron in the excited orbital which is weakly coupled to the magnetic axis giving a resultant  $\Omega = \Omega_c \pm 1/2$ . This type of coupling is called  $\Omega$ -s or  $\Omega, \omega$  coupling and is similar to J-j coupling in atoms. The molecule as a whole has  $\Lambda$  and  $\Omega$  as good quantum numbers while S has lost its significance. The selection rules which govern transitions between states with  $\Omega, \omega$  coupling are as follows:

- (1) transitions within the core are the same as if the excited electron were absent ( $\Delta\Lambda_c, \Delta\Omega = 0, \pm 1$  with  $\Delta\Omega_c = \Delta\Lambda_c$ ) and
- (2)  $\Delta\Omega = 0, \pm 1$ .

Because  $\Omega, \omega$  coupling depends on strong spin-orbit coupling in the core, one might expect it to be modified by a tendency toward atomic spin-orbit (case (c)) coupling, in which case  $\Lambda_c = \Lambda$  is not well defined and the rules  $\Delta\Lambda = 0, \pm 1$  and  $\Delta\Lambda = \Delta\Omega_c$  are not strict. Transitions from ordinary case (a) or (b) to  $\Omega, \omega$  states are governed by  $\Delta\Omega = 0, \pm 1$ ,  $\Delta\Lambda = 0, \pm 1$  with no  $\Delta\Omega = \Delta\Lambda$  restriction.

From a study of experimental and theoretical values of  $\Delta\nu$ , the intervals between the (0,0) bands of two  $^3\Pi$  systems of each molecule, Mulliken (14,15) concluded that in the electronic levels of the halogen molecules, the coupling is, for the most part, between the  $\Lambda, s$  and  $\Omega, \omega$  types, but has strong tendencies, especially in

the heavier atoms, toward separate atom case (c) coupling. On this basis he predicted a number of states in the halogen molecules some of which are shown as dotted curves in the potential energy diagrams (Figures 1,2 and 3).

### Halogen Atom Recombination Studies

The experimental techniques used to produce the high concentrations of atomic species necessary for recombination studies fall into three categories: thermal methods, photochemical dissociation, and electrical discharge.

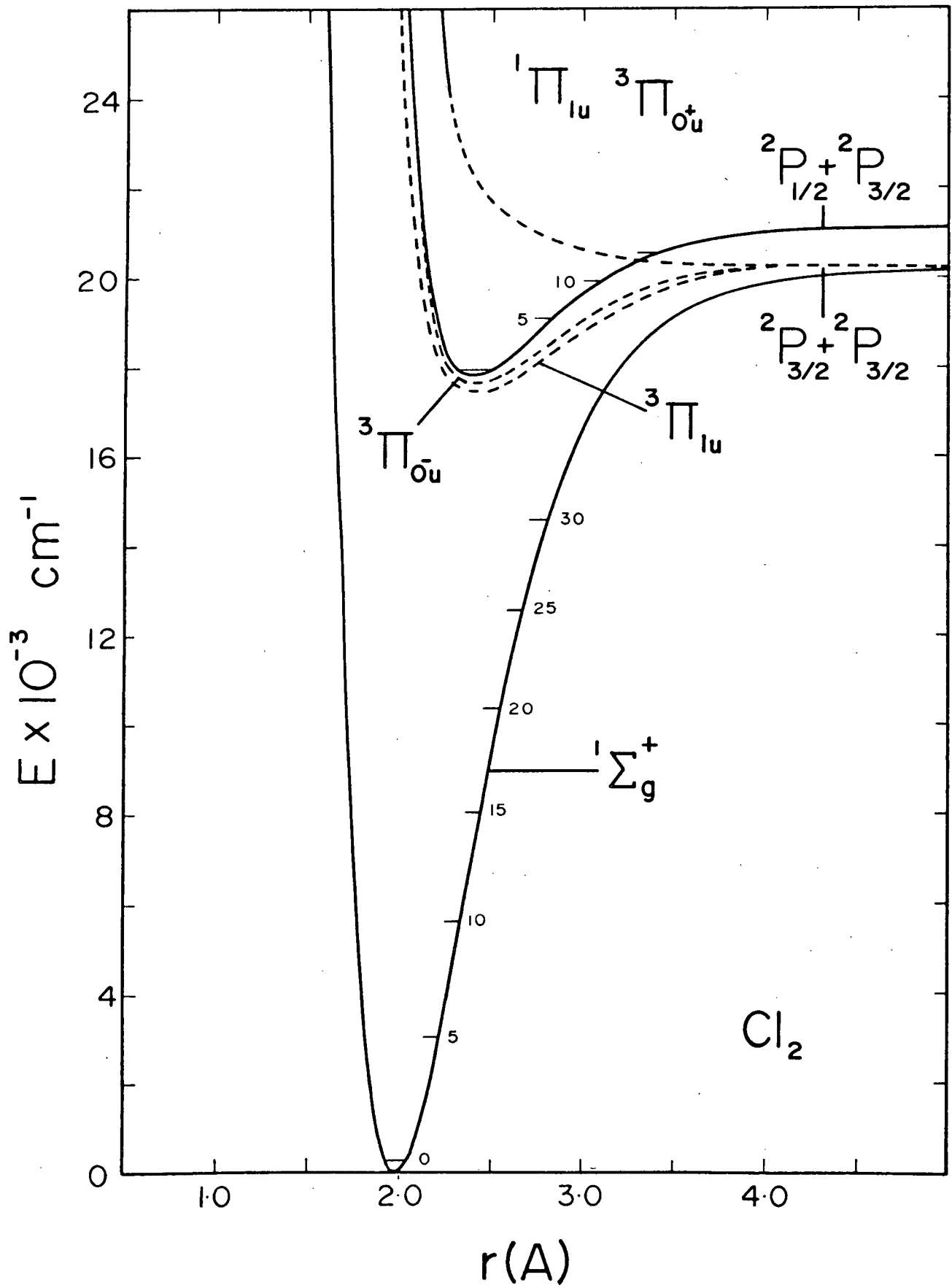
The first studies were conducted by heating the halogens in sealed tubes (16, 17) to approximately 1300°K at which temperature the gases were found to emit visible radiation. The same phenomenon is observed in shock tubes and extensive study of shock heated chlorine and bromine has been made by Palmer (18, 19), Palmer and Hornig (20), Britton (21) and Burns and Hornig (22).

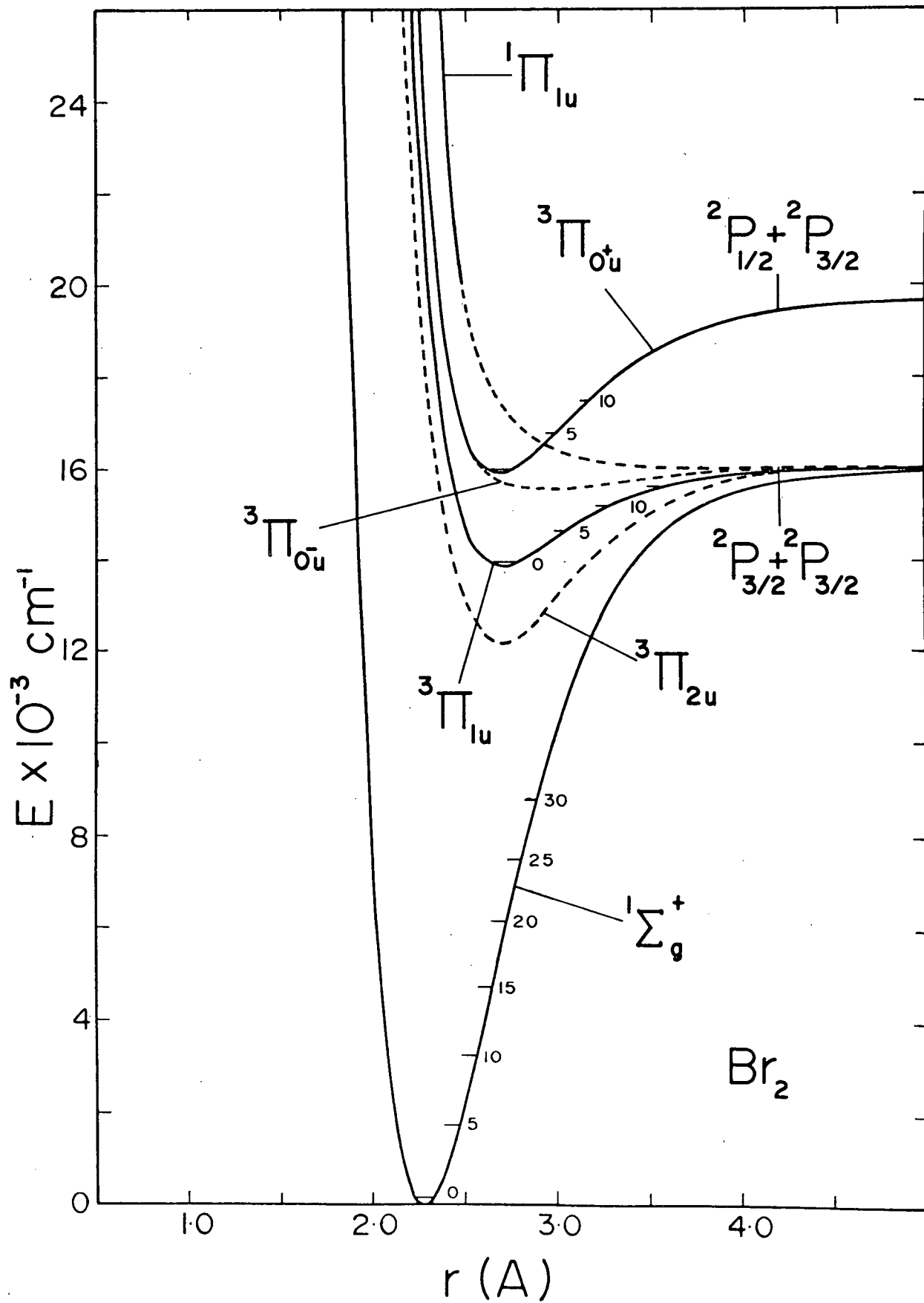
Direct photolysis of the halogens was used by Rabinowitch and Wood (23) to determine the rates of atom recombination in the presence of many foreign gases. However, the greatest advance in this technique came with the development of flash photolysis. This method is particularly suited to the study of iodine because its large extinction coefficient allows a high

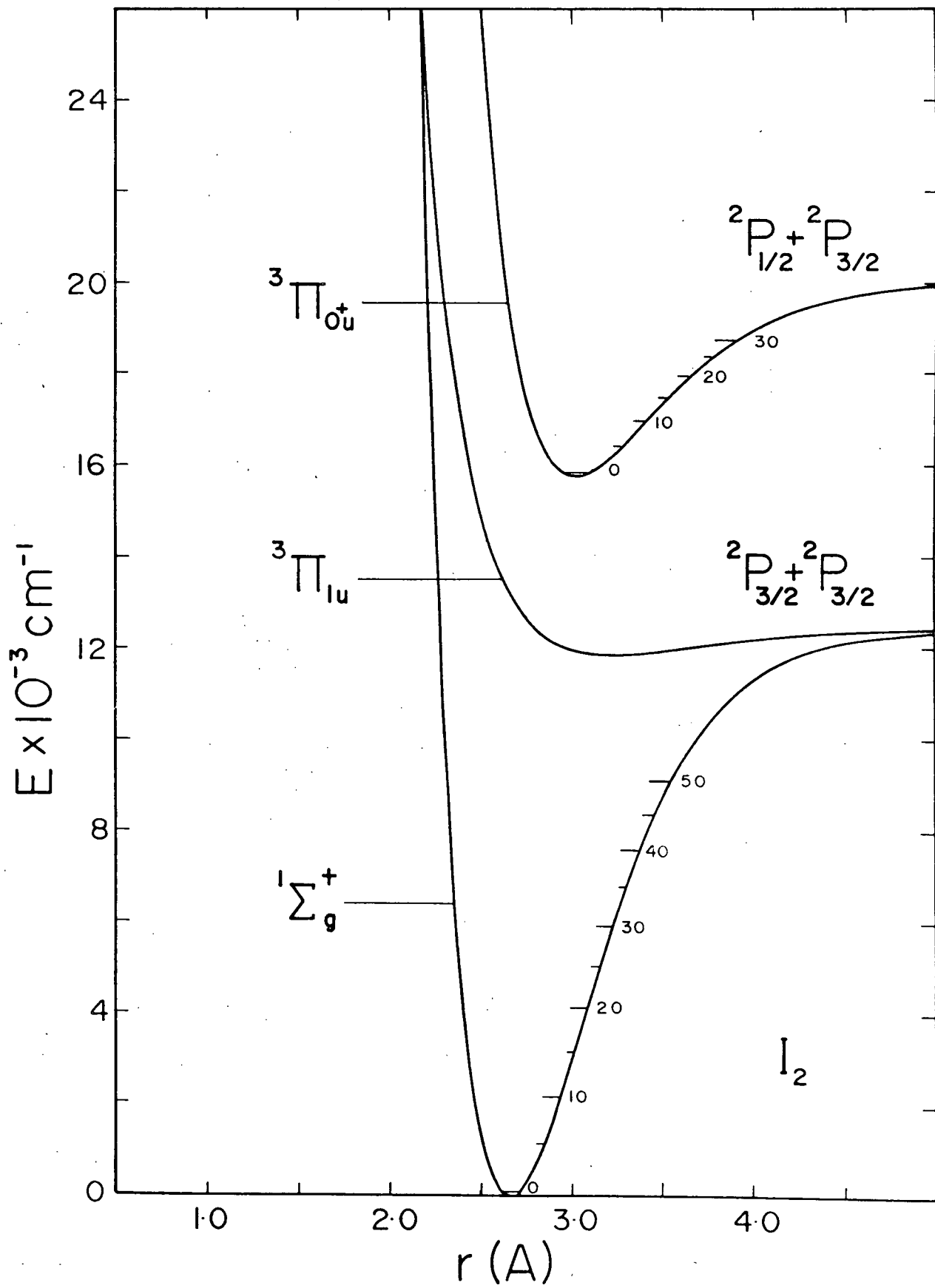
Figure 1. Chlorine potential energy diagram.

Figure 2. Bromine potential energy diagram.

Figure 3. Iodine potential energy diagram.







initial concentration of atoms to be formed, and the decay can be easily followed photometrically. The numerous publications by Porter (see, for example, reference 24) are evidence of the stimulus which this technique has given to the study of atom recombination.

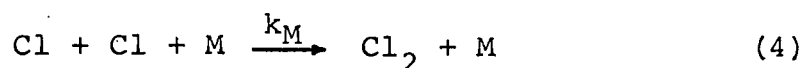
Although electrical discharge techniques were very early shown to be useful for  $N_2$  and  $O_2$  studies, the fact that metal electrodes were used limited the types of gases which could be studied. This problem was circumvented by the advent of the radio frequency and microwave discharges which utilized external antennae and resonance cavities to sustain the discharge and thus avoided contamination of the gas under study.

Investigations of the halogens, however, seem to have been discouraged by the work of Schwab (25) who reported that chlorine and bromine atoms recombined so rapidly on glass and quartz that their study in a discharge-flow system was impossible. In 1961 Ogryzlo (6) reported that certain oxy-acids (called "poisons") when coated on the walls of a flow system reduced wall recombination to such an extent that large atom concentrations could be easily maintained. Although any non-metal oxy-acid was found to be effective, phosphoric acid seemed to be the best poison for halogen atoms.

Rate Studies On Halogen Atom Recombination

Since chlorine has a very low extinction coefficient, the technique of flash photolysis is not suitable for studying the kinetics of recombination, and most quantitative work has been carried out using flow systems. The early work in this field has been reviewed (26) and only the recent work will be considered here.

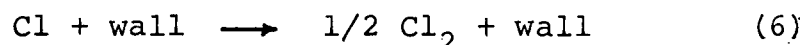
For the termolecular recombination reaction



Bader (26) found  $k_{\text{Cl}_2} = 2.45 \times 10^{16} \text{ cm}^6 \text{ moles}^{-2} \text{ sec}^{-1}$  and  $k_{\text{He}} = 0.3 \times 10^{16} \text{ cm}^6 \text{ moles}^{-2} \text{ sec}^{-1}$  where  $k_M$  is defined by

$$-\frac{d[\text{Cl}]}{dt} = 2k_M [\text{Cl}]^2 [\text{M}] \quad (5)$$

For the concurrent wall recombination reaction



he found  $k = 3.9 \text{ sec}^{-1}$  from which the surface recombination coefficient was found to be  $\sigma = 6.81 \times 10^{-5}$ . These values were later confirmed by Hutton and Wright (27) whose value of  $k_{\text{Cl}_2} = 2.0 \times 10^{16} \text{ cm}^6 \text{ moles}^{-2} \text{ sec}^{-1}$  was in good agreement with Bader, but both were almost two orders of magnitude greater than that reported by Linnett and Booth (28).

In contrast to the dearth of material available on  $\text{Cl}_2$  recombination, a great deal of data have been published on  $\text{Br}_2$  and  $\text{I}_2$ . The first extensive work on iodine

and bromine atom recombination was done by Rabinowitch (29) who derived values of  $k_M$  for a variety of gases from photostationary measurements. The development of flash photolysis has made possible the direct measurement of the recombination of bromine and iodine atoms and  $k_M$  values for a large number of gases have been obtained. Some of these values are given in Table 1. The method of flash photolysis uses the absorption of  $\text{Br}_2$  or  $\text{I}_2$  in the ground state to measure the concentration of atoms at any time after the flash. Implicit in this measurement is the assumption that most of the atoms undergo a direct recombination into the ground state. If, however, a large percentage of the atoms combine through a bound excited state before being relaxed to the ground state, the measurement of these rate constants could be in error. Discharge-flow experiments, on the other hand, do not suffer from this problem because the atom concentration is measured directly.

Two principal experimental facts have evolved from studies of the rate of halogen atom recombination: (1) the efficiency of various third bodies varies over a factor of at least  $10^3$  and (2) the rate constants exhibit a negative temperature dependence. Two theoretical approaches have been utilized to explain these experimental findings.

The first is the energy transfer mechanism which

TABLE 1

## RATE OF RECOMBINATION OF IODINE ATOMS

## AT ROOM TEMPERATURE

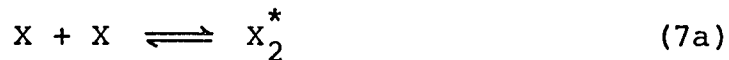
Diluent Gas	$k \times 10^{-16}$ $\text{cm}^6 \text{mole}^{-2} \text{sec}^{-1}$	Reference
He	0.15	24
Ar	0.30	24
O <sub>2</sub>	0.67	24
CO <sub>2</sub>	1.34	24
Benzene	7.95	24
Toluene	19.3	24
CH <sub>3</sub> CH <sub>2</sub> I	26.0	24
Mesitylene	40.2	24
I <sub>2</sub>	138.0	24

## RATE OF RECOMBINATION OF BROMINE ATOMS

## AT ROOM TEMPERATURE

Diluent Gas	$k \times 10^{-16}$ $\text{cm}^6 \text{mole}^{-2} \text{sec}^{-1}$	Reference
He	0.13	22
Ar	0.3	22
N <sub>2</sub>	0.17	36
CO <sub>2</sub>	0.39	37
O <sub>2</sub>	0.40	36
Br	13.0	37

may be represented by the following equations:



$X_2^*$  is a collision complex with a definite lifetime, and it is supposed that a net recombination occurs if this complex collides during its lifetime with a third body M, transferring to it (with a certain probability P) enough energy so that the molecule  $X_2$  cannot subsequently dissociate. The third-order rate constant  $k_r$  for recombination is given by

$$k_r = PgZK \quad (8)$$

where Z is the collision number for reaction (7b) and K is the equilibrium constant for reaction (7a). g is the electronic degeneracy factor which arises because each of the two ground state ( $^2P_{3/2}$ ) atoms has its lowest energy level split into four components by interaction with the other. Of the resulting 16 possible combinations only one leads to the  $^1\Sigma_g^+$  ground state, so that if no electronic transitions occur,  $g = 1/16$ . This theory predicts the correct magnitude of  $k_r$ , but cannot account for the negative temperature dependence unless P is assumed to vary with temperature (30).

The alternate mechanism,

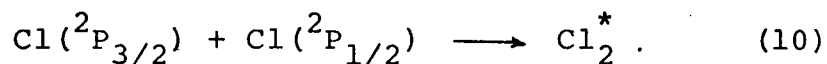


has also been shown to be in substantial accord with the observations (31,32). For this scheme to predict the correct temperature dependence, the intermediate species XM must be bound, the well depth of the intermolecular potential being of the order of a few kilocalories (33).

At present, an unequivocal choice between these two theoretical approaches cannot be made.

### Studies on the Luminescence from Halogen Atom Recombination

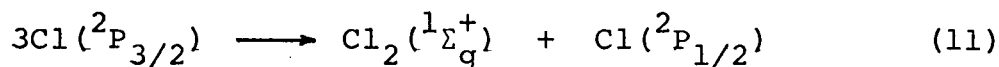
The first studies of emission in the visible from the halogens were reported by Kondratjew and Leipunsky (16). By heating the halogens in quartz tubes to 1300°K they produced an emission which at low pressures consisted of bands in the long wavelength region and a continuum in the violet. An increase in the pressure was found to eliminate the band structure until, at a few hundred mm. Hg, only the continuum remained. Since emission was found at wavelengths shorter than the convergence limit, these investigators suggested that two body recombination followed by the immediate emission of a quantum of radiation was the predominant process:



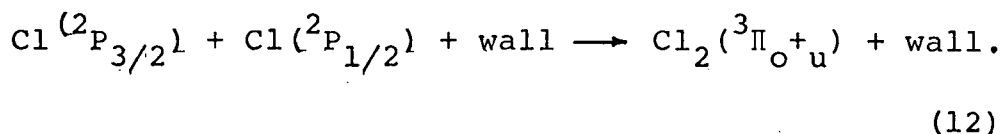
Photometric measurements of the change of intensity of the continuum with temperature, compared to that predicted from simple kinetic theory, was considered

reasonable confirmation that the two body process was responsible for the continuum.

Uchida (17) later studied the halogens by heating the gas in a capillary of 0.5 mm diameter and observing the emission spectra. He found that at long wavelengths the emission was almost exclusively banded and raising the pressure did not eliminate the bands, but caused them to be overwhelmed by the intensity of the continuum. By taking spectra of the emission near the walls and in the middle of the capillary, he discovered that the bands originated near the walls and the continuum predominated in the middle of the tube. He suggested that the wall acted as an energy sink, stabilizing the recombination of a  $^2P_{3/2}$  and a  $^2P_{1/2}$  atom into the  $^3\Pi_{O+u}$  state, which then radiated. Uchida found evidence that the intensity of the bands and also of the continuum was proportional to the fourth power of the degree of dissociation. This he took to be proof that atoms in the  $^2P_{1/2}$  state were produced by the process



and then the formation of the  $^3\Pi_{O+u}$  proceeded via



Recent investigations of halogen emissions have been conducted in flow systems at low pressures where banded

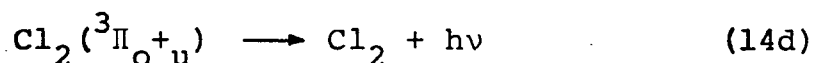
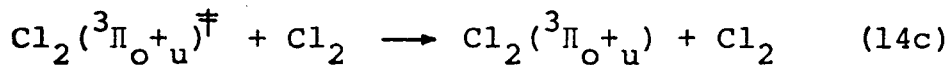
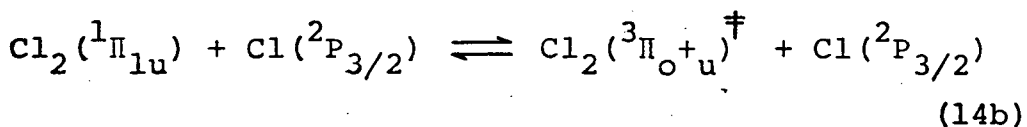
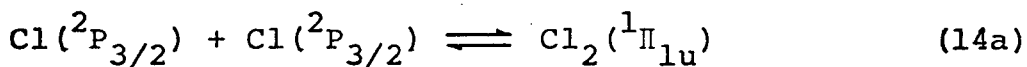
emission predominates. Using a photographic method to determine intensities, Bader and Ogryzlo (34) concluded that the emission intensity varied according to

$$I = k[\text{Cl}]^2[\text{Cl}_2] \quad , \quad (13)$$

which is in contradiction to the findings of Uchida.

The bands were identified as belonging to the  ${}^3\Pi_{o+u}$

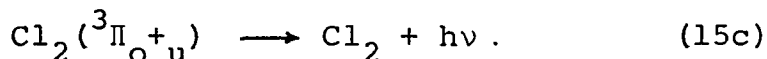
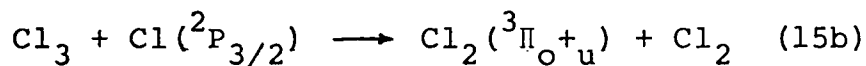
→  ${}^1\Sigma_g^+$  transition in accord with earlier work, but they noted a change in spectral distribution with pressure which had not previously been seen, higher pressures favouring the longer wavelength emission. The fact that no transitions above  $v' = 13$  were observed, they took as evidence of the crossing of the  ${}^3\Pi_{o+u}$  state by the  ${}^1\Pi_{1u}$ , leading to the mechanism



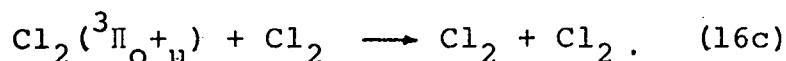
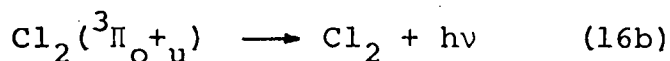
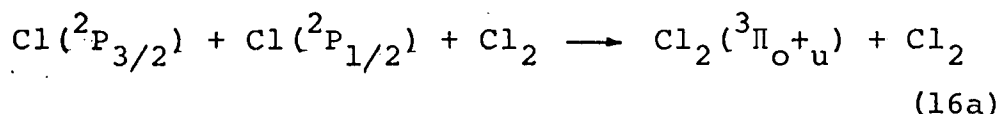
and predicting  $I = k[\text{Cl}({}^2P_{3/2})]^2[\text{Cl}_2]$ . Here, the notation  $\text{Cl}_2({}^3\Pi_{o+u})^\ddagger$  represents a vibrationally excited molecule.

Bader and Ogryzlo were, however, unable to decide between this mechanism and the following, which predicts the same kinetic order but does not require the intermediate

formation of the  $^1\Pi_{1u}$  state:



In a similar study of chlorine atom recombination, Hutton and Wright (27) also found the emission intensity to be proportional to the square of the atom concentration and to the first power of the  $\text{Cl}_2$  pressure. They reported the absolute rate constant for the chlorine emission to be  $1.5 \times 10^{13} \text{ cm}^6 \text{ mole}^{-2} \text{ sec}^{-1}$ . This determination, however, was made over the region  $5200\text{\AA}$  to  $8000\text{\AA}$ , since they could not detect longer wavelength emission, so that this constant may not represent the absolute rate if the emission extends beyond their measureable range. These authors favoured the direct formation of the  $^3\Pi_{o^+u}$  state from one ground state  $^2P_{3/2}$  and one excited  $^2P_{1/2}$  atom, since at  $20^\circ\text{C}$  the equilibrium concentration of  $\text{Cl}(^2P_{1/2})$  is 1% that of  $\text{Cl}(^2P_{3/2})$ . They therefore proposed the following mechanism to explain the emission kinetics:



Equation (16c) represents a deactivation of the excited state by  $\text{Cl}_2$ , and was invoked by Hutton and Wright because they found that the emission intensity was independent of  $[\text{Cl}_2]$  for pressures above 2 torr. Bader and Ogryzlo, on the other hand, attributed this observation to a shift in the emission maximum to longer wavelengths.

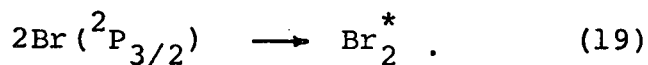
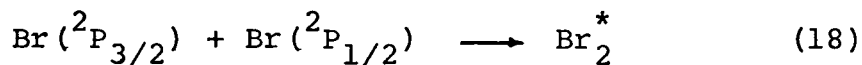
Much less work has been done on radiative recombination from bromine largely owing to the greater difficulties involved in atom detection. Using an isothermal calorimetric detector and a photographic method of determining intensities similar to that employed by Bader and Ogryzlo, Gibbs (35) investigated the bromine afterglow emission. He found that, as in the case of chlorine, the emission intensity was proportional to the square of the atom concentration and the first power of the  $\text{Br}_2$  concentration:

$$I = k[\text{Br}]^2[\text{Br}_2] . \quad (17)$$

The spectrum of the afterglow was found to consist of a large number of bands degraded towards the red which Gibbs assigned to the  $\text{Br}_2( {}^3\Pi_{0+u} \rightarrow {}^1\Sigma_g^+ )$  transition.

At the pressures and temperatures encountered in discharge-flow experiments, the banded emission arising from three-body processes predominates over any contribution from two-body atom recombinations, which

would give rise to continuous emission. At the high pressures and temperatures used in shock tube experiments, however, the emission spectrum is continuous. A study of the emission from shock heated bromine led Palmer (18) to conclude that two body recombination can take place into the  $\text{Br}_2(^3\Pi_{1u})$ ,  $\text{Br}_2(^3\Pi_{0+u})$  and  $\text{Br}_2(^1\Pi_{1u})$  states via the processes



In a similar, but more quantitative investigation of the chlorine emission, Palmer (19, 20) suggested a means of calculating the concentrations of excited  $\text{Cl}_2$  molecules in attractive or repulsive states based on equilibrium statistical mechanics.

### Purpose Of This Investigation

The purpose of this research was to study the luminescence from halogen atom recombination in order to gain a better understanding of the role played by electronically excited states in the total recombination process. To do this, we hoped to be able to:

- (a) devise a method of producing iodine atoms in a discharge flow-system and of observing the recombination emission,
- (b) study the entire afterglow spectra of  $\text{Br}_2$  and  $\text{Cl}_2$  and identify the electronic state(s) giving rise to the luminescence.

We also hoped to determine the kinetic order of the emission intensity with respect to atom concentration and pressure. Using the  $\text{O} + \text{NO}$  glow as a standard of emission intensity, we undertook to determine the absolute rate constants for emission in the halogen afterglows and from these measurements, to estimate the fraction of the total recombination proceeding through electronically excited states. Finally, from an analysis of these data, and those of other workers, we hoped to be able to give a general mechanism for recombination into excited states in the halogens.

## EXPERIMENTAL

### The Flow System

All discharge-flow experiments were performed using a flow system, part of which is illustrated in figure 4. The apparatus consisted of a purification line, a main flow system, in which the reaction tube was located, and four auxiliary gas storage bulbs and capillary flow meters connected to the vacuum system at points A, B and C (figure 4). Since it was periodically necessary to remove the reaction tube for cleaning and poisoning, this section of the vacuum system was constructed to allow for its complete removal.

A number of different types of reaction tube were used in this work; details of the one used for bromine are shown in figure 5. To prevent light from the discharge region being reflected (or conducted) by the glass into the observation section, two right-angled light traps were placed at the end of the discharge tube. The outside of these light traps was painted with flat black enamel. Multiple inlet jets A and B were used to introduce NO, NO<sub>2</sub> and NOCl into the main

Figure 4. Schematic diagram of experimental apparatus.

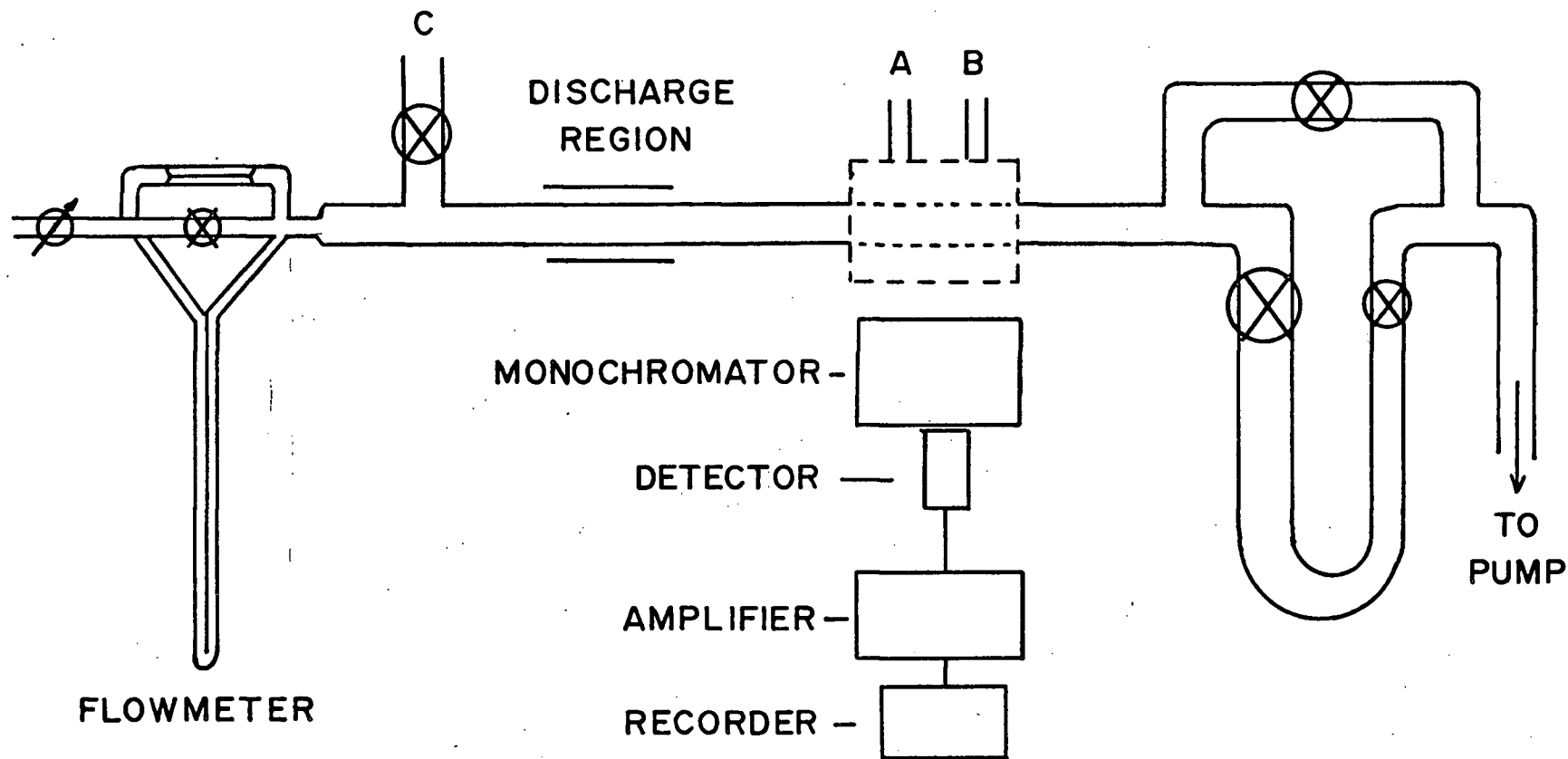
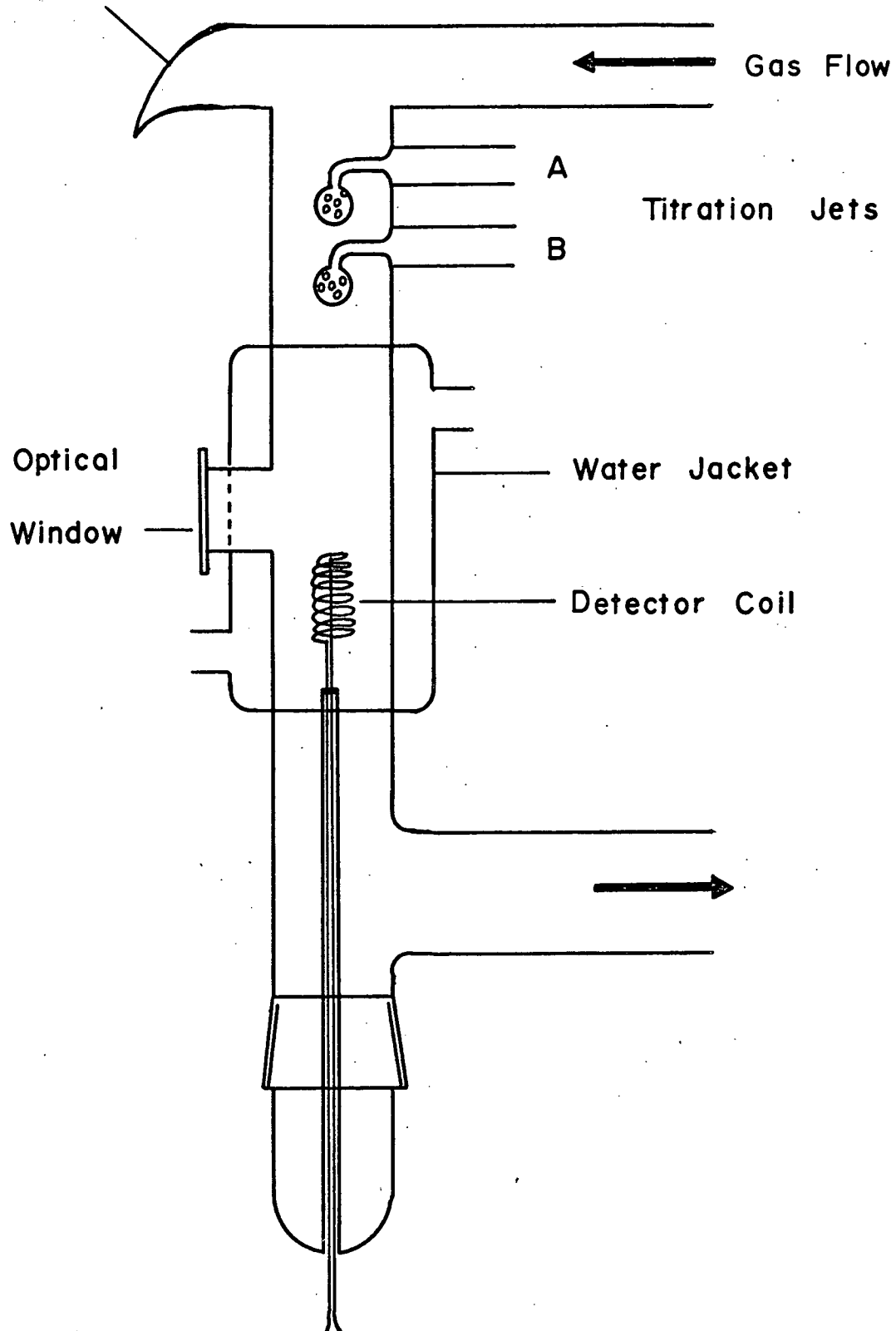


Figure 5. Reaction tube used in bromine after-glow studies.

Light Trap



Gas Flow

Titration Jets

A

B

Optical

Window

Water Jacket

Detector Coil

gas stream and were found to give the best mixing characteristics of any type tested. The section of the reaction tube viewed by the spectrophotometer was covered by an optically flat quartz window.

The walls of the vessel surrounding the detector coil were maintained at a constant temperature of 25°C by circulating water from a temperature bath through the water jacket. Although the detector operates isothermally, and therefore will not cause a temperature variation of the walls after equilibrium has been obtained, it was found that relatively small changes in room temperature could cause appreciable deviations in the detector current. This difficulty was overcome by circulating water from a constant temperature bath through a water jacket surrounding the detector coil.

In spectroscopic experiments which required maximum intensity from the afterglows so that small slitwidths could be used, another type of reaction tube was employed. This vessel was one inch in diameter, four inches long and was viewed "end on" by the spectrophotometer. The walls of this tube were coated with MgO which has 98% reflectivity (38) and which helped to increase the intensity. This type of tube was impractical for kinetic measurements, however, because of the decrease in the intensity of the emissions down the length of the tube, particularly at higher pressures.

Gas flow rates were measured by observing the pressure difference established across a capillary as the gas flowed through it. This pressure difference was indicated on a U-tube manometer filled with either sulfuric acid or dibutylphthalate, since most of the gases used attacked mercury. Calibration of these flowmeters, in the case of non-condensable gases, consisted of collecting a measured volume of the pump exhaust, noting the time required, and applying the ideal gas laws to calculate the flow rate. The flow rate of nitric oxide was assessed each time it was used by observing the pressure drop in the storage bulb in a fixed interval of time. To measure the flow rates of  $\text{Cl}_2$ ,  $\text{NOCl}$  and other condensible gases with vapour pressures greater than one atmosphere, a special calibration bulb was constructed. The volume of this bulb was determined accurately and the pressure of any gas contained in it could be read directly from a mercury manometer. A U-tube filled with dibutylphthalate and an air-bleeding system separated the mercury manometer from the bulb, and permitted pressure measurements without having the gas come into contact with the mercury. Flow rates of bromine and nitrogen dioxide were calculated by trapping out the gas and weighing it in a specially constructed thin-walled weighing vessel. Since no attempt was made to construct the capillaries of the

flowmeters in such a way that gas flow through them conformed to the Poiseuille equation (51), each value of the total system pressure required a separate calibration of the flowmeters.

Gas flows were controlled by either of two types of needle valve. In most cases, Edwards high vacuum needle valves proved to be satisfactory, but when exposed to the halogens they were found to become corroded. For this reason, a Fischer-Porter glass and teflon valve was used for bromine, while the tank regulator was found to give sufficiently fine control in the case of chlorine.

Total system pressure was measured by either of two tilting McLeod gauges, one containing mercury, the other sulfuric acid. The latter was designed to have a pressure measuring range of 0.1 to 5 torr and was calibrated against the mercury gauges.

The total pressure at any flow rate of the gas could be varied by partially closing a 20 mm. stopcock just upstream from the liquid nitrogen cold trap. Originally, a constriction was placed at this point so that the pressure could be varied by changing the flow rate. This procedure was later abandoned because it permitted the use of only one flow rate at a particular pressure.

Although pumping speed is irrelevant in the case of condensable gases, since the effective pressure at the liquid nitrogen trap is zero, it is important when working with oxygen. Initially a Welsh Duo-Seal model 1397 vacuum pump was used which had a pumping speed of 425 l./min. This was later replaced by two pumps, a Welsh model 1403 and a 1405H, operated in parallel. Both pumps were used only for oxygen studies and during the O + NO calibration.

### Materials

Chlorine from Matheson of Canada Limited (99.5% minimum purity) was used without further purification.

Nitrosyl chloride was obtained from Matheson (93% minimum purity) and was further purified by trap to trap distillation using dry ice-acetone and alcohol slush baths and stored in a 22 l. bulb. The infra-red absorption spectra of samples withdrawn from the storage bulb and from the pump trap showed that little or no decomposition had resulted from passing the gas through the metal needle valves.

Nitrogen dioxide was obtained from Matheson Company and traces of the chief impurity, NO, were removed by storing the gas with oxygen until the solid was pure white in colour. The gas was kept trapped down with dry ice and before being used, was expanded into a 2 l. bulb.

Nitric oxide was obtained from Matheson and its chief impurity was found to be  $\text{NO}_2$ . Trap to trap distillations using liquid nitrogen and an ethanol slush bath were performed until the gas was colourless and the solid was pure white. The nitric oxide was stored, ready for use, in a 2 l. bulb with a mercury manometer attached, the latter serving to measure the bulb pressure and scavenge any  $\text{NO}_2$  formed after purification. Reagent grade bromine from the Baker Chemical Company was first dried over silica gel, thoroughly de-gased by freezing and pumping, and then the middle fraction was slowly distilled into the cold trap of a 22 l. storage bulb. When not in use, the bromine was kept trapped down in a dry ice-acetone bath to avoid contamination.

Matheson extra dry grade oxygen was found to contain little  $\text{N}_2$ , the most objectionable impurity in gas-discharge experiments, and was used directly from the cylinder without further purification.

#### Production of the Excited Species

##### (a) Chlorine and Bromine Atoms

Atoms were formed in an electrodeless discharge produced by applying 2450 mc./sec. microwave power from a Raytheon generator to the discharge region of the reaction tube. Since the fluctuation of line

voltage affected the atom concentrations quite markedly, the microwave generator was run off a 220 V Sola transformer to stabilize the voltage. A  $\frac{1}{4}$  wave discharge cavity constructed from the specifications of Broida et al (39) was found to be the most satisfactory type of cavity for halogen studies. Adjustments could be made for tuning this cavity to resonance and also for optimizing the reflected power. The increased efficiency thus obtained extended the pressure range over which the discharge could be maintained and, in fact, it was found that oxygen discharges could be sustained at pressures close to one atmosphere. It appears that high concentrations of halogen atoms are obtained when the discharge region is quite hot, so that the highly localized discharge produced by this cavity proved to be advantageous. The discharge tube was constructed of 12 mm. diameter pyrex and cooling was achieved by blowing a stream of air through the inlet provided on the cavity.

In order to decrease wall recombination to an acceptable level, the technique first used by Ogryzlo (6) of coating the walls of the reaction vessel with phosphoric acid was employed. In practice only the walls of the discharge region were "poisoned" since this seemed to be sufficient. Coating the walls of the whole system was undesirable since this caused fogging

of the optical windows. The surface of the glass was prepared by cleaning it thoroughly with soap and water and then with hot, concentrated NaOH solution before the poison was applied. The tube was then filled with a 20% solution of  $H_3PO_4$ , drained, and then evacuated to remove the excess water. Finally the tube was thoroughly dried by discharging pure argon through it for an hour before any experiments were performed.

(b) Production Of Iodine Atoms In A Flow System

In the hope that this study could be extended to an investigation of  $I_2$ , some preliminary experiments on the production of iodine atoms in a flow system were undertaken. The main problem encountered was that of obtaining a high enough flow rate of iodine through the system to produce measurable quantities of iodine atoms. Initially, this problem was overcome by heating the iodine crystals in a small glass furnace. This furnace was connected to the discharge tube through a capillary and both the furnace and capillary were wrapped with heating wire and insulating material. The discharge tube was maintained at a high temperature by surrounding it with a jacket filled with  $CCl_4$  which was heated by the discharge itself. Carbon tetrachloride was used for this purpose since it does not absorb the microwave radiation.

A second method used to provide high concentrations of iodine, and one which was found useful when using  $I_2$  as a titrant in gas reactions, was to pass an inert gas through a vessel of heated iodine crystals.

Because the high rate of recombination of iodine atoms caused a rapid decay of intensity down the reaction tube, observations of the emission were done very close to the discharge region. Two right-angled light traps ensured that light from the discharge did not enter the monochromator slit. The walls of the reaction tube were jacketed so that the entire vessel could be heated and a removable cold trap was placed immediately after the tube. This trap permitted easy removal of the iodine after it had passed through the system.

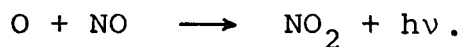
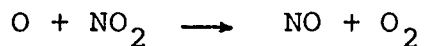
Because of the obvious difficulties entailed in the measurement of iodine flowrates, no attempt was made to perform any quantitative experiments. Since the emission was expected to be in the infrared, the PbS detector was employed for all observations.

#### Atom Detection and Measurement

The two most widely used methods for measuring atom concentration in flow systems are chemical titration and isothermal-calorimetric detection. In order to utilize a titration procedure a substance must be available which reacts rapidly and stoichiometrically

with the atomic species but does not generate a product which reacts with the atoms at a comparable rate.

Spealman and Rodebush (40) first suggested the use of  $\text{NO}_2$  for the titration of oxygen atoms:



When  $\text{NO}_2$  is added to a stream of oxygen atoms, the characteristic green air afterglow is observed and as more  $\text{NO}_2$  is added, the intensity of this emission reaches a maximum (when the flow of  $\text{NO}_2$  is about  $\frac{1}{2}$  of the oxygen atom flow). Addition of more  $\text{NO}_2$  causes the intensity of the glow to diminish and finally extinguishes it sharply to within 3 cm. of the gas inlet, the latter distance being governed by the mixing characteristics of the inlet jet. At this point the flow of  $\text{NO}_2$  is equal to the flow of oxygen atoms. A precaution necessary in this procedure is to keep the  $[\text{O}]/[\text{O}_2]$  ratio small so that no significant pressure change occurs during the titration for oxygen atoms. Kaufman (8) found that efficiency of the discharge changed with total pressure thus causing a change in the oxygen atom flow rate.

The use of  $\text{NOCl}$  as a titrant for chlorine atoms was first suggested by Ogryzlo (6) and was used by

Hutton and Wright (27) for atom concentration measurements. The reaction is

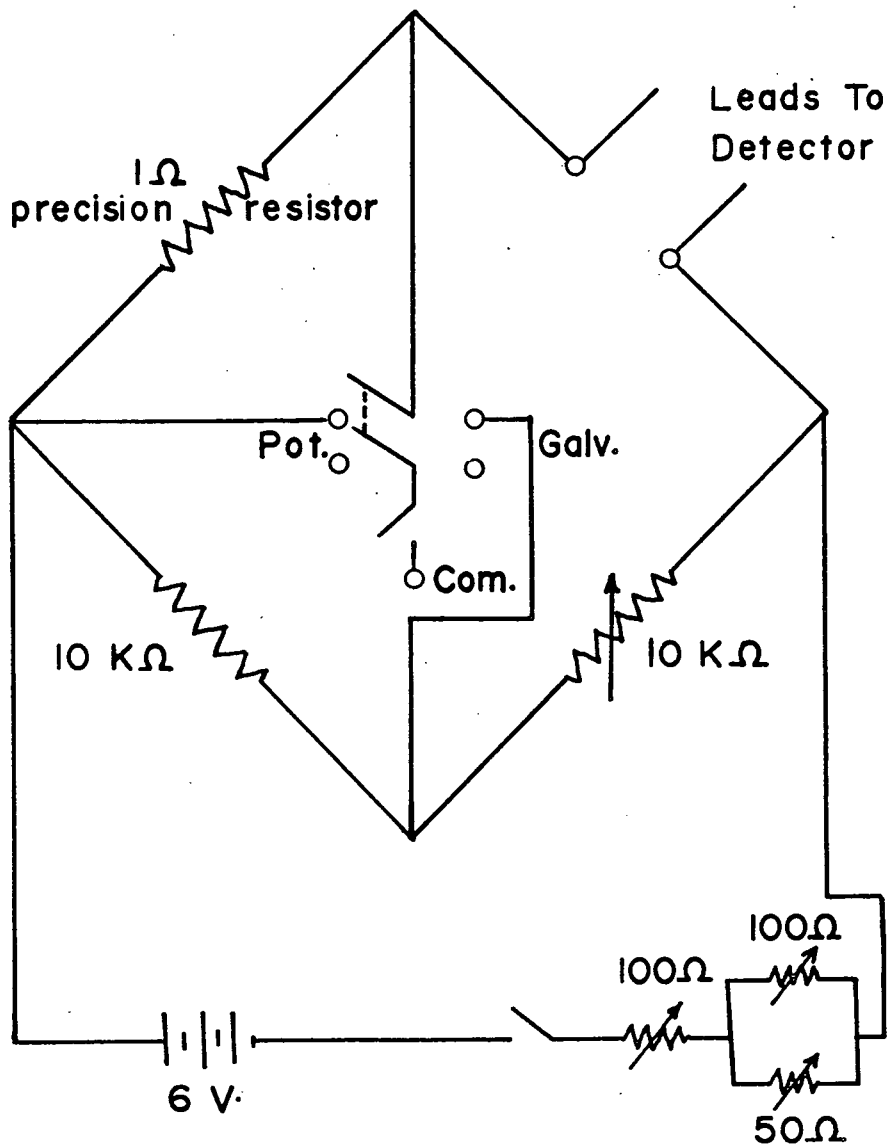


Although this reaction is reasonably fast (41), our preliminary experiments showed that the extinction of the chlorine afterglow did not provide a satisfactory endpoint for the titration. When a photomultiplier was placed 10 cm. downstream from the inlet jet, as suggested by Hutton and Wright, and NOCl was added until extinction of the chlorine afterglow occurred at this point, analysis of the reaction products showed the presence of considerable NOCl. This fact, and the observation that this procedure gave consistently higher atom flow rates than indicated by the isothermal detector, leads us to believe that this is not a very satisfactory procedure. For this reason, and also because no satisfactory chemical titration procedure has been found for bromine, the isothermal calorimetric detector was used for all halogen atom measurements.

The isothermal calorimetric detector was first described by Ogryzlo (42) who used it in the measurement of oxygen atoms and later found it to be useful for the halogen atoms (6). The detector, in the form in which it was used for chlorine and bromine atoms,

consisted of a helically wound spiral of platinum wire electroplated with nickel. The nickel was plated from a solution of nickel chloride and ammonium chloride using a plating current of about 10 milliamps supplied from a 6 volt storage battery. Halogen atoms recombine on the nickel surface with almost 100% efficiency releasing an amount of heat equal to the dissociation energy per pair of combining atoms. By controlling the current to the detector one is able to hold the temperature constant so that the detector operates isothermally. The decrease in current necessary to maintain the detector temperature from the value with no atoms flowing, to that when atoms are recombining on the surface, permits calculation of the atomic flow rate. The galvanometer-potentiometer and associated wiring used for the control and measurement of the detector current is shown in figure 6. The detector forms one arm of a Wheatstone bridge. In operation, the bridge is first balanced with the discharge off, by adjustment of the current and/or the decade resistance box. The current passing through the detector is found by measuring the potential drop across a 1 ohm precision resistor. The discharge is then initiated and the current through the detector is reduced to maintain the detector at its initial temperature. The current is read again and the atom flow rate

Figure 6. Circuit diagram of the detector  
bridge



calculated from the formula

$$\text{atom flow} = \frac{\Delta(i^2)R}{4.18 D/2} \quad \text{gm. atom/sec.} \quad (22)$$

where  $\Delta(i^2)$  is the current squared decrease =  $i_1^2 - i_2^2$

R = resistance of the detector in ohms

D = dissociation energy of the bond being formed  
(cal./mole)

4.18 = the electrical power to heat conversion  
factor (4.18 joules/cal.)

The concentration of gas in the system can be calculated using the ideal gas laws which are assumed to be valid for this work.

A number of problems were encountered in using the detector for halogen atom measurements. The most serious problem which arose in the work with chlorine was that when the detector coil was exposed to high atom concentrations, a contamination of the nickel surface occurred after a period of time. This caused a reduction in the recombining efficiency of the coil and was readily recognized by the appearance of the afterglow downstream from the detector. At moderate atom flow rates, this contamination usually required up to two hours before atoms began to sweep past the detector. When this occurred, the detector current reading began rising slowly so that the bridge could no longer be properly balanced and the orange chlorine

afterglow was visible downstream from the nickel coil. Since this phenomenon had not been reported in previous work using this technique, a systematic search for the source of the trouble was undertaken. First, further purification and drying of the chlorine was carried out with no noticeable effect on the rapidity of contamination. Further evidence that impurities were not causing loss of efficiency was provided by the fact that undischarged chlorine did not cause contamination over a period of six hours. To ensure that the phosphoric acid poisoning was not being transferred to the detector, only the discharge region was coated. The water was then thoroughly removed by baking the tube at 200°C under vacuum for two hours before placing the detector back into the system. This procedure did not produce any change. Finally, a number of different techniques of plating the nickel onto the coil were tried, from using different electroplating currents to deposit the nickel, to heat treating the coil. Again this did not produce any noticeable improvement. Consequently, measurements had to be taken rapidly, within the lifetime of a given coil. This was feasible because it was observed that the loss of detector efficiency occurred rather suddenly and was easily recognized by a sudden increase in detector current and appearance of the afterglow behind the coil. Although undoubtedly

the contamination proceeded at a constant rate, the large area provided by the long coil of nickel wire meant that contamination occurred first at the top of the coil and then proceeded to the bottom. Evidence for this was that initially only the first coil of wire was needed to kill all the atoms, even at high flow rates. The second effect which made the use of this technique possible was that the coil could be re-activated in situ merely by applying 1.5-2 amps to the coil for about one minute. At first, the number of atoms being swept by the coil increased sharply and then slowly decreased until no atoms were getting by. The detector current was then reduced to its original value and allowed to re-equilibrate. Initially a second photomultiplier was placed downstream of the detector so that any emission in this region could be detected, but since all experiments were performed in the dark, it became obvious that the eye could detect this as quickly as the photomultiplier.

In using this technique to find bromine atom concentrations, quite a different problem arose. Because of its higher molecular weight, bromine did not transfer heat from the coil to the walls of the reaction tube as quickly as did chlorine. As a result the detector operated at a higher temperature, and if high

atom flows were used, nickel was found to distill off the coil and onto the walls. This resulted in a continuous increase in the detector current but at no time was there any evidence that atoms were being swept by the coil. Further verification of this phenomenon came with the discovery that upon removing the detector and allowing discharged oxygen to flow through the system, a band of violet chemiluminescence on the walls of the reaction tube marked the former position of the detector coil. This glow has recently been identified (43) as the Herzberg bands of  $O_2$  which are produced in the catalyzed recombination of oxygen atoms on metal surfaces. This problem was circumvented by using low Br flow rates and operating the detector at low current values.

### Spectroscopic Measurements

#### (a) Equipment

A Hilger and Watts large aperture prism monochromator No. D285 equipped with interchangeable glass and quartz prisms was used for most spectroscopic measurements. This instrument was well suited for the low light intensities encountered in this work because of its  $f/4.5$  aperture, its high transmission, resulting from the use of front surfaced mirrors for internal focusing, and the wide slit widths obtainable (to

1.25 mm.). Although the glass prism and associated calibrated wavelength drum were used for most experiments, the quartz prism was used in investigations of emissions beyond  $2\mu$  because of the higher transmission of quartz in the infrared. When working in the infrared region, the monochromator was sealed and flooded with dry nitrogen to reduce absorption due to atmospheric  $\text{CO}_2$  and water. A wavelength drive mechanism utilizing a 1 rpm synchronous motor was added and by means of interchanging gears, any of four drive speeds could be selected. The wavelength calibration of the instrument was checked periodically using the mercury emission lines from a low pressure mercury lamp or using neon or argon lamps in the infrared.

(b) Measurement of Spectra

The procedure used to measure accurately band head positions in  $\text{Cl}_2$  and  $\text{Br}_2$  emission spectra was as follows. First, a neon spectrum was recorded and measured. The position and wavelength of a number of the bands were then used to compute the linear dispersion curve of the monochromator by fitting a cubic equation to the data. When the emission spectra were recorded, the  $7503\overset{\circ}{\text{A}}$  Ne line was superimposed on the recorder trace. The band heads were then measured relative to this line and these measurements were

used to find the correct wavelength from the dispersion curve. These calculations were carried out on the IBM 7044 computer and the program also calculated vacuum wave numbers.

(c) Signal Detection

Since the systems studied emitted radiation over a wide wavelength range, it was necessary to use three different detectors. An RCA 7265 photomultiplier, operated at a voltage of 1750 volts, detected radiation in the visible region. In the near infrared region ( $6800\text{\AA} - 12000\text{\AA}$ ) an RCA 7102 photomultiplier was used, operated at 1250 volts and cooled with liquid nitrogen. Both photomultipliers were adapted to fit into a metal casing on which was mounted a metal dewar. The glass envelope of each phototube came into contact with a brass ring attached to the bottom of this dewar so that efficient cooling could be achieved. The metal casing could be evacuated and the optical window was fitted with a heater to prevent fogging. Because condensation on the resistors and associated wiring was found to cause a sharp increase in the noise level, a heater was placed around the resistor chain and provision was made for blowing dry nitrogen through the wiring associated with the phototube. Stabilized D.C. voltages were supplied from an Interstate power supply model 304.

The determination of absolute emission intensities requires a high degree of photomultiplier stability and for this reason, careful warmup procedures were followed before each experiment was performed. Both tubes were run at operating voltages for one hour before being used. In addition, the RCA 7102 was cooled for one hour before the voltage was applied. Neither tube was exposed to light of high intensity while being used.

Using a calibrated lamp and a stable A.C. power supply, the output current of the photomultipliers was found to be a linear function of the exciting illumination at intensities similar to those encountered in an experiment. At high intensity levels, the phototubes were observed to undergo some fatigue after prolonged exposure, but this was not expected to be a problem since the emission intensities observed in an experiment were very low. To check for slight sensitivity changes from day to day, the signal from a tungsten strip lamp operated at set voltage and current was measured.

In the medium infrared region ( $1.2\mu - 2.6\mu$ ) emission was detected by a lead sulfide photoconductive cell obtained from Infrared Industries Incorporated. The sensitive area of this detector was 2.54 mm. by 5.08 mm. and it was mounted inside a dewar equipped with a sapphire optical window. The detector was

operated in series with a 500 K $\Omega$  load resistor and voltage was supplied from a 300 v. battery. The cell and associated wiring were mounted inside a grounded brass case. Since optimum values of signal to noise ratio and sensitivity were obtained when the cell was operated at  $-78^{\circ}\text{C}$ , the dewar was filled with dry ice and acetone before the voltage was applied. A small, front-surfaced spherical mirror was used to focus the light coming from the exit slit of the monochromator onto the sensitive area of the photocell. The apparatus was carefully shielded to prevent extraneous light from entering the photocell.

#### (d) Signal Amplification

Light striking the entrance slit of the monochromator was chopped at 165 c.p.s. by a rotating toothed wheel so that the output of all the detectors could be amplified as an A.C. signal. A lock-in amplifier constructed by Electronics, Missiles and Communications Incorporated amplified the output from the photomultipliers and the signal was displayed on a Leeds and Northrup Speedomax G recorder. One of the problems associated with absolute emission studies is that radiation of widely varying intensities must be compared. For example, the  $\text{O} + \text{NO}$  afterglow, by which the detectors were calibrated, was much more intense than the emission from the recombination of halogen

atoms. However, the use of the precision step attenuators on the amplifier greatly simplified this procedure and made the use of "neutral density" filters unnecessary.

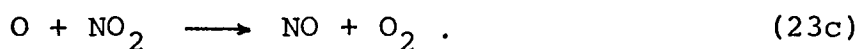
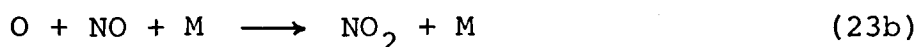
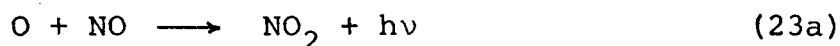
Although a gain of  $1.2 \times 10^4$  was obtainable from the lock-in amplifier, the weak output from the lead sulfide detector necessitated the use of a pre-amplifier. A low noise Princeton Applied Research (model CR-4) amplifier having an internal power supply, (a rechargeable nickel-cadmium battery pack) was used in this application. The small physical size of this unit permitted its placement close to the photocell so that short leads could be used. The output of this pre-amplifier was fed into the lock-in amplifier.

In some experiments, the simultaneous use of two detector systems was necessary. For this purpose a second phototube, chopper, and frequency sensitive amplifier were used. This amplifier was sensitive to a frequency of 27.5 Hz and had an overall gain of  $10^4$ .

(e) Calibration of Detectors for Absolute  
Emission Intensities

Because gas phase chemiluminescent reactions are diffuse sources of light, their characterization with respect to absolute quantum yields is difficult. In these systems, the normal calibration procedures

applicable to point sources of light cannot be used. Recently, however, Fontijn, Meyer and Schiff (9) have studied the rate of light emission from the reaction of oxygen atoms with NO and have suggested its use as a standard. The kinetics of the overall reaction have been investigated by Kaufman (8) and can be represented by



Since reaction (23c) is very much faster than (23a) or (23b) the NO concentration remains essentially constant during the course of the reaction. The process may then be considered simply as a nitric oxide catalyzed recombination of oxygen atoms. The light intensity is proportional to the product  $[\text{O}][\text{NO}]$  and is independent of the total pressure at pressures above 0.1 torr. The procedure used in finding the rate constant of emission of a reaction is simply to observe the intensity of the O + NO glow in the same reaction tube and under the same conditions (ie. spectrometer slitwidth, etc.) as the unknown glow. The use of this procedure makes it unnecessary to know the true spectral distribution of the unknown emission and since both the O + NO glow and the unknown glow

emit in the same volume, all geometric factors cancel out.

Let us suppose that the afterglow under study radiates according to the rate equation  $I = k_o [B]^n$ . The intensity of this emission in a wavelength interval  $\Delta\lambda$  centred at a wavelength  $\lambda$ , is

$$I_o(\lambda_1) = \frac{F_o(\lambda_1)\Delta\lambda_1 k_o [B]^n V}{L_o} = K(\lambda_1) A_o i_o(\lambda_1) \quad (24)$$

In this equation  $F_o(\lambda_1)$  is the spectral flux density (photons/cc/sec/Å) and  $L_o$  is the total intensity in comparable units, ie.

$$L_o = \int_0^{\lambda_{\max}} F_o(\lambda) d\lambda \quad (25)$$

$V$  is the volume of the radiating gas,  $k_o$  is the total light production rate constant for the unknown glow and  $[B]$  is the measured concentration of the emitting species. The constant  $K(\lambda)$  contains all the geometrical factors, the transmission of the observation tube window and the monochromator and the phototube sensitivity. Since the monochromator is a prism instrument, the constant  $K(\lambda)$  would also account for the variation in spectral slit width,  $\Delta\lambda$ , with wavelength. Finally,  $i_o(\lambda_1)$  is the photomultiplier current produced by  $I_o(\lambda_1)$  and  $A_o$  is the amplifier attenuation, the latter

being the only parameter varied in the detector system between observation of the O + NO "continuum" and the unknown afterglow.

A similar equation to (24) can be written for the intensity of the NO<sub>2</sub> "continuum" in the same wavelength interval  $\Delta\lambda$  centred at  $\lambda_1$ :

$$I_s(\lambda_1) = \frac{F_s(\lambda_1)\Delta\lambda_1 k_s [O][NO]V}{L_s} = K(\lambda_1)A_s i_s(\lambda_1) \quad (26)$$

where the symbols all have their former meaning, the subscript s denoting the parameters of the "standard" reaction. Dividing equation (1) by (3) we get

$$\frac{F_o(\lambda_1)k_o}{L_o} = \frac{A_o i_o(\lambda_1)F_s(\lambda_1)k_s [O][NO]}{[B]^n A_s i_s(\lambda_1) L_s} \quad (27)$$

Integrating over all wavelengths between  $\lambda_{\min}$  and  $\lambda_{\max}$ , between which all of the intensity of the unknown emission lies, we obtain the following equation for the total light producing rate constant

$$k_o = \frac{k_s [O][NO]A_o}{[B]^n A_s} \frac{\int_{\lambda_{\min}}^{\lambda_{\max}} F_s(\lambda) \frac{i_o(\lambda)}{i_s(\lambda)} d\lambda}{\int_{\lambda_{\min}}^{\lambda_{\max}} F_s(\lambda) d\lambda} \quad (28)$$

In equation (28)  $k_s$  and  $F_s$  can be found using the data of Fontijn, Meyer and Schiff (9) and all the other values can be found experimentally.

If, for example, a monochromator trace is obtained for an unknown emission, the curve is first corrected by taking intensity readings at a number of wavelengths and multiplying each of these by  $F_s(\lambda)/i_s(\lambda)$ . The curve is then re-plotted and the integral in the numerator of equation (28) is evaluated by finding the area under this curve. This was done originally by a procedure of cutting and weighing, or by the use of a planimeter. However the whole calculation was eventually carried out numerically on the IBM 7044 computer.

In order to ensure that the reaction tube did not change position relative to the spectrometer slit between calibrations, it was clamped so that if its removal was necessary, it could be relocated in its original position.

Before using the O + NO calibration procedure, the only change made to the system was to remove the detector coil since the products of this reaction quickly contaminated the metal surface of the detector. Also, a small coil of silver wire was placed downstream from the reaction tube to destroy the oxygen atoms in the gas stream and thereby prevent ozone from collecting in the liquid nitrogen cold traps.

The O + NO glow was observed at a total system pressure of 1 torr and at an oxygen flowrate of between 50 and 100  $\mu$  moles/sec. The gas flows were allowed to

equilibrate for an hour before the spectrum was scanned. After scanning the spectrum the NO flow was cut off and the NO<sub>2</sub> titration for oxygen atoms was quickly performed. This procedure was repeated three or four times and an average of the results was taken.

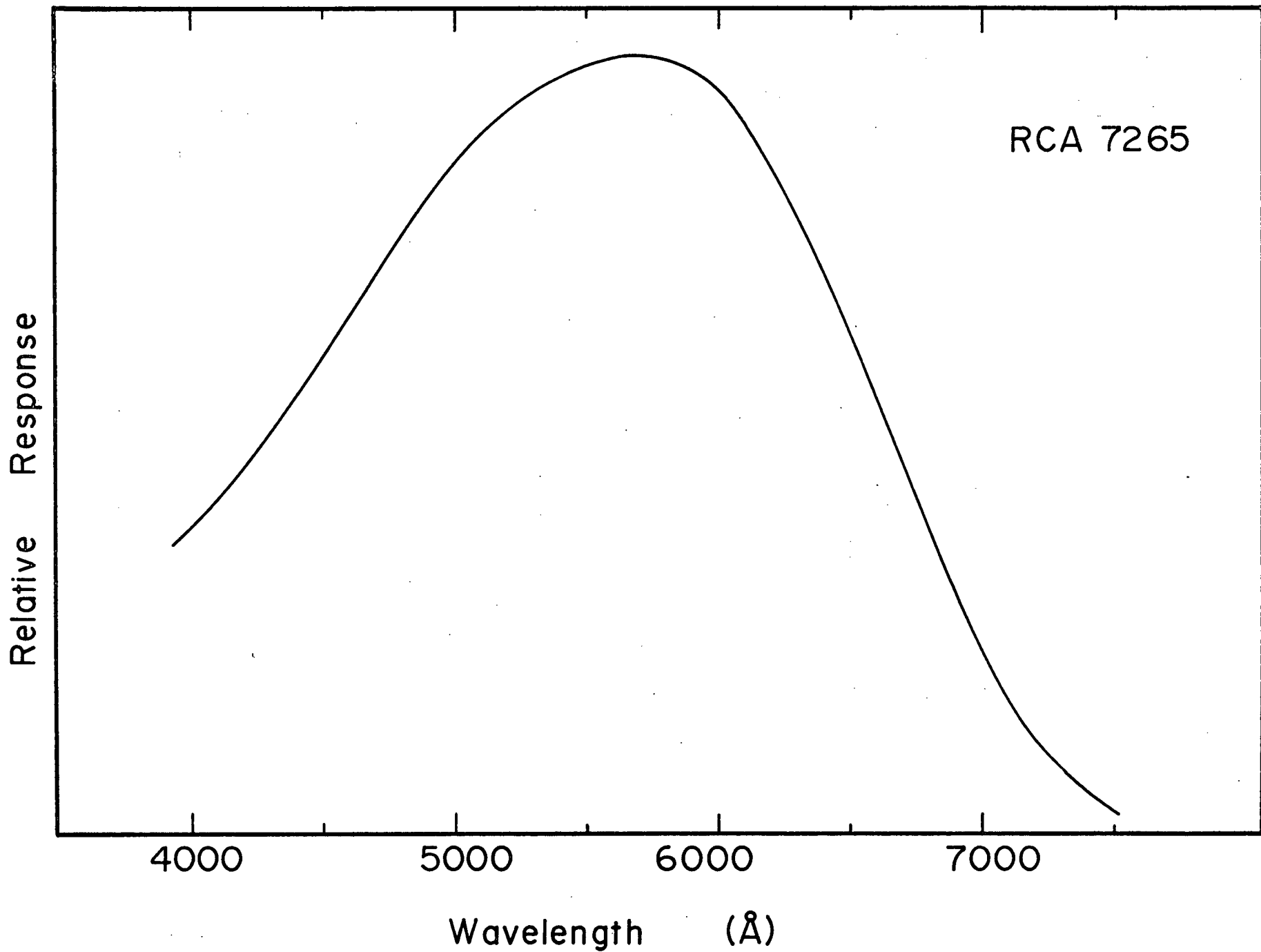
Although the use of this calibration procedure made the determination of the spectral sensitivity of the monochromator-photomultiplier combination unnecessary over the region covered by the NO<sub>2</sub> "continuum", this function had to be known for emissions beyond 1.4 $\mu$ . The use of this function then permitted the calculation of the true spectral distribution of such emissions. A lamp of standard spectral irradiance operated from a constant current power supply (the unit was obtained from Electro Optics Associates) was used for this purpose. The lamp was calibrated against a black-body radiation source and covered the region from 0.25 to 2.5 $\mu$  .

(f) Experimental Determination of the Transmission of the Optical System and Detector Sensitivity

In order to compare the spectral response of the detectors used in this investigation, relative spectral sensitivity curves were found for each detector. These curves represent not only the response of each detector, but also the transmission of the entire optical system including the monochromator and all optical windows

used in the course of a normal experiment. They were obtained using the lamp of standard spectral irradiance, described in the previous section, in conjunction with a number of neutral density filters which were needed to reduce the high intensity of the 100 watt quartz-iodine lamp. Figure (7) was obtained using the RCA 7265 photomultiplier at room temperature operated at 1750 volts and using a monochromator slitwidth of  $200\mu$ . Figure (8) shows the relative spectral sensitivity of the RCA 7102 phototube cooled to liquid nitrogen temperature and operated at 1250 volts. The spectral response of the pbs cell (cooled to  $-78^{\circ}\text{C}$ ) is shown in figure 9.

Figure 7. Relative response of the RCA 7265  
photomultiplier and monochromator  
(slitwidth 0.2 mm).



RCA 7265

Relative Response

4000

5000

6000

7000

Wavelength (Å)

Figure 8. Relative response of the RCA 7102  
photomultiplier and monochromator  
(slitwidth 0.1 mm).

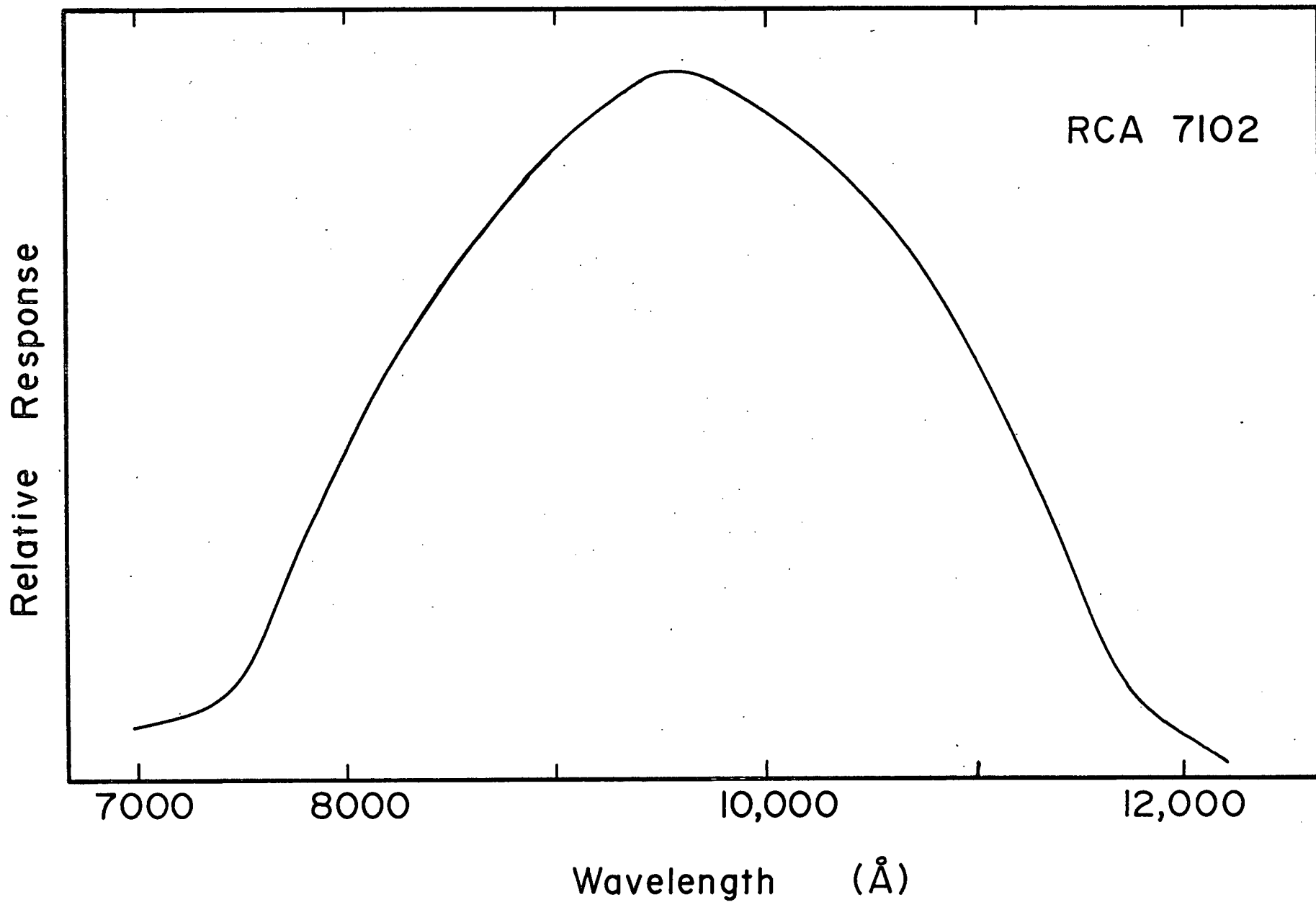
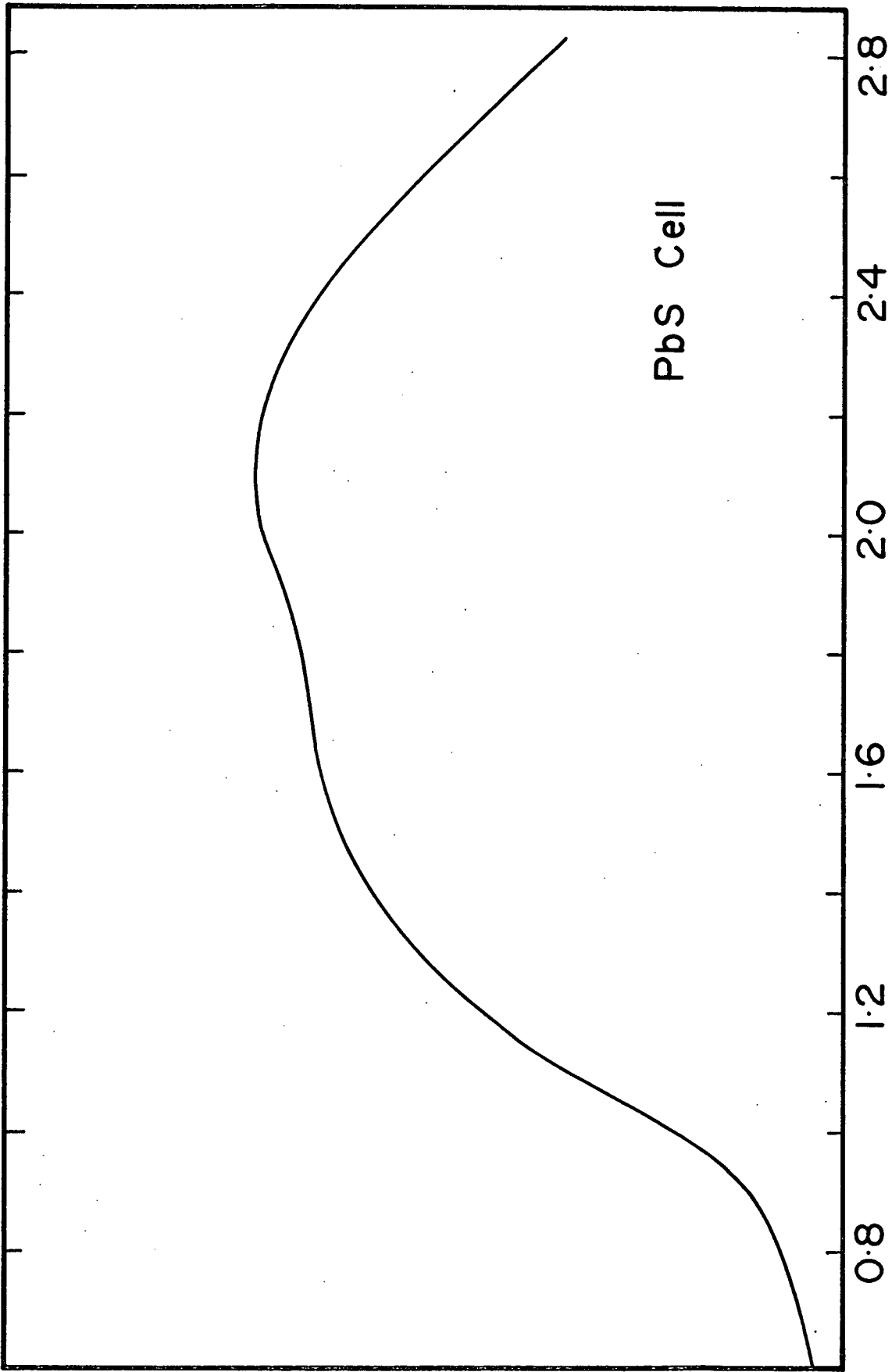


Figure 9. Relative response of PbS detector  
and monochromator (slitwidth 0.15 mm).



Relative Response

PbS Cell

Wavelength (microns)

## RESULTS

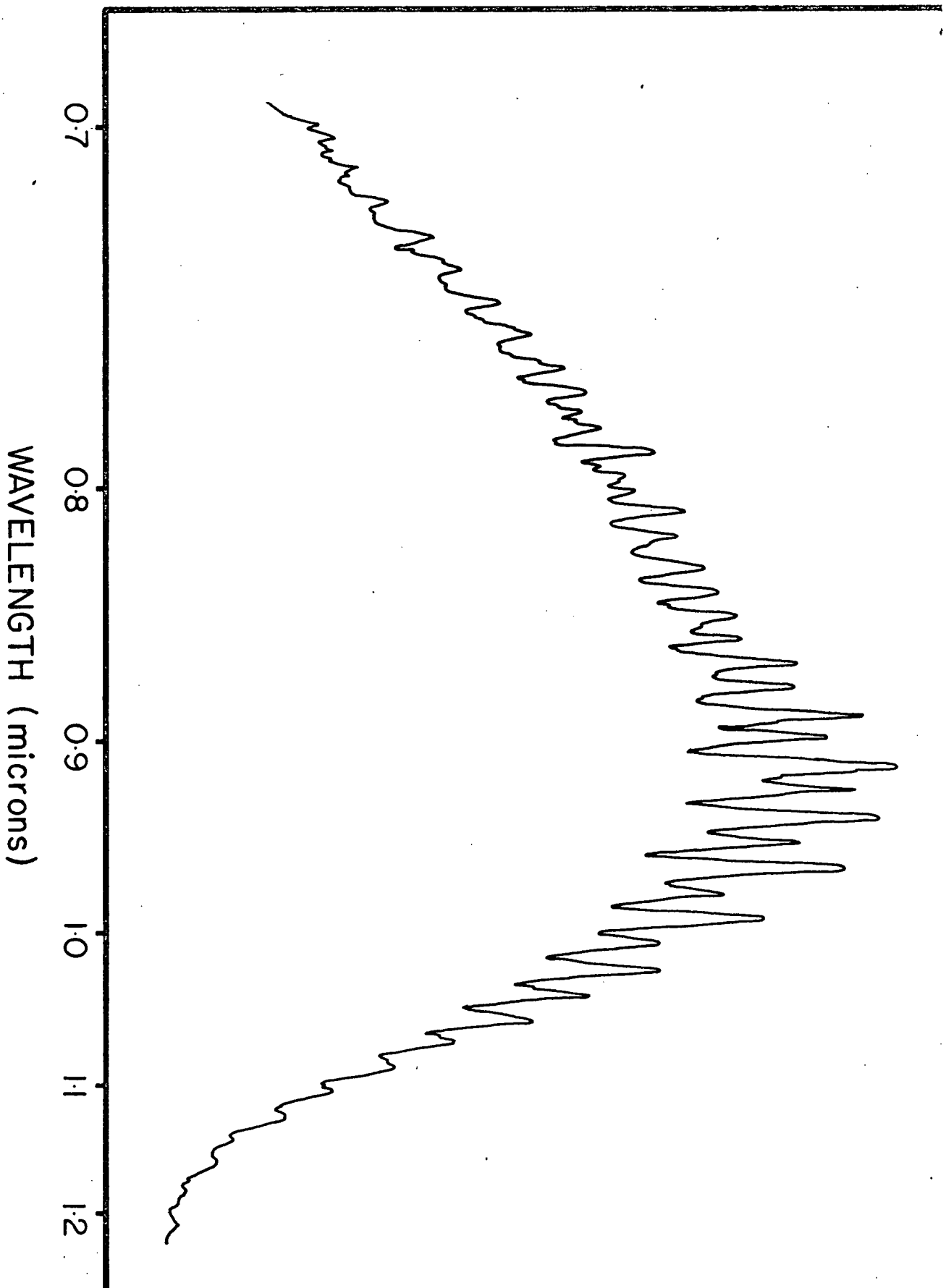
### The Bromine Afterglow Spectrum

When a discharge is initiated in gaseous bromine, a faint red glow visible to the eye is produced. The spectrum of this emission was recorded using the Hilger-Watts monochromator and the RCA 7102 photomultiplier cooled to liquid nitrogen temperature. The high rate of bromine atom recombination, resulting in a rapid decay of the afterglow down the length of the reaction tube, limited the pressure range over which the emission could be studied. At pressures above 2 torr, the intensity of the emission was insufficient to allow detection at reasonable slit widths. A typical recorder trace of the bromine spectrum measured at a pressure of 0.8 torr is shown in figure 10.

Variation of the conditions of pressure and atom concentration under which the spectrum was recorded had a marked effect on the appearance of the bands. Not only was the relative intensity of each band found to be a function of pressure, but in some cases the position of the band appeared to shift. This latter effect was most noticeable in the infrared region of

Figure 10. Recorder trace of the bromine after-glow spectrum.

INTENSITY



the spectrum where the lower dispersion of the monochromator could cause extensive overlapping of the bands. Thus, before any assignment of these bands was attempted, a high resolution spectrum of the bromine afterglow was examined.

This bromine afterglow spectrum was photographed with a Czerny-Turner f/6.3 plane-grating spectrograph blazed at  $7500\text{\AA}$  on Kodak 1-N plates so that the region between  $7200\text{\AA}$  and  $8400\text{\AA}$  was recorded. The spectrum was observed to be quite complex, consisting of a large number of red degraded bands and exhibiting extensive overlap in some regions. The recorded band heads are listed in Table 2 together with the proposed assignments. The values of  $\nu_{\text{calc.}}$  were calculated using the spectroscopic constants of the  ${}^3\Pi_{1u}$  state given by Darbyshire (44) and Horsley (45) and for the  ${}^3\Pi_{0+u}$  state, calculations were based on the constants given by Horsley and Barrow (46). The bands have been assigned to the  ${}^3\Pi_{1u} \rightarrow {}^1\Sigma_g^+$  and  ${}^3\Pi_{0+u} \rightarrow {}^1\Sigma_g^+$  transitions of molecular bromine. The emission from the  ${}^3\Pi_{1u}$  state was observed to originate in vibrational levels higher than  $v' = 5$  while assignments corresponding to  $v' = 1$  and 2 have been made for the  ${}^3\Pi_{0+u}$  (figure 11).

The band positions measured on the spectrophotometer traces are given in Table 3 together with their tentative

TABLE 2

MEASUREMENT OF THE BAND HEADS OF THE Br<sub>2</sub> AFTERGLOW

IN THE REGION 7000 - 8300Å

$\nu_{\text{vac.}}$ (cm <sup>-1</sup> )	Relative Intensity	${}^3\Pi_{1u} \rightarrow {}^1\Sigma_g^+$			${}^3\Pi_{0+u} \rightarrow {}^1\Sigma_g^+$		
		$\nu'$	$\nu''$	$\nu_{\text{calc.}}$ (cm <sup>-1</sup> )	$\nu'$	$\nu''$	$\nu_{\text{calc.}}$ (cm <sup>-1</sup> )
11689.5	S	5	9	11671.2			
11702.1	M				1	14	11704.9
11716.6	M	11	11	11715.9			
11734.0	M	8	10	11727.5			
11798.8	M	6	9	11798.7			
11835.0	W	9	10	11831.0			
		4	8	11839.2			
11984.4	S	5	8	11975.1			
11991.3	S				1	13	11997.9
12004.3	M	11	10	12015			
		(3	7)	(12000.8)			
12032.1	W	8	9	12029.2			
12046.0	W						
12104.6	S	6	8	12102.5			
12143.2	W	(9	9)	12132.7			
		4	7	12145.2			
(12172.6)	W	(13	10)	12171.2			
12227.8	W	7	8	12221.8			
		10	9	12228.6			
		14	10	12238.8			

TABLE 2 Continued

$\nu_{\text{vac.}}$ ( $\text{cm}^{-1}$ )	Relative Intensity	${}^3\Pi_{1u} \rightarrow {}^1\Sigma_g^+$			${}^3\Pi_{0^+u} \rightarrow {}^1\Sigma_g^+$		
		$\nu'$	$\nu''$	$\nu_{\text{calc.}}$ ( $\text{cm}^{-1}$ )	$\nu'$	$\nu''$	$\nu_{\text{calc.}}$ ( $\text{cm}^{-1}$ )
12277.9	S	(5	7)	(12289.3)			
12297.9	S				1	12	12293.2
12336.0	M	8	8	12333.1			
12417.6	S	6	7	12408.6			
12437.7	S	9	8	12436.6			
12488.6	M	(13	9)	12472.9			
12533.7	S	7	7	12527.8			
		10	8	12532.5			
12543.9	W	14	9	12540.5			
12575.7	S						
12595.6	S	5	6	12589.3	1	11	12590.5
12638.8	M	8	7	12639.1			
12717.7	S	6	6	12716.8			
12736.3	S	9	7	12742.6			
12774.6	W	13	8	12776.8			
12841.0	S	7	6	12836.0			
		10	7	12838.5			
12848.2	W	14	8	12844.4			
12895.0	M	5	5	12899.7	1	10	12890.1
12926.5	W	11	7	12927.0			
12948.6	M	8	6	12947.3			

TABLE 2 Continued

$\nu_{\text{vac.}}$ ( $\text{cm}^{-1}$ )	Relative Intensity	${}^3\Pi_{1u} \rightarrow {}^1\Sigma_g^+$			${}^3\Pi_{0+u} \rightarrow {}^1\Sigma_g^+$		
		$\nu'$	$\nu''$	$\nu_{\text{calc.}}$ ( $\text{cm}^{-1}$ )	$\nu'$	$\nu''$	$\nu_{\text{calc.}}$ ( $\text{cm}^{-1}$ )
13019.9	W	(12	7)	(13008.4)			
13035.6	S	6	5	13027.1			
13051.7	S	9	6	13050.8	2	10	13051.0
13149.0	S	7	5	13146.4			
		10	6	13146.7			
		14	7	13150.4			
13192.1	M				1	9	13191.8
13240.3	W	11	6	13235.2			
		5	4	13212.2			
13259.7	W	8	5	13257.7			
13318.2	M	12	6	13316.6			
13337.9	M	6	4	13339.6			
13359.5	M	9	5	13361.2	2	9	13352.7
13392.2	W	13	6	13391.0			
13461.1	S	7	4	13458.9			
		10	5	13457.1			
		14	6	13458.6			
13502.4	M				1	8	13495.7
13544.0	W	11	5	13545.6			
13572.6	M	8	4	13570.2			
13626.0	S	12	5	13627.0			

TABLE 2 Continued

$\nu_{\text{vac.}}$ ( $\text{cm}^{-1}$ )	Relative Intensity	${}^3\Pi_{1u} \rightarrow {}^1\Sigma_g^+$			${}^3\Pi_{0+u} \rightarrow {}^1\Sigma_g^+$		
		$\nu'$	$\nu''$	$\nu_{\text{calc.}}$ ( $\text{cm}^{-1}$ )	$\nu'$	$\nu''$	$\nu_{\text{calc.}}$ ( $\text{cm}^{-1}$ )
13700.7	W	13	5	13701.3			
13768.9	S	7	3	13773.6			
		10	4	13769.6			
		14	5	13769.0			

Figure 11. Assignments to the  ${}^3\Pi_{0^+u} \rightarrow {}^1\Sigma_g^+$  transition in the spectrum of discharged bromine. Full line 0.7 torr, broken line 1.5 torr.

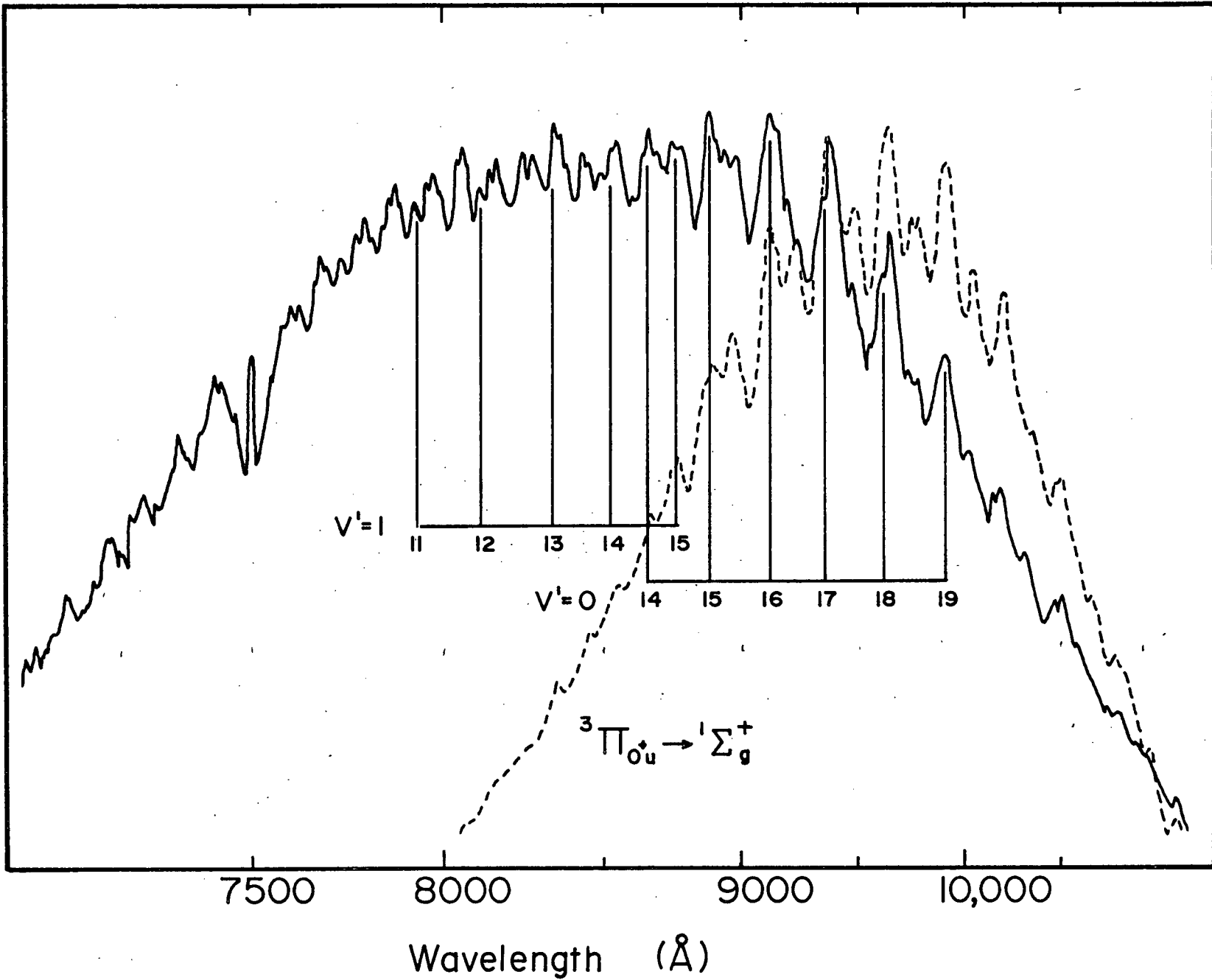


TABLE 3  
 BANDS IN THE Br<sub>2</sub> AFTERGLOW SPECTRUM  
 RECORDED BY HILGER MONOCHROMATOR

$\nu_{\text{vac.}}$ (cm <sup>-1</sup> )	${}^3\Pi_{1u} \rightarrow {}^1\Sigma_g^+$			${}^3\Pi_{0+u} \rightarrow {}^1\Sigma_g^+$		
	$\nu'$	$\nu''$	$\nu_{\text{calc.}}$ (cm <sup>-1</sup> )	$\nu'$	$\nu''$	$\nu_{\text{calc.}}$ (cm <sup>-1</sup> )
14604	(18	3)	(14603)			
14417				1	5	14420
14286	(18	5)	(14288)	2	6	14271
14120				1	6	14110
13985	9	3	13988			
13962				2	7	13962
13876	8	3	13885			
13807				1	7	13802
13648				2	8	13657
13629	12	5	13627			
	7	4	13459			
13447	10	5	13457			
	14	6	13459			
13350				2	9	13352
13492				1	8	13496
13186				1	9	13192
	7	5	13146			
13134	10	6	13146			
	14	7	13150			

TABLE 3 Continued

$\nu_{\text{vac.}}$ ( $\text{cm}^{-1}$ )	${}^3\Pi_{1u} \longrightarrow {}^1\Sigma_g^+$			${}^3\Pi_{0^+u} \longrightarrow {}^1\Sigma_g^+$		
	$\nu'$	$\nu''$	$\nu_{\text{calc.}}$ ( $\text{cm}^{-1}$ )	$\nu'$	$\nu''$	$\nu_{\text{calc.}}$ ( $\text{cm}^{-1}$ )
13038	6	5	13027	2	10	13051
12948	8	6	12947			
12881	(5	5)	(12899)	1	10	12890
12839	7	6	12836			
	10	7	12839			
12742	9	7	12743			
12709	6	6	12717			
12596	5	6	(12589)* (12607)†	1	11	12591
12526	7	7	12528			
12418	6	7	12409			
12304				1	12	12293
12279	5	7	(12281)* (12298)†			
12229	7	8	12222			
12131	9	9	12133			
12079	6	8	(12103)* (12071)†			
11971	5	8	11975			
11839	9	10	11831			
	4	8	(11839)*			

TABLE 3 Continued

$\nu_{\text{vac.}}$ ( $\text{cm}^{-1}$ )	${}^3\Pi_{1u} \rightarrow {}^1\Sigma_g^+$			${}^3\Pi_{0^+u} \rightarrow {}^1\Sigma_g^+$		
	$\nu'$	$\nu''$	$\nu_{\text{calc.}}$ ( $\text{cm}^{-1}$ )	$\nu'$	$\nu''$	$\nu_{\text{calc.}}$ ( $\text{cm}^{-1}$ )
11756	1	7	(11762)†			
11710				1	14	11705
11673	5	9	(11671)*			
11599	2	8	(11598)†			
11540				0	14	11541
11416				1	15	11414
11370	5	10	(11370)* (11387)†			
11248	(4	10)	(11261)†	0	15	11250
11153	1	9	(11152)†			
11098	5	11	(11088)†			
10950	4	11	(10962)†	0	16	10961
10859	1	10	(10851)†			
10673				0	17	10674
10648	2	11	(10636)*			
	4	12	(10664)†			
10528	3	12	(10532)†			
10389	(4	13)	(10369)†	0	18	10389
10230	3	13	(10238)†			
	1	12	(10254)†			

TABLE 3 Continued

$\nu_{\text{vac.}}$ ( $\text{cm}^{-1}$ )	${}^3\Pi_{lu} \rightarrow {}^1\Sigma_g^+$			${}^3\Pi_{o+u} \rightarrow {}^1\Sigma_g^+$		
	$\nu'$	$\nu''$	$\nu_{\text{calc.}}$ ( $\text{cm}^{-1}$ )	$\nu'$	$\nu''$	$\nu_{\text{calc.}}$ ( $\text{cm}^{-1}$ )
10080	(4	14)	(10076)†	0	19	10107
9827	0	13	(9811)†	0	20	9827
9782						
9678						
9531	0	14	9518	0	21	9549
9483						
9231	0	15	(9227)†			
9065	1	16	(9035)†			
8940	0	16	(8938)†			

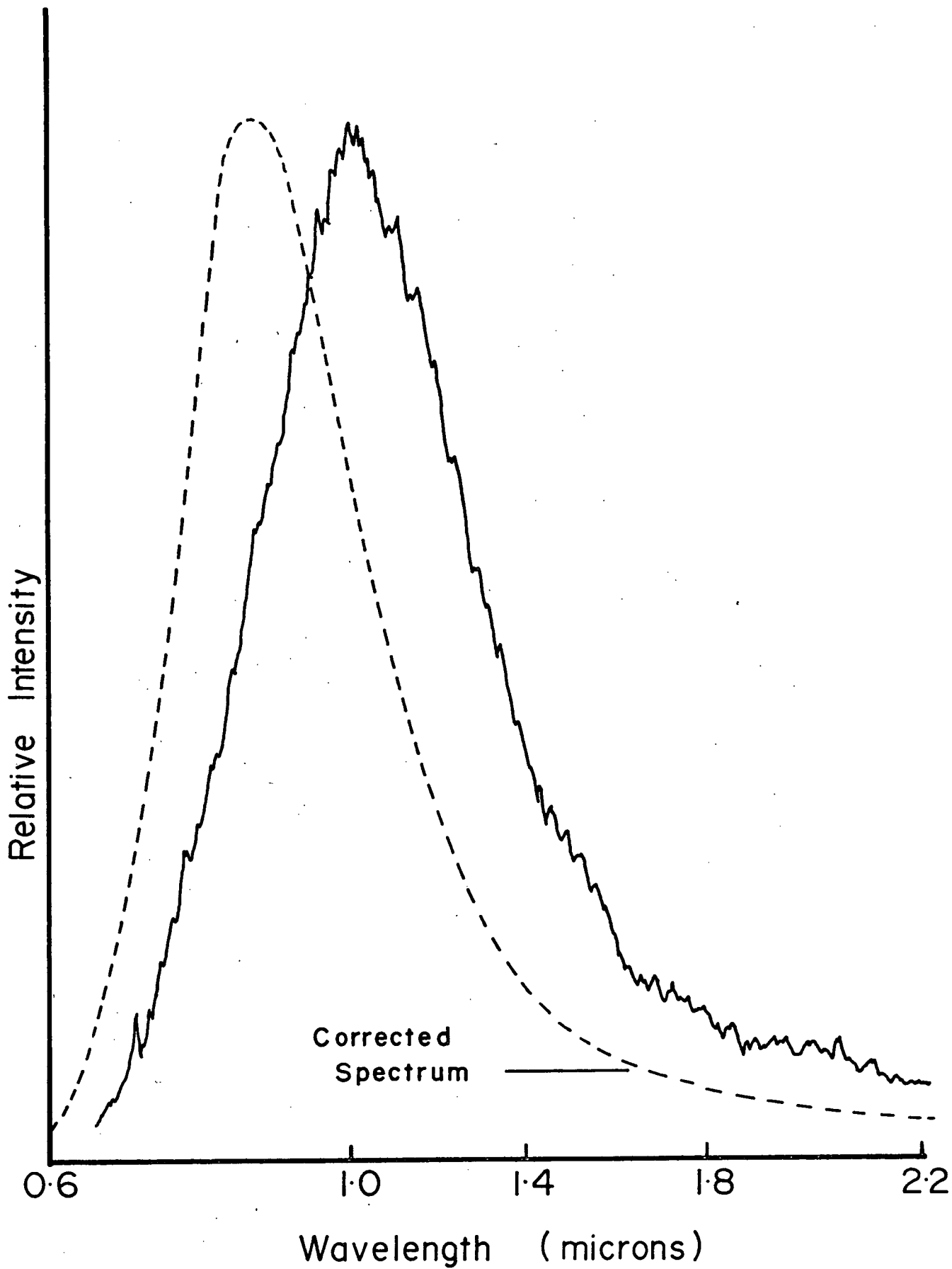
i

\*  $\nu$  calculated from references 44 and 45.†  $\nu$  calculated from reference 48.

assignments. In the region between 11,500 and 14,000  $\text{cm}^{-1}$  the measured bands show good agreement with the strong (s) bands which appear on the photographic plate and band assignments in this region were made by comparing the two spectra. In the more interesting spectral region around 10,000  $\text{cm}^{-1}$ , a number of intense and well separated peaks are observed but the origin of these bands was more difficult to determine for two reasons. First of all, the linear dispersion of the monochromator is quite low in this region so that measurement of band positions is less accurate than in the higher energy region. Secondly, since absorption has never been observed into levels below  $v' = 6$  in the  ${}^3\Pi_{1u}$  state (44, 47), the spectroscopic constants given by Darbyshire (44) may not be valid for the lowest vibrational levels. For those assignments which are in question, the band positions calculated from the revised constants given by Clyne and Coxon (48) are also shown in Table 3.

To find the wavelength range over which the emission extended, the RCA 7265 photomultiplier and the Infracron PbS detector were used to find the high and low energy limits respectively. The bromine afterglow intensity was below the limits of the detectors at wavelengths less than 6000 $\overset{\circ}{\text{A}}$  and greater than 19000 $\overset{\circ}{\text{A}}$ . The spectral distribution, obtained using the lead sulfide cell, is shown in figure 12.

Figure 12. Spectral distribution of the bromine  
afterglow spectrum obtained by PbS  
detector.



The spectral distribution of the bromine afterglow was found to be dependent upon atom concentration and total pressure. Under conditions of low pressure and high atom concentration the maximum intensity appeared at  $7700\text{\AA}$  as shown in figure 13(a). At pressures above 0.5 torr the maximum intensity appeared at  $9400\text{\AA}$  (figure 13(b)). This spectrum was recorded at a total pressure of 1 torr using argon as a diluent and was unusual in that very little emission below  $8000\text{\AA}$  was observed. These last two spectra represent the true spectral distribution of the bromine afterglow and were obtained by correcting the original spectra for transmission of the optical system and sensitivity of the photomultiplier. The spectra were then reconstructed point by point on a scale linear in wavelength.

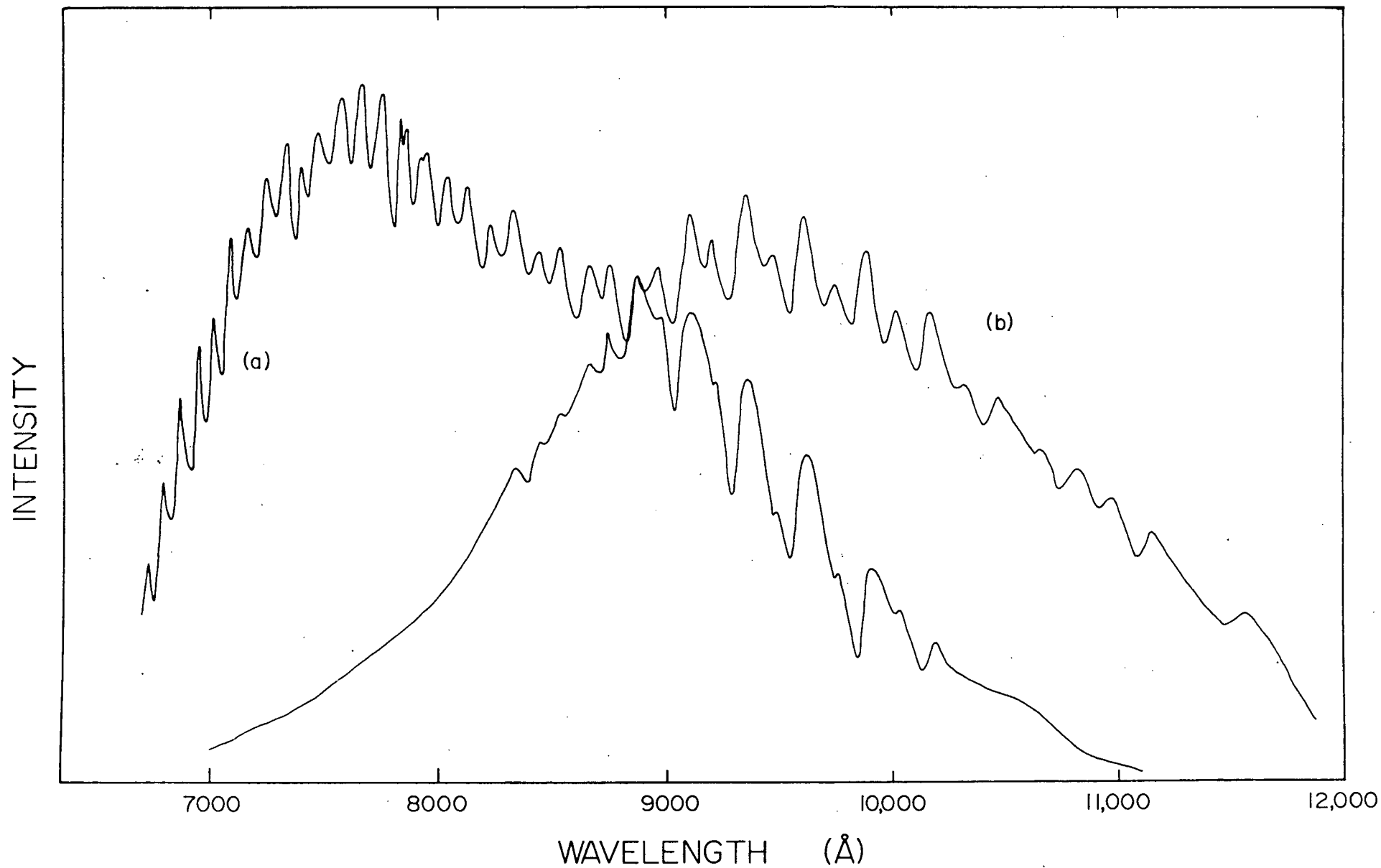
#### Kinetics Of The Bromine Afterglow

Before measuring the rate constants for the total emission, a more quantitative study of the variation of spectral distribution with atom concentration and pressure was undertaken. To do this, the intensities in narrow bands centred at a number of wavelengths across the afterglow spectrum were observed as a function of  $[\text{Br}]$  and  $[\text{Br}_2]$ . At the same time, the dependence

Figure 13. True spectral distribution of the  
bromine afterglow spectrum.

Curve (a): pressure = 0.25 torr

Curve (b): pressure = 1 torr



of the integrated emission intensity on atom concentration and pressure was investigated.

(a) Dependence Of Emission Intensity On [Br]

At a fixed total pressure, the intensity in a small wavelength interval,  $I_\lambda$ , was measured at various atom concentrations. These measurements were repeated at a number of pressures between 0.5 and 2 torr. The results obtained for bands centred at  $7200\text{\AA}$ ,  $8400\text{\AA}$  and  $10400\text{\AA}$  are listed in Table 4. The region of the spectrum covered by each of these bands is:  $7165\text{\AA} < \lambda < 7235\text{\AA}$  for the  $7200\text{\AA}$  band,  $8335\text{\AA} < \lambda < 8465\text{\AA}$  for the band centred at  $8400\text{\AA}$ , and  $10395\text{\AA} < \lambda < 10505\text{\AA}$  for the  $10400\text{\AA}$  band.

If the dependence of  $I_\lambda$  on [Br] is assumed to be of the form  $I_\lambda \propto [\text{Br}]^n$ , then a plot of  $\log I_\lambda$  against  $\log [\text{Br}]$  (figures 14(a) and 15(a)) will yield a value of the parameter  $n$ . When this was done, it was found that  $1.2 \leq n \leq 2$ , and only at the high energy end of the spectrum did  $n$  approach a value of 2 (Table 5).

The integrated emission intensities ( $\int I_\lambda d\lambda$ ) between  $6800\text{\AA}$  and  $12000\text{\AA}$  were obtained by scanning the emission spectrum using large monochromator slitwidths to obtain structureless spectra. These spectra were then corrected to obtain the true spectral distributions and the areas under these curves were measured. The dependence of the integrated intensity on atom concentration is shown in Table 4. Plots of  $\log (\int I_\lambda d\lambda)$  against [Br] (figures 14(b),

TABLE 4  
 THE DEPENDENCE OF  $I_\lambda$  UPON [Br].  
 INTENSITY IN ARBITRARY UNITS

Pressure (torr)	[Br] x $10^9$ (m/cc)	$I_{7200}$	$I_{8400}$	$I_{10400}$	$\int_{6000\text{\AA}}^{12000\text{\AA}} I_\lambda d\lambda$
0.53	0.079	1.0	9.0	18.0	70.7
"	0.32	7.0	45.0	96.0	312
"	0.55	16.0	114	210	709
0.92	0.45	4.80	43.2	91.2	288
"	0.68	13.7	93.8	186	608
"	0.99	22.0	176	346	1120
"	1.44	50.0	310	540	1900
"	0.15	0.65	7.15	17.6	57.0
"	0.56	7.50	70.0	139	450
"	2.36	70.0	700	1200	4800
1.18	0.67	12.8	104	208	679
"	1.00	28.4	211	384	1300
"	0.58	8.8	61.3	119	413
"	0.80	16.0	128	238	790
"	1.43	50.0	325	550	1920
"	0.150	0.0	9.6	20.0	69.8
1.50	0.41	8.0	34.4	72.0	234
"	0.34	4.0	29.6	56.0	188
"	0.60	10.0	70.0	152	492
"	0.82	15.7	126	246	830

TABLE 4 Continued

Pressure (torr)	[Br] x 10 <sup>9</sup> (m/cc)	I <sub>7200</sub>	I <sub>8400</sub>	I <sub>10400</sub>	$\int_{6000\text{\AA}}^{12000\text{\AA}} I_{\lambda} d\lambda$
1.82	0.064	1.2	9.6	19.2	64.2
"	0.12	2.4	23.2	48.0	157
"	0.18	0.8	13.6	28.8	93.0
"	0.23	2.4	29.6	57.0	189
"	0.31	4.0	43.2	88.0	286
"	0.37	5.6	54.5	117	372
"	0.47	12.5	99.0	182	612

TABLE 5

VALUES OF  $n$  IN THE EXPRESSION  $I_\lambda \propto [\text{Br}]^n$ 

Pressure (torr)	n			
	$I_{7200}$	$I_{8400}$	$I_{10400}$	$\int_{6000\text{\AA}}^{12000\text{\AA}} I_\lambda d\lambda$
0.52	$1.5 \pm 0.2$	$1.2 \pm 0.2$	$1.2 \pm 0.2$	$1.2 \pm 0.2$
0.92	$2.0 \pm 0.1$	$1.6 \pm 0.1$	$1.5 \pm 0.1$	$1.6 \pm 0.1$
1.18	$2.0 \pm 0.1$	$1.6 \pm 0.1$	$1.5 \pm 0.1$	$1.7 \pm 0.1$
1.50	-	$1.8 \pm 0.1$	$1.7 \pm 0.1$	$1.7 \pm 0.1$
1.82	$2.3 \pm 0.2$	$1.8 \pm 0.1$	$1.6 \pm 0.1$	$1.8 \pm 0.1$

Figure 14: Plots of (a)  $\log I_\lambda$  vs.  $\log [\text{Br}]$  and  
(b)  $\log \left( \int I_\lambda d\lambda \right)$  vs.  $\log [\text{Br}]$  for a  
pressure of 0.92 torr. Intensity in  
arbitrary units.

Points in (a) obtained for bands centred  
at the following wavelengths:  $\Delta$  7200 $\overset{\circ}{\text{A}}$ ,  
 $\square$  8400 $\overset{\circ}{\text{A}}$ ,  $\blacksquare$  10400 $\overset{\circ}{\text{A}}$ .

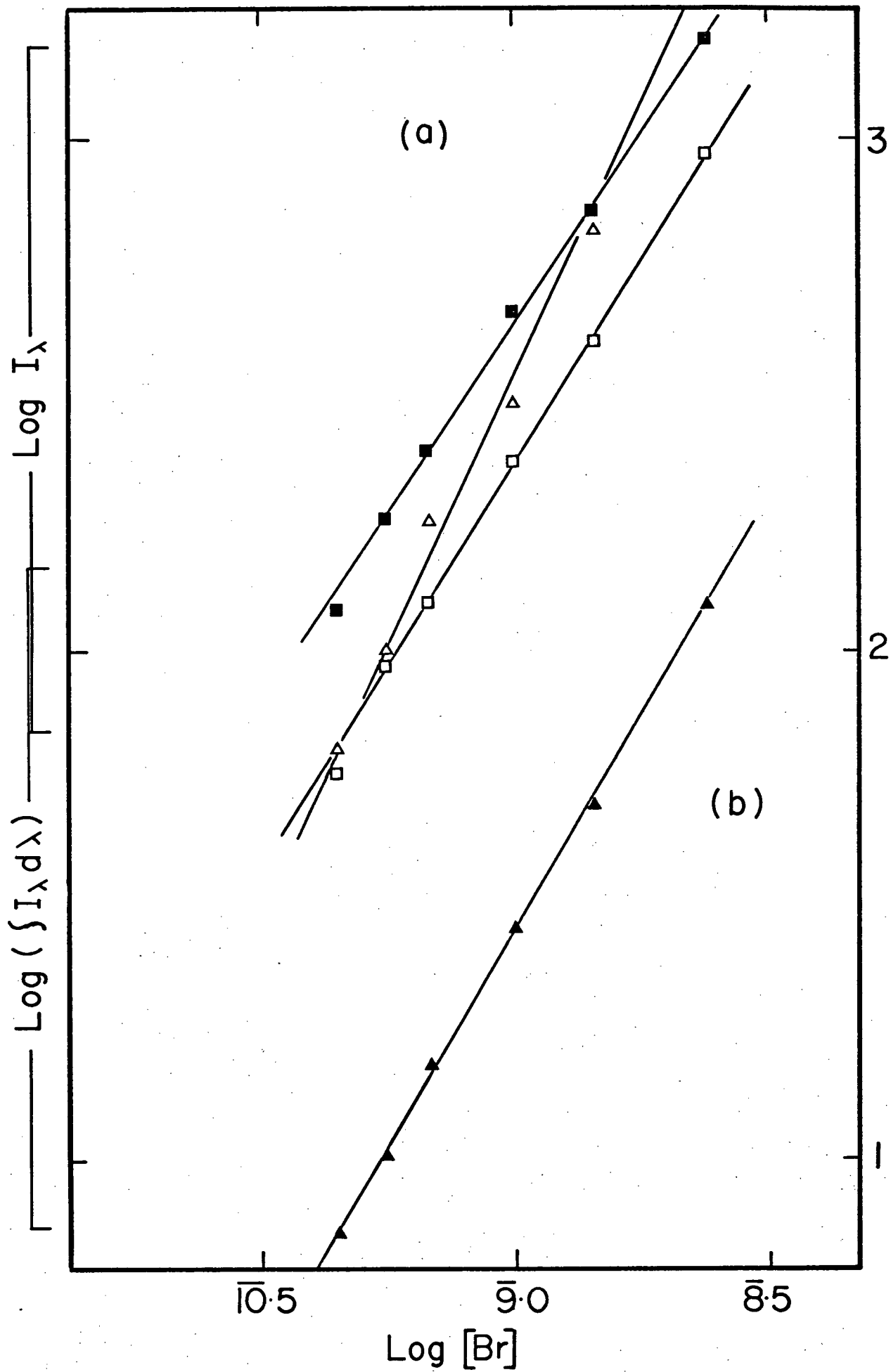
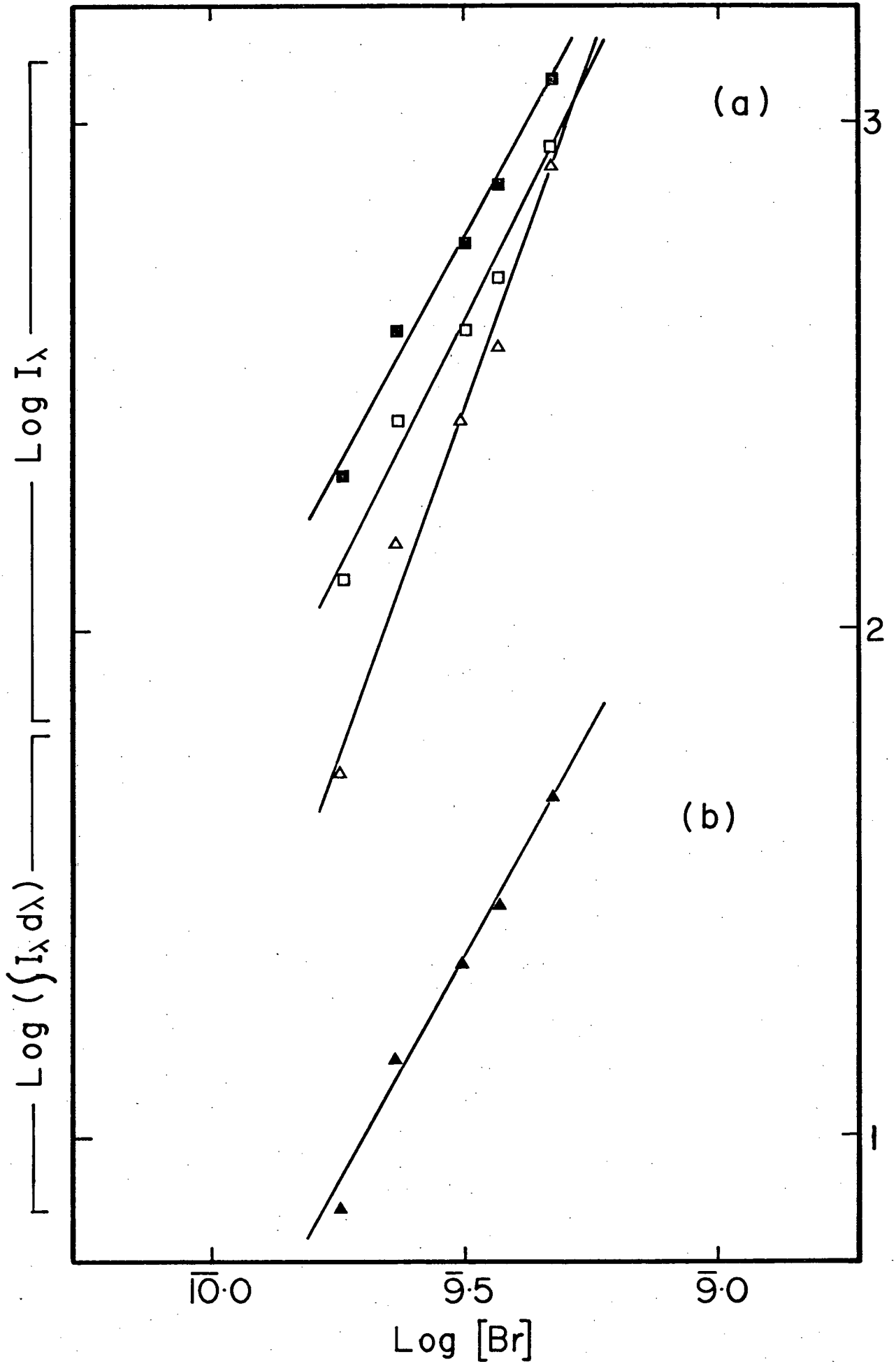


Figure 15. Plots of (a)  $\log I_\lambda$  vs.  $\log [\text{Br}]$  and  
(b)  $\log (\int I_\lambda d\lambda)$  vs.  $\log [\text{Br}]$  for a  
pressure of 1.82 torr. Intensity in  
arbitrary units.

Points in (a) obtained for bands centred  
at the following wavelengths:  $\Delta$  7200 $\overset{\circ}{\text{A}}$ ,  
 $\square$  8400 $\overset{\circ}{\text{A}}$ , and  $\blacksquare$  10400 $\overset{\circ}{\text{A}}$ .



15(b) and Table 5) indicate that the dependence of the integrated intensity upon  $[\text{Br}]$  increases with increasing pressure, but does not show a squared dependence even at the highest pressure studied.

(b) Pressure Dependence Of The Emission Intensity

Since it was not possible to devise an experiment in which the total pressure was varied while the atom concentration remained constant, an attempt was made to obtain the variation of  $I_\lambda$  with  $[\text{Br}_2]$  by interpolation of the  $I_\lambda$  vs.  $[\text{Br}]$  data. However, owing to the large amount of scatter in the results, no positive correlation could be made.

The variation of the integrated intensity with pressure was, however, obtained by interpolation, although the data show considerable scatter. At  $[\text{Br}] = 5.0 \times 10^{-10}$  moles/cc., these results indicate that  $I_\lambda d\lambda \propto [\text{Br}_2]^{0.0 \pm 0.2}$  over the pressure range 0.5 to 1.8 torr. This dependence could not be determined at higher  $[\text{Br}]$  values because of the limited range of atom concentration over which the data overlapped.

(c) Absolute Rate Constant Measurements

If the apparent rate constant for the emission is defined as

$$k_{\text{app}} = I_{\text{total}} / [\text{Br}]^2 [\text{Br}_2], \quad (29)$$

then equation 28 can be rewritten, for the case of the bromine afterglow, to give:

$$k_{\text{app}} = \frac{k_s [\text{O}] [\text{NO}] A_{\text{Br}_2}}{[\text{Br}]^2 [\text{Br}_2] A_s} \frac{\int_{6000\text{\AA}}^{12000\text{\AA}} F_s(\lambda) i_{\text{Br}_2}(\lambda) d\lambda}{\int_{6000\text{\AA}}^{12000\text{\AA}} i_s(\lambda) d\lambda} \frac{\int_{6000\text{\AA}}^{12000\text{\AA}} F_s(\lambda) d\lambda}{\int_{6000\text{\AA}}^{12000\text{\AA}} F_s(\lambda) d\lambda} \quad (30)$$

where all symbols have their former meaning.

For each value of  $[\text{Br}]$  and  $[\text{Br}_2]$  a structureless spectrophotometer trace was obtained, using a slitwidth of 500 microns, for emission from  $6000\text{\AA}$  to  $12000\text{\AA}$ . Values of  $i_{\text{Br}_2}(\lambda)$  were read from these traces at  $200\text{\AA}$  intervals and the integral in the numerator of equation (30) was evaluated numerically. The values of  $k_{\text{app}}$  found in this way are listed in Table 6.

Since a significant contribution to the total emission intensity is made by radiation beyond  $12000\text{\AA}$ , the rate constants calculated above will be lower than those calculated for the total emission. To estimate the fraction of the total emission which appears beyond  $12000\text{\AA}$ , spectra were recorded using the lead sulfide detector, and then corrected to yield the true spectral distribution. However, because of the low intensity levels involved, and since the signal/noise ratio of this detector is far below that of the photomultipliers, spectra at

TABLE 6

VALUES OF  $k_{app}$  FOR EMISSION BETWEEN 6000Å AND 12000Å IN THE BROMINE AFTERGLOW

Pressure torr	Flow of Br <sub>2</sub> μ moles/sec	Flow of Br μ moles/sec	[Br <sub>2</sub> ] × 10 <sup>8</sup> moles/cc	[Br] × 10 <sup>9</sup> moles/cc	$k_{app} \times 10^{-14}$ cm <sup>6</sup> moles <sup>-2</sup> sec <sup>-1</sup>
0.53	17.6	0.048	2.88	0.0785	12.7
"	17.6	0.193	2.86	0.316	3.88
"	17.6	0.335	2.85	0.548	2.94
0.92	18.6	0.168	4.98	0.451	1.01
"	18.6	0.253	4.96	0.680	0.939
"	18.6	0.370	4.95	0.994	0.813
"	18.6	0.534	4.93	1.44	0.667
"	18.6	0.0564	4.99	0.152	1.76
"	18.6	0.208	4.97	0.559	1.03
"	18.6	0.879	4.88	2.36	0.625
1.18	18.6	0.193	6.38	0.665	0.852
"	18.6	0.292	6.36	1.01	0.715
"	18.6	0.168	6.38	0.579	0.684
"	18.6	0.231	6.37	0.796	0.695

TABLE 6 Continued

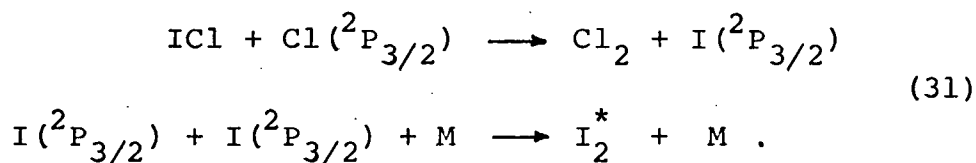
Pressure torr	Flow of Br <sub>2</sub> μ moles/sec	Flow of Br μ moles/sec	[Br <sub>2</sub> ] x 10 <sup>8</sup> moles/cc	[Br] x 10 <sup>9</sup> moles/cc	k <sub>app</sub> x 10 <sup>-14</sup> cm <sup>6</sup> moles <sup>-2</sup> sec <sup>-1</sup>
1.18	18.6	0.416	6.34	1.43	0.524
"	18.6	0.0433	6.40	0.149	1.74
1.50	18.7	0.0937	8.13	0.408	0.612
"	18.7	0.0769	8.13	0.335	0.730
"	18.7	0.138	8.12	0.601	0.596
"	18.7	0.188	8.11	0.819	0.542
1.82	21.5	0.0140	9.88	0.0644	5.56
"	21.5	0.0271	9.88	0.125	3.64
"	21.5	0.0510	9.88	0.235	1.24
"	21.5	0.0692	9.87	0.318	1.02
"	21.5	0.0805	9.87	0.370	0.976
"	21.5	0.1030	9.86	0.474	0.985

low atom concentrations could not be measured. Using high atom concentration, 13% of the emission was observed to lie beyond  $12000\overset{\circ}{\text{A}}$  at 0.28 torr and this value increased to 22% for pressures above 0.5 torr. In view of the fact that emission in the infrared is favoured by low [Br], the rate constants for the total emission are probably in the range of 20 to 30% higher than those listed in Table 6.

#### Emission From Iodine Atom Recombination

Two methods of producing iodine atoms in a flow system were used: direct discharge of iodine and the chemical titration of chlorine atoms with ICl. The emission produced in each case was of low intensity and appeared in the region  $0.8\mu$  to  $2.4\mu$ . The spectra obtained using the PbS detector are shown in figures 16 and 17. The intensity of the emission was lower than that of the other halogen afterglows because high concentrations of iodine were difficult to obtain in the flow system.

The production of excited iodine atoms by the chemical titration procedure occurs via the following steps:



However, in using this method, care had to be taken not

Figure 16. The spectrum of discharged  $I_2$ .

DISCHARGED I<sub>2</sub>

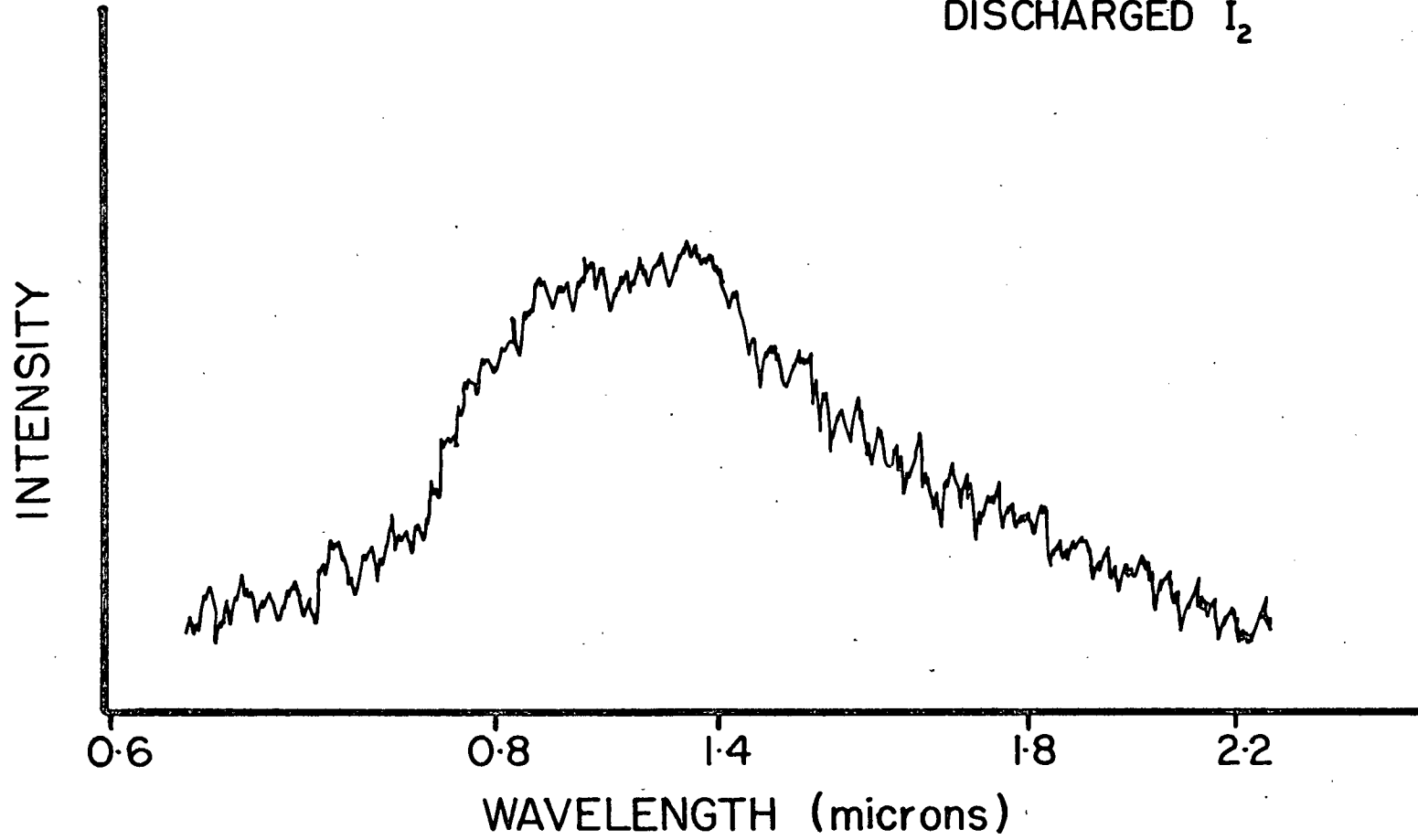
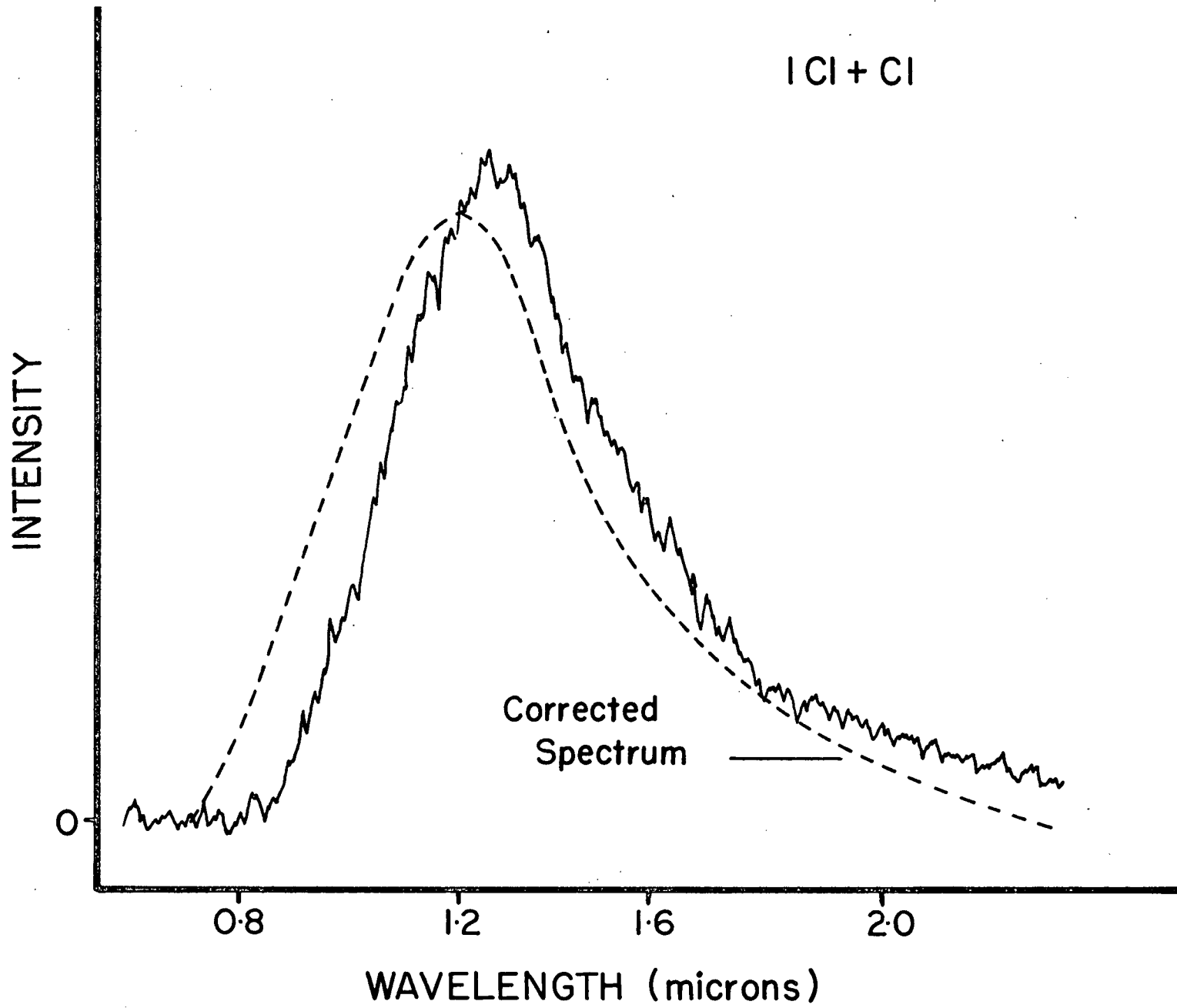
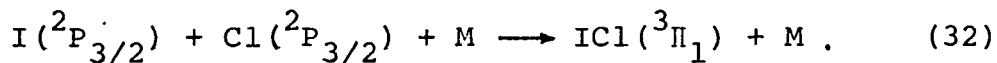


Figure 17. Iodine afterglow spectrum produced by  $\text{ICl} + \text{Cl}$  reaction. Broken curve gives the true spectral distribution.



to titrate more than a stoichiometric amount of ICl into the stream of chlorine atoms. This was necessary to ensure that emission arising from the formation of excited ICl did not contribute to the afterglow:



Clyne and Coxon (50) studied the emission spectrum of ICl produced in a discharge-flow system, and found a number of strong transitions below  $8000\overset{\circ}{\text{A}}$ . The fact that no emission below  $8000\overset{\circ}{\text{A}}$  was detected in our experiments was taken to indicate that reaction (32) did not contribute significantly to the afterglow.

Because of the difficulties involved in measuring iodine flow rates and atom concentrations, kinetic measurements on the iodine afterglow were not attempted.

#### The Chlorine Afterglow Spectrum

The emission from the recombination of chlorine atoms was observed to extend from  $5000\overset{\circ}{\text{A}}$  to  $15000\overset{\circ}{\text{A}}$ . The region from  $6000\overset{\circ}{\text{A}}$  to  $11000\overset{\circ}{\text{A}}$  in the emission spectrum was characterized by a large number of red-degraded bands, the position of which was determined by measuring the monochromator traces. Thirty band heads in the afterglow were measured, and these have all been identified as arising from the  $^3\Pi_{o+u} \longrightarrow ^1\Sigma_g^+$  transition of molecular chlorine. The calculated band head positions shown in Table 7 are

TABLE 7

BAND HEADS RECORDED FROM THE CHLORINE AFTERGLOW SPECTRUM

wavelength ° (Å)	$\nu_{\text{vac.}}$ ( $\text{cm}^{-1}$ )	${}^3\Pi_{\text{O}^+ \text{u}} \rightarrow {}^1\Sigma_{\text{g}}^+$		$\nu_{\text{calc.}}^{\dagger}$
		$\nu'$	$\nu''$	
10551	9474	2	17	9455
10071	9926	0	15	9909
9618	10394	0	14	10388
		2	15	10396
9195	10872	0	13	10872
8979	11134	1	13	11121
8814	11342	0	12	11362
		2	13	11359
8611	11610	1	12	11610
8441	11886	0	11	11857
		2	12	11849
8265	12096	1	11	12105
8108	12330	0	10	12357
		2	11	12344
7944	12585	3	11	12571
		1	10	12606
7780	12850	2	10	12844
7635	13094	3	10	13072
		1	9	13112
7480	13365	2	9	13350
7360	13583	3	9	13578
7226	13835	2	8	13856
7100	14081	3	8	14086
6992	14302	4	8	14305
6868	14572	3	7	14605
6750	14811	4	7	14821
6655	15032	5	7	15029

TABLE 7 Continued

wavelength ° (Å)	$\nu_{\text{vac.}}$ ( $\text{cm}^{-1}$ )	$3\Pi_{\text{O}^+u} \xrightarrow{\nu'} 1\Sigma_{\text{g}}^+ \xleftarrow{\nu''}$	$\nu^{\dagger}$ calc.
6580	15193	6      7	15226
6522	15333	4      6	15343
6438	15528	5      6	15551
6364	15718	6      6	15748
6296	15879	4      5	15871
6225	16071	5      5	16078
6154	16255	6      5	16276
6083	16442	7      5	16461
6020	16607	5      4	16611

† calculated from reference (50)

based on the revised spectroscopic constants of Clyne and Coxon (50).

Spectral distribution changes similar to those exhibited by the bromine afterglow were observed in the chlorine emission. Maintaining the total pressure at a constant value while varying the atom concentration had the effect of shifting the intensity maximum from shorter wavelengths, at high  $[Cl]$ , to longer wavelengths at low  $[Cl]$  (figure 18). On the other hand, high pressures were found to favour emission in the red region while lowering the pressure shifted the intensity maximum towards the blue (figure 19).

The true spectral distribution of the chlorine afterglow spectrum is shown in figure 20. These curves were constructed in a manner similar to those of figure 13 for the bromine emission.

In order to rule out the possibility that these intensity shifts were due to changing discharge temperatures, experiments were performed to investigate the effect of varying the reaction tube temperature on the spectrum. However, no measurable change in intensity distribution was observed when the temperature of the walls of the reaction tube was varied over the range of  $-20^{\circ}C$  to  $150^{\circ}C$ .

Figure 18. The change in the spectral distribution of the  $\text{Cl}_2$  afterglow with atom concentration. Pressure fixed at 1.0 torr.

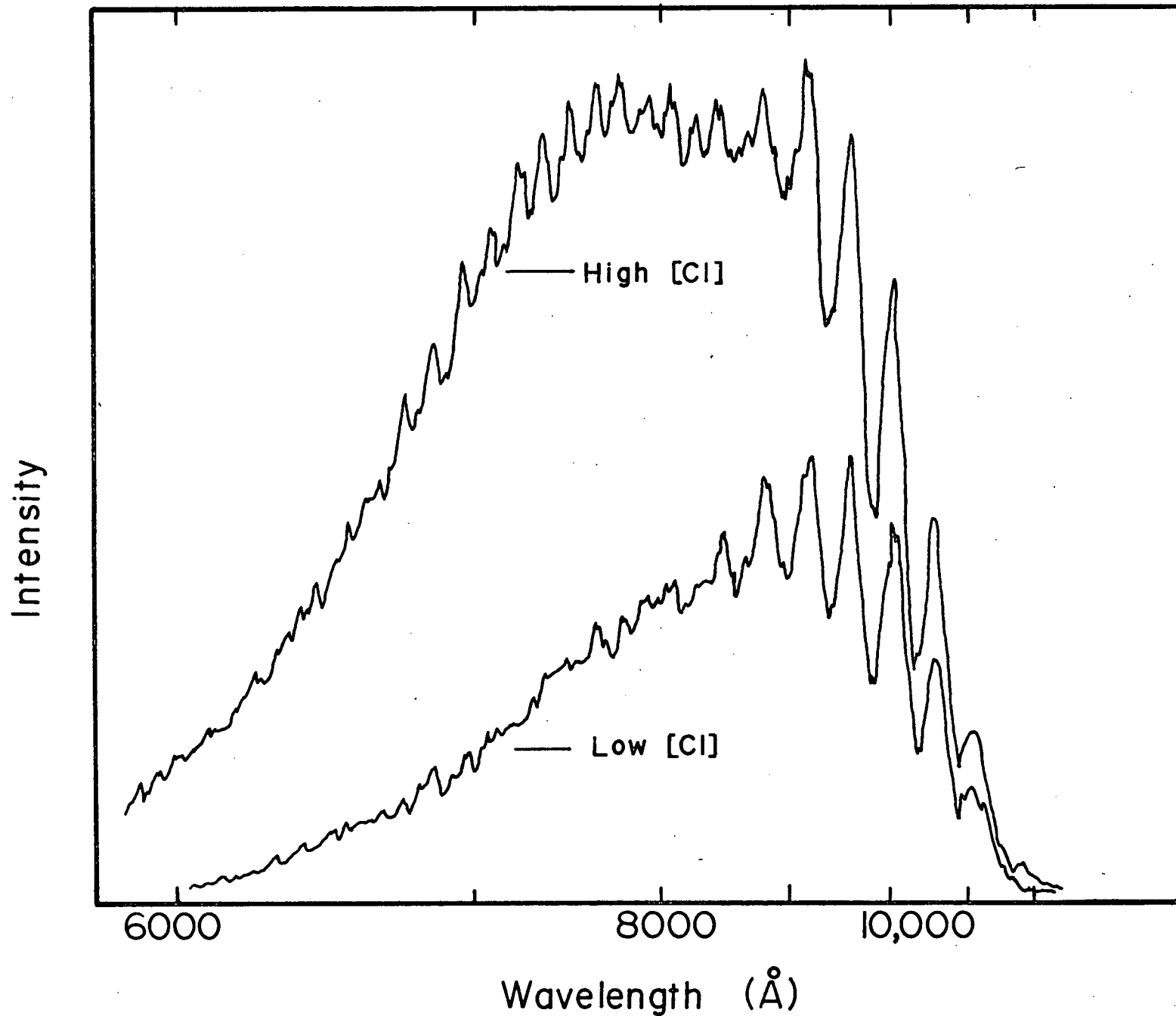


Figure 19. The change in spectral distribution of the  $\text{Cl}_2$  afterglow spectrum with pressure.  $[\text{Cl}] = 1.2 \times 10^{-9}$  mole/cc, monochromator slitwidth = 0.5 mm, pressures in torr.

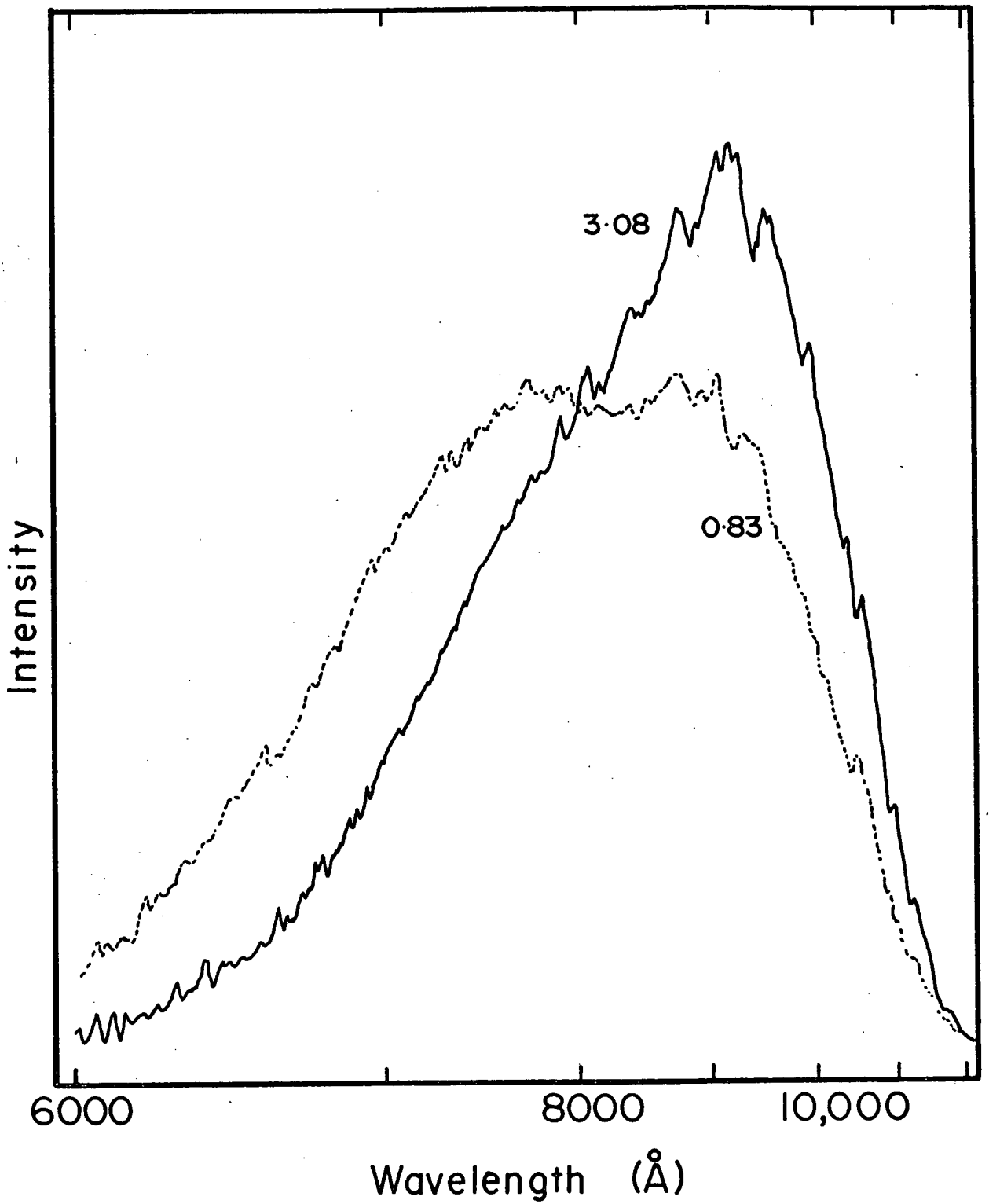
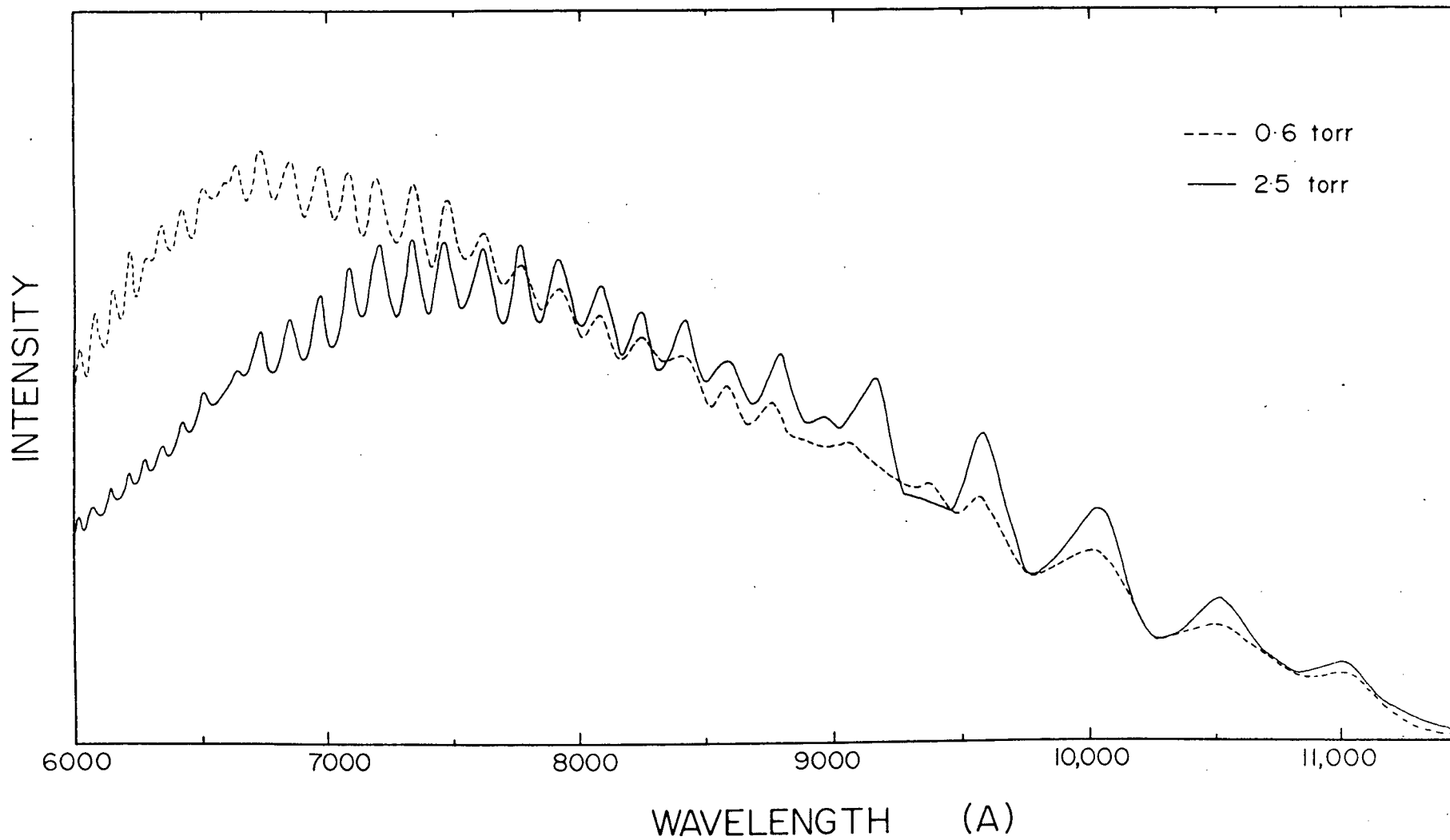


Figure 20. True spectral distribution of the chlorine afterglow spectrum.



## Kinetics Of The Chlorine Afterglow Emission

Since the chlorine afterglow emission was found to extend over such a wide wavelength range ( $5000\text{\AA}$  to  $15000\text{\AA}$ ) and because no single detector was suitable for studying the entire spectrum, the emission was studied in three regions. The RCA 7265 photomultiplier was used to study the region between  $5000\text{\AA}$  and  $6800\text{\AA}$  (hereafter called the visible region), while the portion from  $6800\text{\AA}$  to  $12000\text{\AA}$  (infrared region) was covered by the RCA 7102 photomultiplier. Beyond  $12000\text{\AA}$ , the emission intensity was low, and measurements with the PbS detector showed that this region contributed not more than 5% to the total intensity. In view of the small contribution from this region and because of the low sensitivity of the PbS detector, detailed kinetic studies were not attempted beyond  $12000\text{\AA}$ .

The visible and infrared regions were studied at a number of different pressures ranging from 0.83 to 3.08 torr. The limits on the pressure range were imposed by the requirement of only a small pressure gradient down the length of the reaction tube and by the need to operate under conditions where emission intensities were easily measurable. At pressures above 3.5 torr, the intensity became too low for detection, and below 0.83 torr the pressure gradient, as calculated from the Poiseuille equation (51), became sizable. At each value of the total system pressure, the atom concentration was varied by adjusting the microwave power or the cavity resonance.

## (a) Dependence Of The Emission Intensity On [Cl]

The emission intensity in various regions of the chlorine afterglow spectrum was studied as a function of atom concentration at constant total pressure. This was done by isolating five regions of the spectrum, the positions and bandwidths of which are listed below.

Band Centre Å	Bandwidth Å
5500	5468 < $\lambda$ < 5532
6200	6152 < $\lambda$ < 6248
7000	6930 < $\lambda$ < 7070
8600	8475 < $\lambda$ < 8725
10600	10390 < $\lambda$ < 10810

The intensity measured in each of these bands at various atom concentrations is listed in Table 8 for five values of the pressure. Plotting the logarithm of  $I_\lambda$  against  $\log [Cl]$  yields a value of  $n$  in the expression  $I_\lambda \propto [Cl]^n$ , and the values of  $n$  obtained in this way are listed in Table 9. Figures 21 and 22 show  $\log I_\lambda$  vs.  $\log [Cl]$  plots for two values of the total pressure.

From an examination of the values of  $n$  listed in Table 9, it appears that the intensity at longer wavelengths depends on the first power of the atom concentration while that at short wavelengths is proportional to the square of the atom concentration.

The integrated emission intensity in the visible and infrared regions was also observed as a function of [Cl]

TABLE 8(a)

DEPENDENCE OF  $I_\lambda$  UPON  $[Cl]$ . INTENSITY IN ARBITRARY UNITS

Pressure torr	$[Cl]$ moles/cc x 10	$I_{5500}$	$I_{6200}$	$\int_{5000\text{\AA}}^{6800\text{\AA}} I_\lambda d\lambda$
0.83	1.29	4.0	24.8	61.4
"	1.80	8.0	46.5	111
"	2.05	11.2	62.5	146
"	2.99	30.4	114	275
"	1.42	4.80	28.0	68.5
"	1.50	4.80	30.4	75.5
"	1.83	8.80	45.6	113
"	2.37	13.6	68.9	169
"	2.84	19.2	103	246
1.32	0.943	1.50	15.2	35.2
"	1.16	3.00	20.0	50.9
"	1.52	4.50	28.5	71.1
"	1.96	8.00	49.5	122
"	2.54	14.4	81.6	199
"	2.54	14.4	80.0	198
"	3.28	25.0	130	316
"	3.09	22.5	118	286
1.70	0.721	1.0	8.0	21.9
"	1.02	2.0	16.0	40.9
"	1.52	6.0	34.0	85.7
"	1.82	8.0	46.0	116
"	2.49	14.3	85.9	21.2
"	2.32	13.0	74.1	186

TABLE 8 (a) Continued

Pressure torr	[Cl] moles/cc x 10	$I_{5500}$	$I_{6200}$	$\int_{5000}^{6800} I_{\lambda} d\lambda$
2.33	0.484	0.7	6.0	16.1
"	0.567	0.8	7.0	18.1
"	0.616	1.0	9.0	23.5
"	0.815	2.0	13.5	35.3
"	1.24	4.5	28.0	72.1
"	1.90	10.5	66.0	165
3.03	0.501	0.8	4.0	11.2
"	0.575	1.2	5.0	13.8
"	0.531	1.0	4.5	11.9
"	1.10	3.0	11.0	30.7
"	1.38	4.5	18.0	48.6

TABLE 8 (b)

DEPENDENCE OF  $I_\lambda$  ON  $[Cl]$ . INTENSITY IN ARBITRARY UNITS

Pressure torr	$[Cl]$ moles/cc x $10^9$	$I_{7000}$	$I_{8600}$	$I_{10600}$	$\int_{6800\text{\AA}}^{12000\text{\AA}} I_\lambda d\lambda$
0.83	1.20	82.5	111	47.5	448
"	1.24	80.0	106	47.5	440
"	1.15	65.0	92.5	40.0	373
"	0.716	27.5	50.0	25.0	198
"	0.153	6.25	17.5	8.00	62.8
1.32	4.62	442	488	195	2030
"	5.24	507	542	208	2280
"	2.95	236	307	132	1240
"	3.21	264	334	144	1370
"	3.96	360	416	176	1730
"	5.83	572	601	247	2560
1.70	0.746	40.0	89.5	41.7	343
"	1.32	89.5	165	72.0	618
"	2.35	196	300	120	1180
"	5.53	485	600	250	2500
"	4.95	430	540	230	2240
"	7.09	816	881	368	3710
"	3.57	296	406	176	1650
"	4.48	400	504	216	2090
"	5.86	540	655	280	2760
"	6.54	663	767	325	3240
2.33	0.434	12.5	40.0	21.2	155
"	1.12	50.0	115	55.0	426
"	0.712	25.0	70.0	35.0	258
"	0.863	30.0	83.9	42.5	310
"	1.28	55.0	125	65.0	473

TABLE 8(b) Continued

Pressure torr	[Cl] moles/cc x 10 <sup>9</sup>	I <sub>7000</sub>	I <sub>8600</sub>	I <sub>10600</sub>	$\int_{6800\text{\AA}}^{12000\text{\AA}} I_{\lambda} d\lambda$
3.08	0.216	8.76	32.5	18.8	124
"	0.299	11.2	45.0	25.0	165
"	0.518	21.2	70.0	40.0	262
"	0.668	32.5	98.9	55.0	372
"	0.953	47.5	135	75.0	505
"	1.26	70.0	180	92.5	664

TABLE 9

VALUES OF  $n$  IN THE EXPRESSION  $I_\lambda \propto [Cl]^n$ 

Pressure torr	n						
	$I_{5500}$	$I_{6200}$	$I_{7000}$	$I_{8600}$	$I_{10600}$	$\int_{5000}^{6800} I_\lambda d\lambda$	$\int_{6800}^{12000} I_\lambda d\lambda$
0.83	2.1 ± 0.1	1.9 ± 0.1	1.5 ± 0.2	1.1 ± 0.2	1.0 ± 0.2	1.8 ± 0.1	1.2 ± 0.2
1.32	2.2 ± 0.1	1.8 ± 0.1	1.3 ± 0.1	1.0 ± 0.1	0.9 ± 0.1	1.7 ± 0.1	1.0 ± 0.1
1.70	2.0 ± 0.1	1.9 ± 0.1	1.3 ± 0.1	1.0 ± 0.1	0.9 ± 0.1	1.8 ± 0.1	1.0 ± 0.1
2.33	2.0 ± 0.1	1.8 ± 0.1	1.6 ± 0.1	1.1 ± 0.1	1.0 ± 0.1	1.7 ± 0.1	1.0 ± 0.1
3.03	1.6 ± 0.1	1.4 ± 0.1	1.2 ± 0.1	1.0 ± 0.1	0.9 ± 0.1	1.4 ± 0.1	1.0 ± 0.1

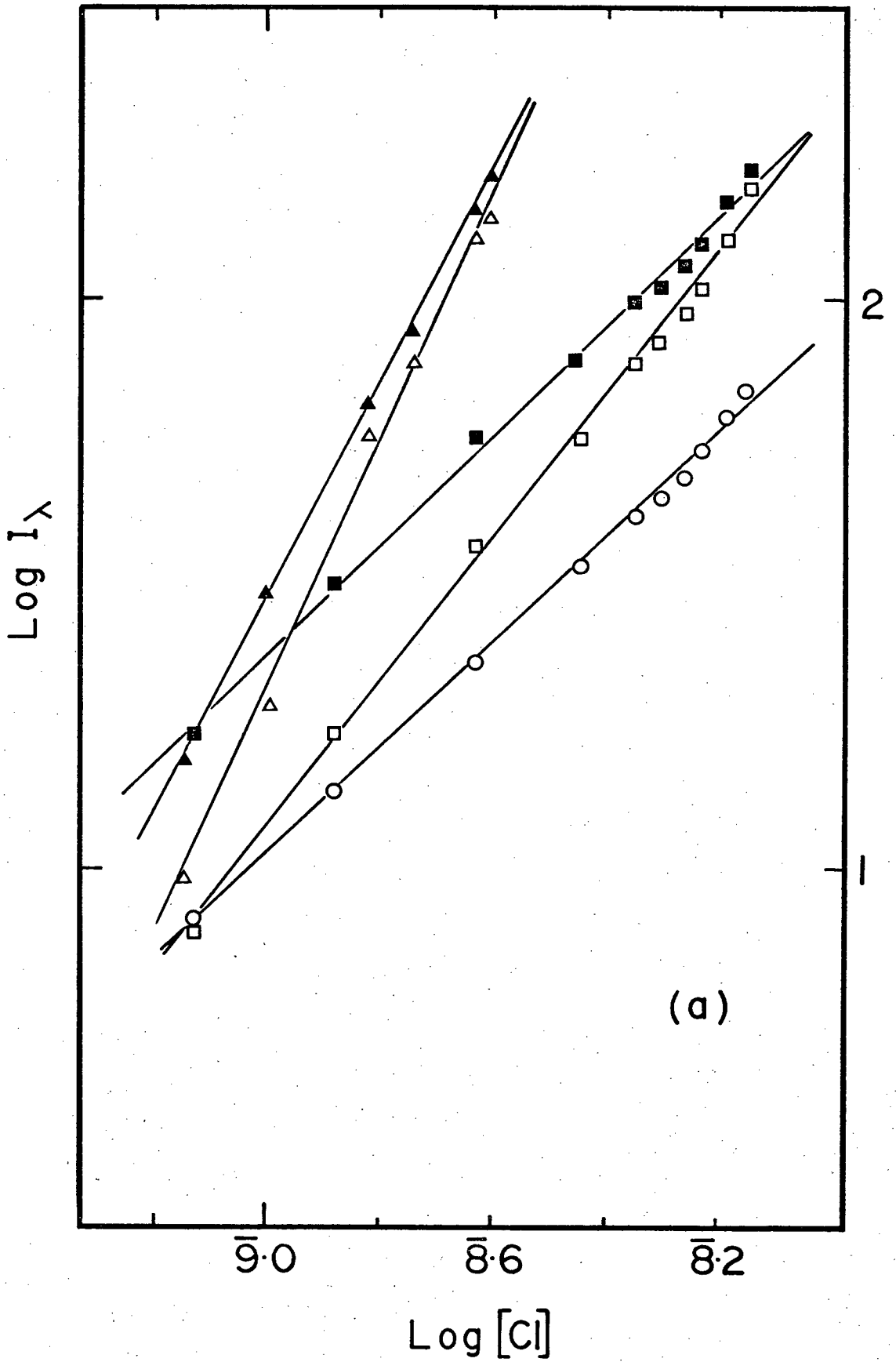
Figure 21(a). Plots of  $\log I_\lambda$  vs.  $\log [Cl]$  for a pressure of 1.70 torr. Intensity in arbitrary units.

Points obtained for bands centred at the following wavelengths:

$\Delta$  5500Å,  $\blacktriangle$  6200Å,  $\square$  7000Å,  $\blacksquare$  8600Å,  $\circ$  10600Å.

Figure 21(b). Plot of  $\log (\int I_\lambda d\lambda)$  vs.  $\log [Cl]$  for a pressure of 1.70 torr.

Closed circles for infrared region (6800Å - 12000Å), open circles for visible region (5000Å - 6800Å).



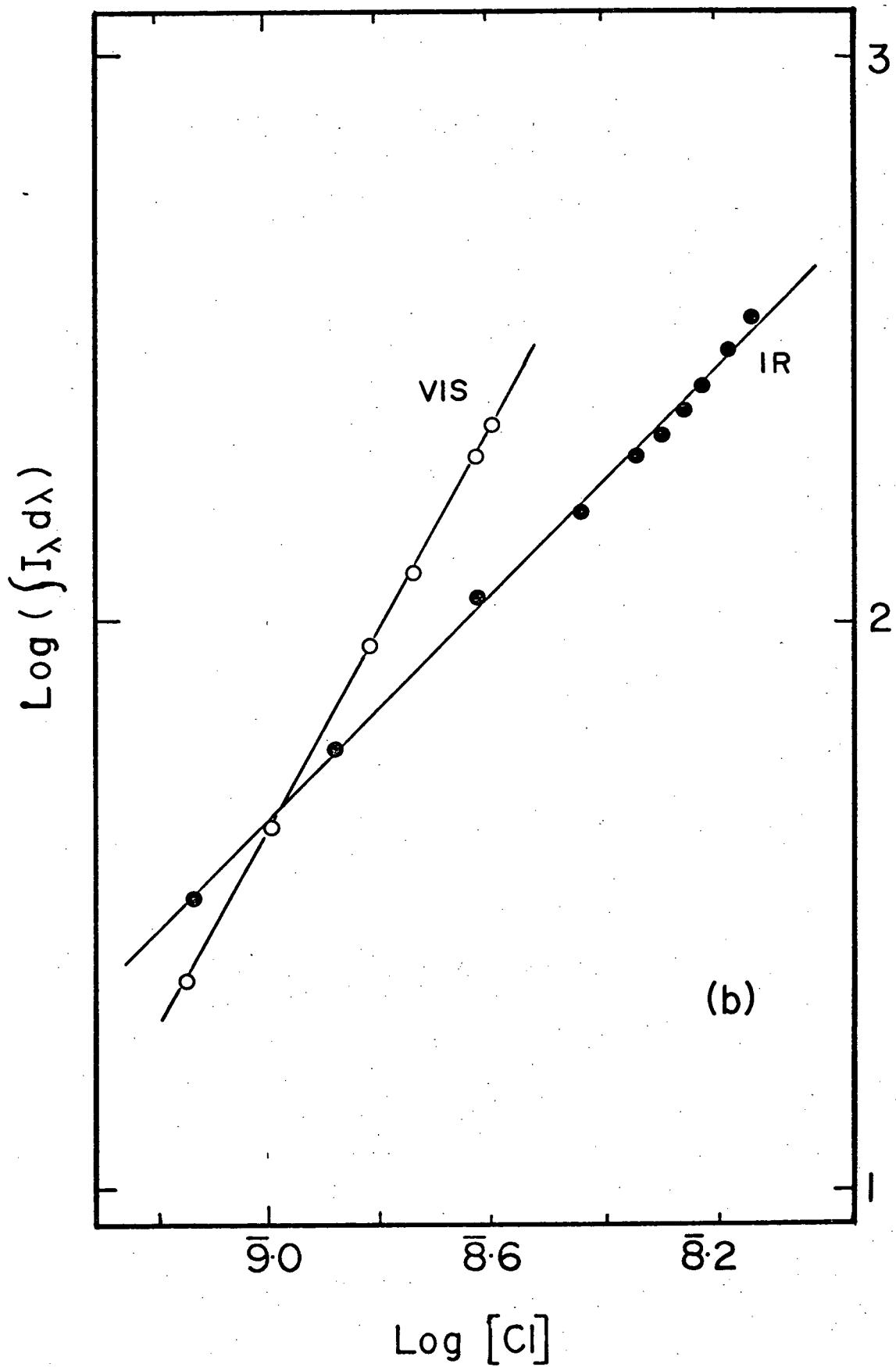


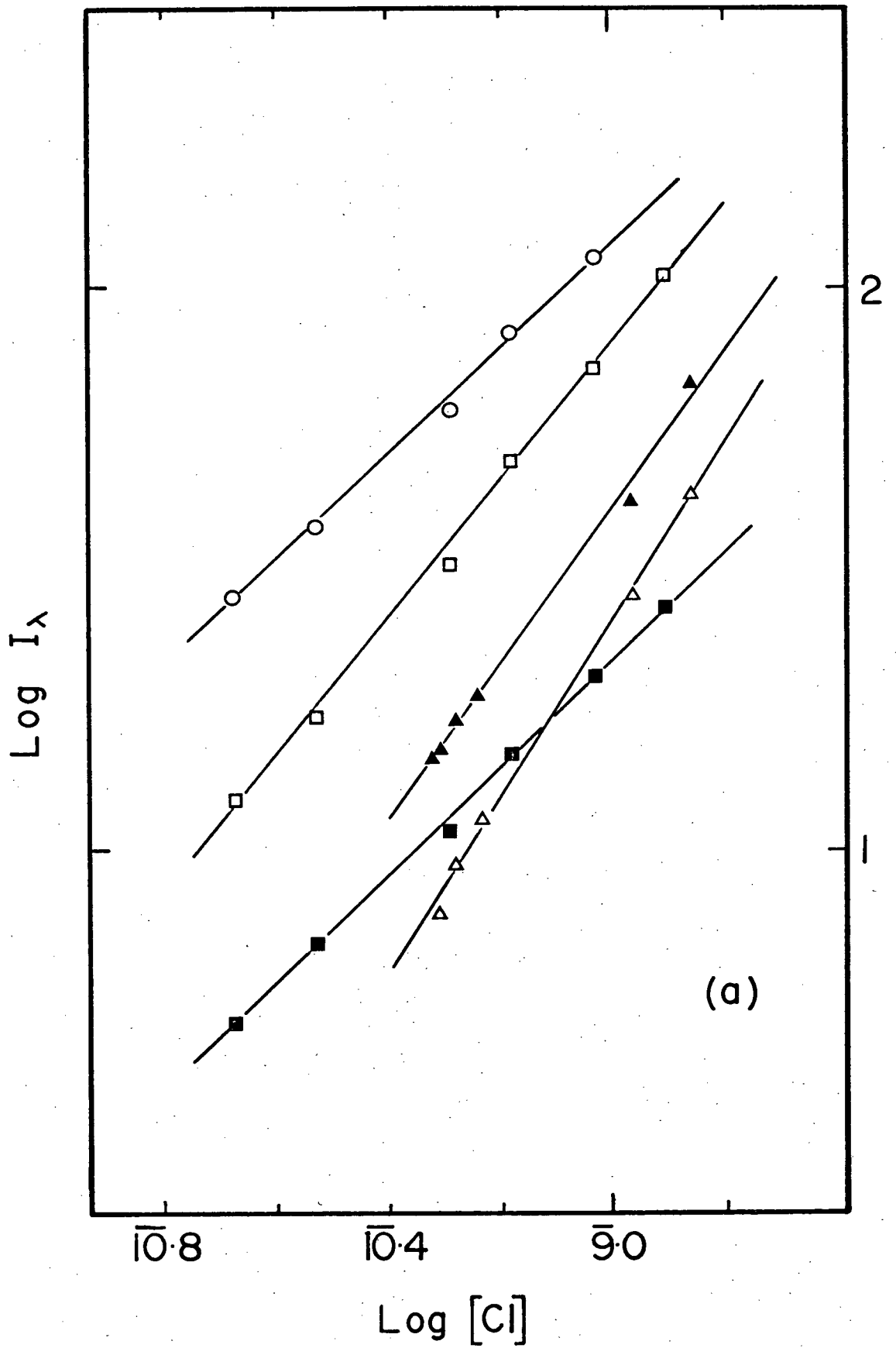
Figure 22(a). Plots of  $\log I_\lambda$  vs.  $\log [Cl]$  for a pressure of 3.08 torr. Intensity in arbitrary units.

Points obtained for bands centred at the following wavelengths:

$\Delta$  5500Å,  $\blacktriangle$  6200Å,  $\square$  7000Å,  $\blacksquare$  8600Å,  
 $\circ$  10600Å.

Figure 22(b). Plot of  $\log (\int I_\lambda d\lambda)$  vs.  $\log [Cl]$  for a pressure of 3.08 torr.

Closed circles for infrared region (6800Å - 12000Å), open circles for visible region (5000Å - 6800Å).



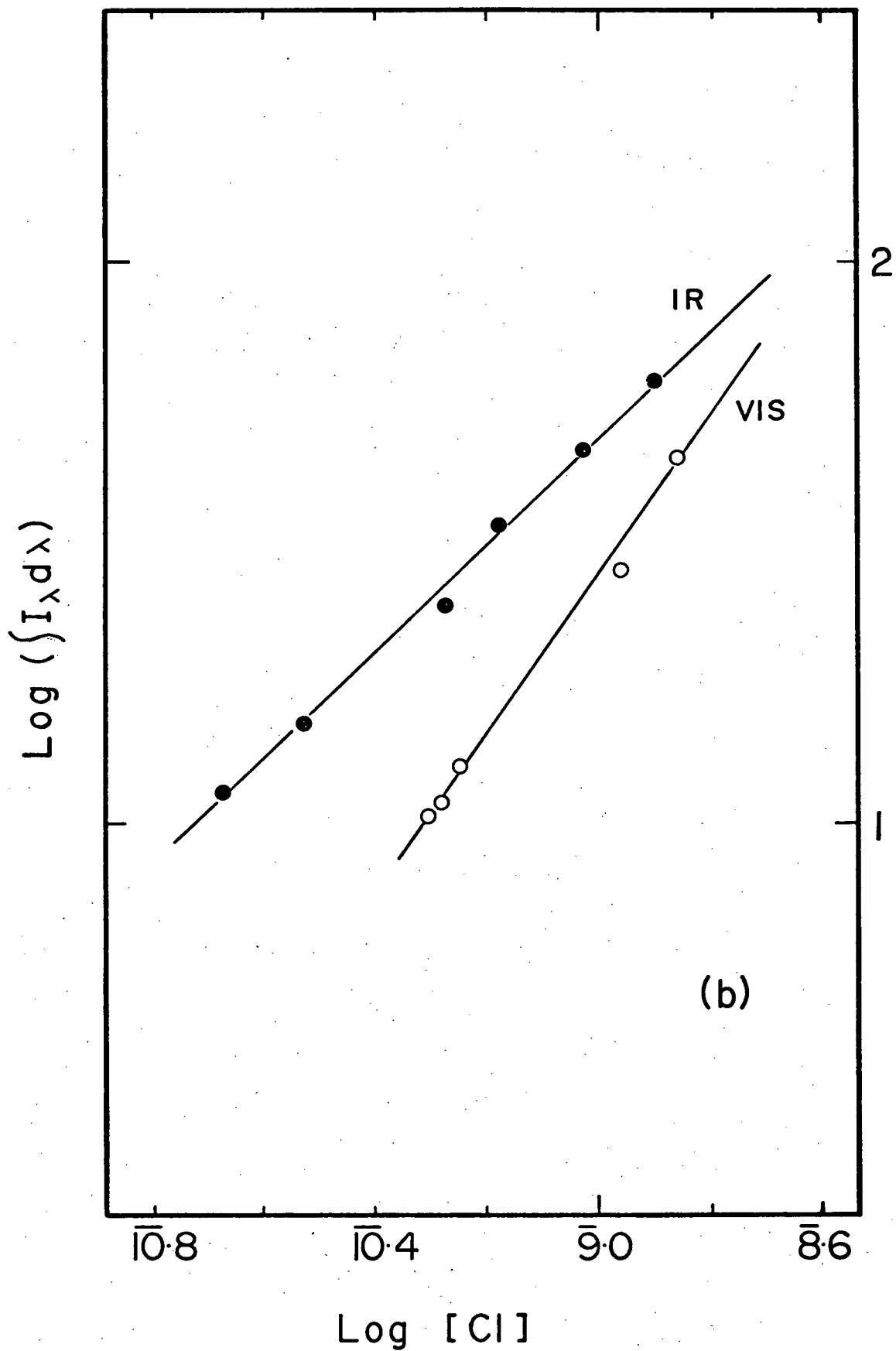


(Table 8 and figures 21 and 22). The visible region was found to exhibit a higher dependence on [Cl] than the infrared region (Table 9). The intensity in this latter portion of the spectrum was found to depend on the first power of the atom concentration at every pressure studied.

(b) Dependence Of The Emission Intensity On [Cl<sub>2</sub>]

Since it was not possible to devise an experiment in which the pressure was varied while the atom concentration was held constant, the dependence of the intensity on pressure had to be found by interpolation of the  $I_\lambda$  vs. [Cl] data. The data obtained in this way exhibit considerable scatter since they are affected by day to day changes in photomultiplier and detector sensitivity. However, values of  $m$  in the expression  $I_\lambda \propto [Cl_2]^m$  have been obtained by plotting  $\log I_\lambda$  against  $\log P$  at constant [Cl] (figure 23), and these are shown in Table 10. These data show that the intensity in the short wavelength region of the spectrum is independent of pressure, but the dependence increases with wavelength until the intensity is found to be proportional to  $[Cl_2]^{0.5 \pm 0.2}$  at 10600Å.

The integrated intensity in the visible region was found to be independent of pressure while that in the infrared region was observed to have small pressure dependence (figure 23 and Table 10).

Figure 23. Plot of  $\log P$  vs.  $\log I_\lambda$  for bands centred at five wavelengths. Atom concentration fixed at  $1.3 \times 10^{-9}$  mole/cc.

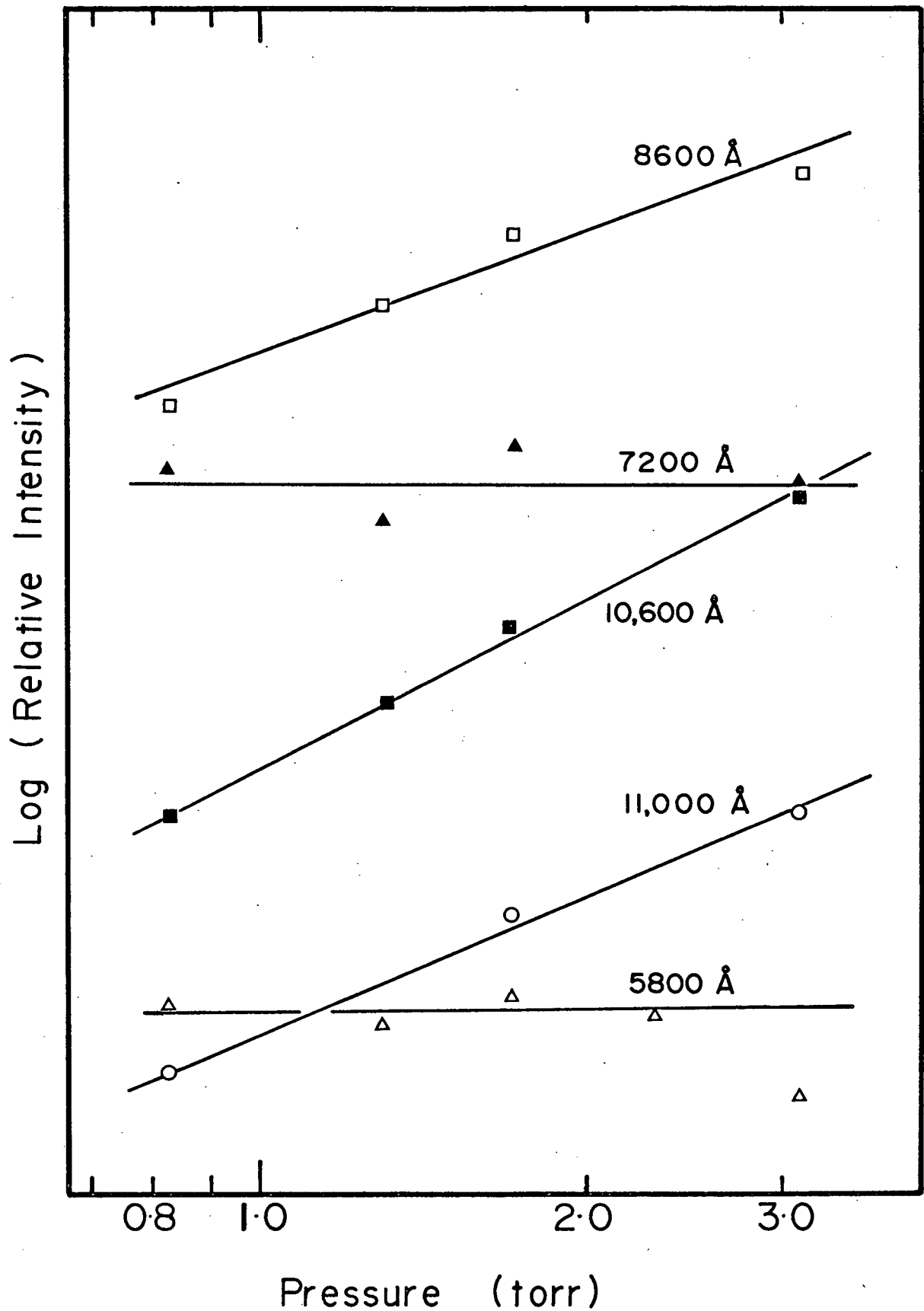


TABLE 10

VALUES OF  $m$  IN THE EXPRESSION  $I_\lambda \propto [Cl_2]^m$ 

[Cl] x 10 <sup>-9</sup> (moles/cc)	m					
	I <sub>5500</sub>	I <sub>7000</sub>	I <sub>8600</sub>	I <sub>10600</sub>	$\int_{5000\text{Å}}^{6800\text{Å}} I_\lambda d\lambda$	$\int_{6800\text{Å}}^{12000\text{Å}} I_\lambda d\lambda$
1.3	0.0 ± 0.2	0.0 ± 0.2	0.3 ± 0.2	0.5 ± 0.2	0.0 ± 0.2	0.3 ± 0.2
2.0	0.0 ± 0.2	0.0 ± 0.2	0.3 ± 0.2	0.4 ± 0.2	0.0 ± 0.2	0.1 ± 0.2

## (c) Absolute Rate Constant Measurements

If we define the apparent rate constant for the chlorine emission as

$$k_{\text{app}} = I_{\text{total}} / [\text{Cl}]^2 [\text{Cl}_2],$$

then the rate constants can be evaluated using equation 28. However, because separate measurements have been carried out in the visible and infrared regions of the chlorine afterglow, rate constants corresponding to the emission in these two regions were calculated,  $k_{\text{app}}^{\text{VIS}}$  for the region 5000 $\text{\AA}$  to 6800 $\text{\AA}$ , and  $k_{\text{app}}^{\text{IR}}$  for the emission between 6800 $\text{\AA}$  and 12000 $\text{\AA}$ . The results of these measurements are listed in Table 11.

The most important data to be extracted from these results are the rate constants for the total emission. A simple addition of the rate constants in the two regions was not possible since both  $k_{\text{app}}^{\text{VIS}}$  and  $k_{\text{app}}^{\text{IR}}$  varied with atom concentration. However, it was found that straight lines were obtained by plotting  $k_{\text{app}}$  against  $1/[\text{Cl}]$  (figures 24 and 25), and this fact made it possible to obtain rate constants for any value of  $[\text{Cl}]$  by interpolation. Thus, the rate constant for the total emission at any atom concentration could be determined by adding the values of  $k_{\text{app}}^{\text{VIS}}$  and  $k_{\text{app}}^{\text{IR}}$  found from these plots. The resultant  $k_{\text{app}}^{\text{TOTAL}}$  vs.  $1/[\text{Cl}]$  plots, constructed in this way, are shown in figure 26. The solid lines in this figure represent the values of  $1/[\text{Cl}]$  over which the  $k_{\text{app}}^{\text{VIS}}$  and  $k_{\text{app}}^{\text{IR}}$  data overlap

TABLE 11

VALUES OF  $k_{app}$  FOR THE CHLORINE AFTERGLOW EMISSION

PRESSURE = 0.83 torr

Spectral Region	Flow of $Cl_2$ $\mu$ moles/sec	Flow of Cl $\mu$ moles/sec	$[Cl_2] \times 10^8$ moles/cc	$[Cl] \times 10^9$ gm atom/cc	$k_{app} \times 10^{-12}$ $cm^6 moles^{-2} sec^{-1}$
	32.1	0.918	4.45	1.29	3.42
	32.1	1.28	4.42	1.80	3.20
	32.1	1.46	4.41	2.05	3.26
	32.1	2.13	4.36	2.99	2.90
5000 - 6800Å	32.1	1.01	4.44	1.42	3.16
	32.1	1.07	4.43	1.50	3.11
	32.1	1.30	4.42	1.83	3.16
	32.1	1.69	4.39	2.37	2.81
	32.1	2.02	4.37	2.84	2.88
	32.1	0.855	4.45	1.20	14.5
6800 - 12000Å	32.1	0.879	4.45	1.24	13.5
	32.1	0.815	4.45	1.15	13.3
	32.1	0.510	4.47	0.716	17.9
	32.1	0.109	4.50	0.153	12.4

TABLE 11 Continued

PRESSURE = 1.32 torr

Spectral Region	Flow of Cl <sub>2</sub> μ moles/sec	Flow of Cl μ moles/sec	[Cl <sub>2</sub> ] × 10 <sup>8</sup> moles/cc	[Cl] × 10 <sup>9</sup> gm atom/cc	k <sub>app</sub> × 10 <sup>-12</sup> cm <sup>6</sup> moles <sup>-2</sup> sec <sup>-1</sup>
	33.0	0.434	7.12	0.943	2.29
	33.0	0.534	7.11	1.16	2.19
	33.0	0.697	7.10	1.52	1.80
5000 - 6800Å	33.0	0.901	7.07	1.96	1.86
	33.0	1.17	7.04	2.54	1.80
	33.0	1.17	7.04	2.54	1.79
	33.0	1.51	7.00	3.28	1.73
	33.0	1.42	7.02	3.09	1.76
	32.6	2.10	6.94	4.62	2.85
	32.6	2.38	6.91	5.24	2.50
6800 - 12000Å	32.6	1.34	7.02	2.95	4.24
	32.6	1.46	7.01	3.21	3.96
	32.6	1.80	6.97	3.96	3.30
	32.6	2.65	6.88	5.83	2.28

TABLE 11 Continued

PRESSURE = 1.70 torr

Spectral Region	Flow of Cl <sub>2</sub> μ moles/sec	Flow of Cl μ moles/sec	[Cl <sub>2</sub> ] x 10 <sup>8</sup> moles/cc	[Cl] x 10 <sup>9</sup> gm atom/cc	k <sub>app</sub> x 10 <sup>-12</sup> cm <sup>6</sup> moles <sup>-2</sup> sec <sup>-1</sup>
	31.0	0.242	9.20	0.721	1.89
	31.0	0.341	9.19	1.02	1.78
5000 - 6800Å	31.0	0.511	9.16	1.52	1.66
	31.0	0.610	9.15	1.82	1.59
	31.0	0.835	9.11	2.49	1.55
	32.8	0.265	9.28	0.746	1.40
	32.8	0.469	9.17	1.32	8.05
	32.8	0.833	9.12	2.35	4.92
	35.1	2.10	8.96	5.53	1.90
6800 - 12000Å	37.5	2.01	8.99	4.95	2.12
	37.5	2.88	8.88	7.09	1.73
	36.7	1.42	9.06	3.57	2.98
	36.7	1.78	9.01	4.48	2.41
	36.7	2.33	8.94	5.86	1.87
	36.7	2.60	8.91	6.54	1.77

TABLE 11 Continued

PRESSURE = 2.33 torr

Spectral Region	Flow of Cl <sub>2</sub> μ moles/sec	Flow of Cl μ moles/sec	[Cl <sub>2</sub> ] x 10 <sup>8</sup> moles/cc	[Cl] x 10 <sup>9</sup> gm atom/cc	k <sub>app</sub> x 10 <sup>-12</sup> cm <sup>6</sup> moles <sup>-2</sup> sec <sup>-1</sup>
	38.2	0.146	12.6	0.484	2.24
	38.2	0.171	12.6	0.567	1.84
5000 - 6800Å	38.2	0.186	12.6	0.616	2.02
	38.2	0.246	12.6	0.815	1.74
	38.2	0.373	12.6	1.24	1.55
	38.2	0.574	12.6	1.90	1.50
	31.2	0.107	12.6	0.434	13.6
	31.2	0.275	12.6	1.12	5.66
6800 - 12000Å	31.1	0.175	12.6	7.12	8.40
	31.1	0.212	12.6	8.63	6.88
	31.1	0.314	12.6	1.28	4.79

TABLE 11 Continued

PRESSURE = 3.08 torr

Spectral Region	Flow of Cl <sub>2</sub> μ moles/sec	Flow of Cl μ moles/sec	[Cl <sub>2</sub> ] × 10 <sup>8</sup> moles/cc	[Cl] × 10 <sup>9</sup> gm atom/cc	k <sub>app</sub> × 10 <sup>-12</sup> cm <sup>6</sup> moles <sup>-2</sup> sec <sup>-1</sup>
	38.1	0.116	16.4	0.501	1.12
	38.1	0.133	16.4	0.575	1.05
5000 -	38.1	0.123	16.4	0.531	1.05
6800Å	38.1	0.255	16.4	1.10	0.634
	38.1	0.320	16.4	1.38	0.639
	38.1	0.0491	16.7	0.216	33.1
	38.1	0.0681	16.7	0.299	23.0
6800 -	38.1	0.118	16.7	0.518	12.2
12000Å	38.1	0.152	16.7	0.668	10.4
	38.1	0.217	16.7	0.953	6.94
	38.1	0.287	16.7	1.26	5.20

Figure 24. Plot of  $k_{app}$  vs.  $1/[Cl]$  for a pressure of 1.70 torr.  $\circ$  visible region (5000Å - 6800Å),  $\bullet$  infrared region (6800Å - 12000Å), --- addition of rate constants for the two regions.

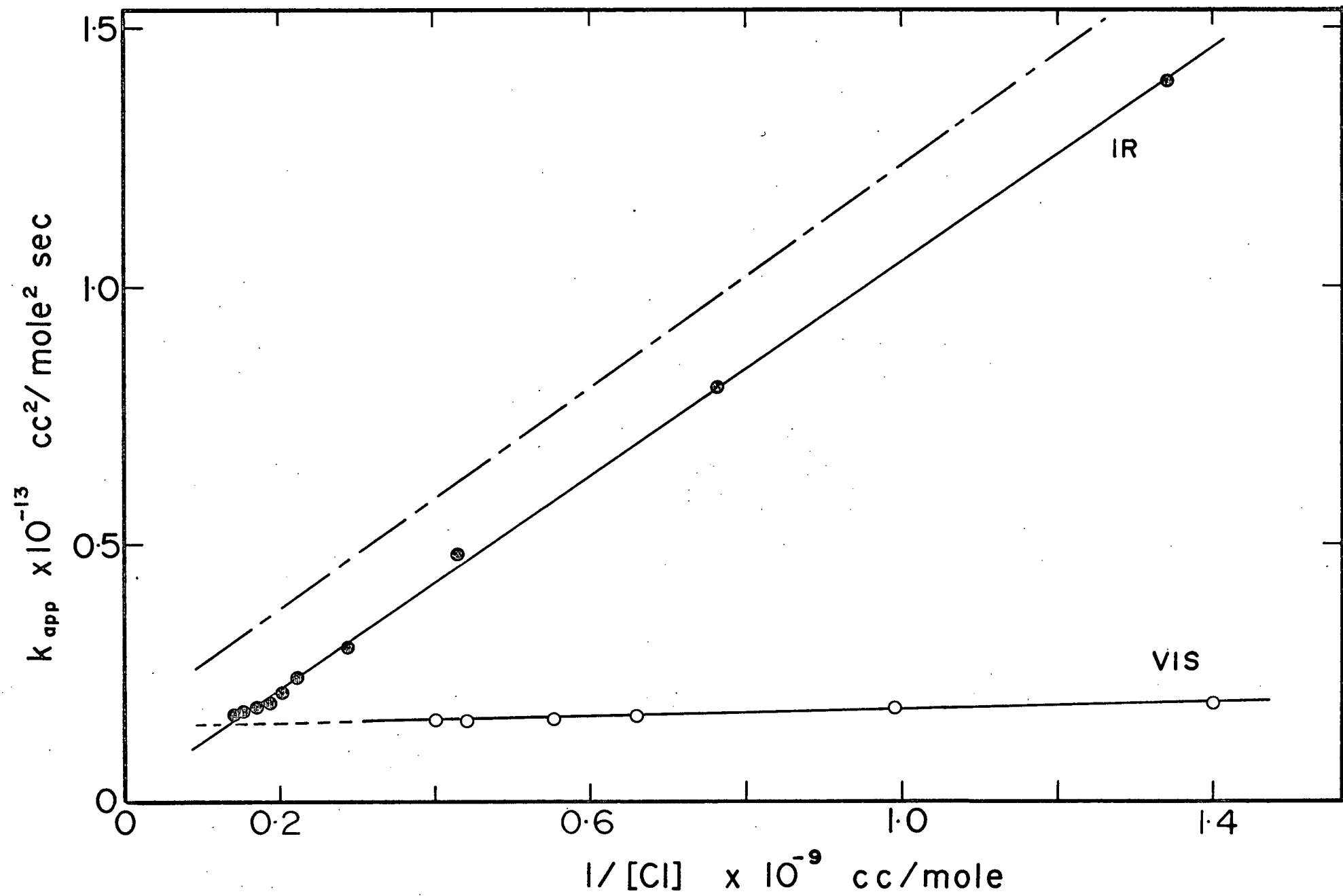


Figure 25. Plot of  $k_{app}$  vs.  $1/[Cl]$  for a pressure of 2.33 torr.  $\circ$  visible region (5000Å - 6800Å),  $\bullet$  infrared region (6800Å - 12000Å), — — — addition of rate constants for the two regions.

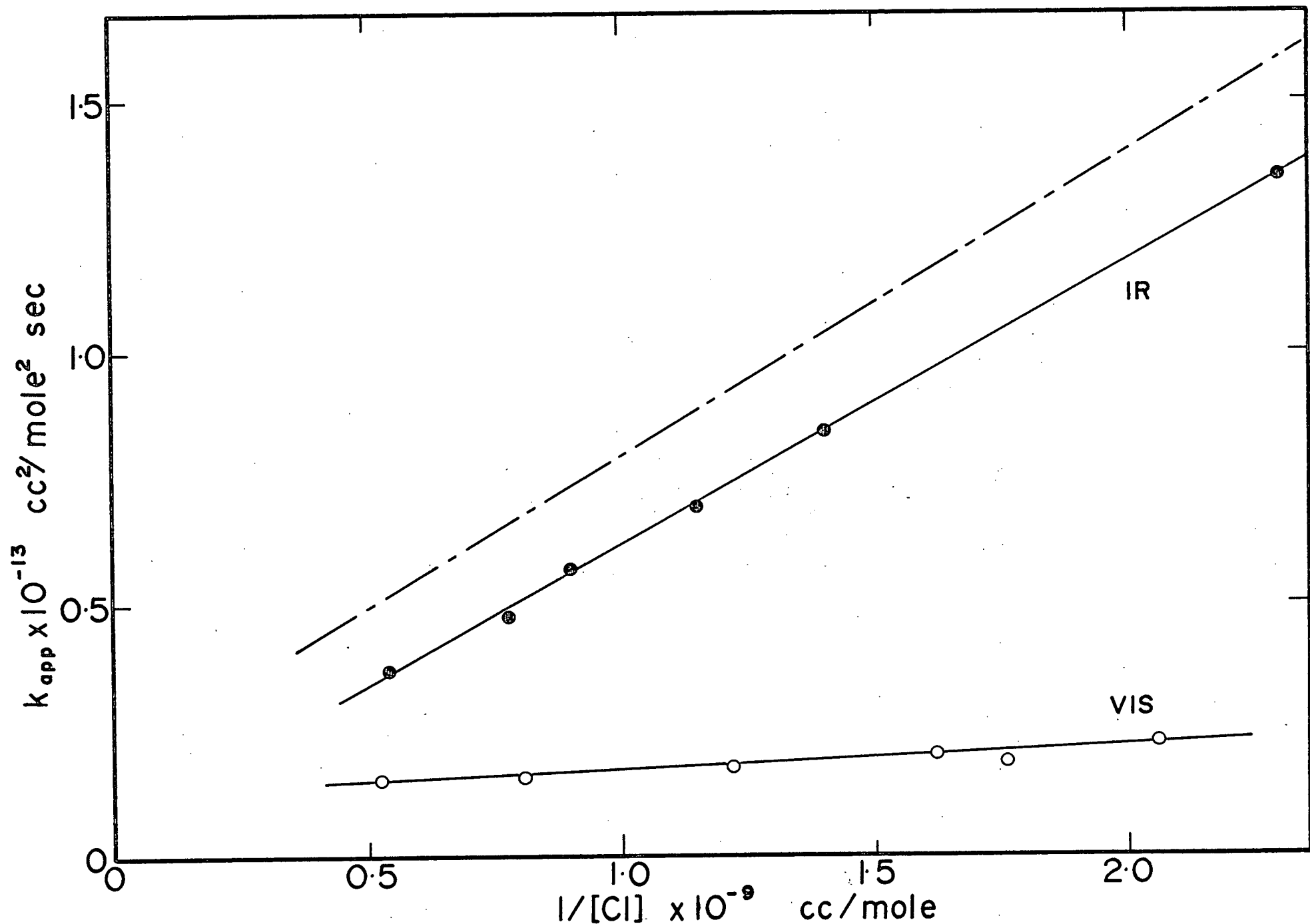
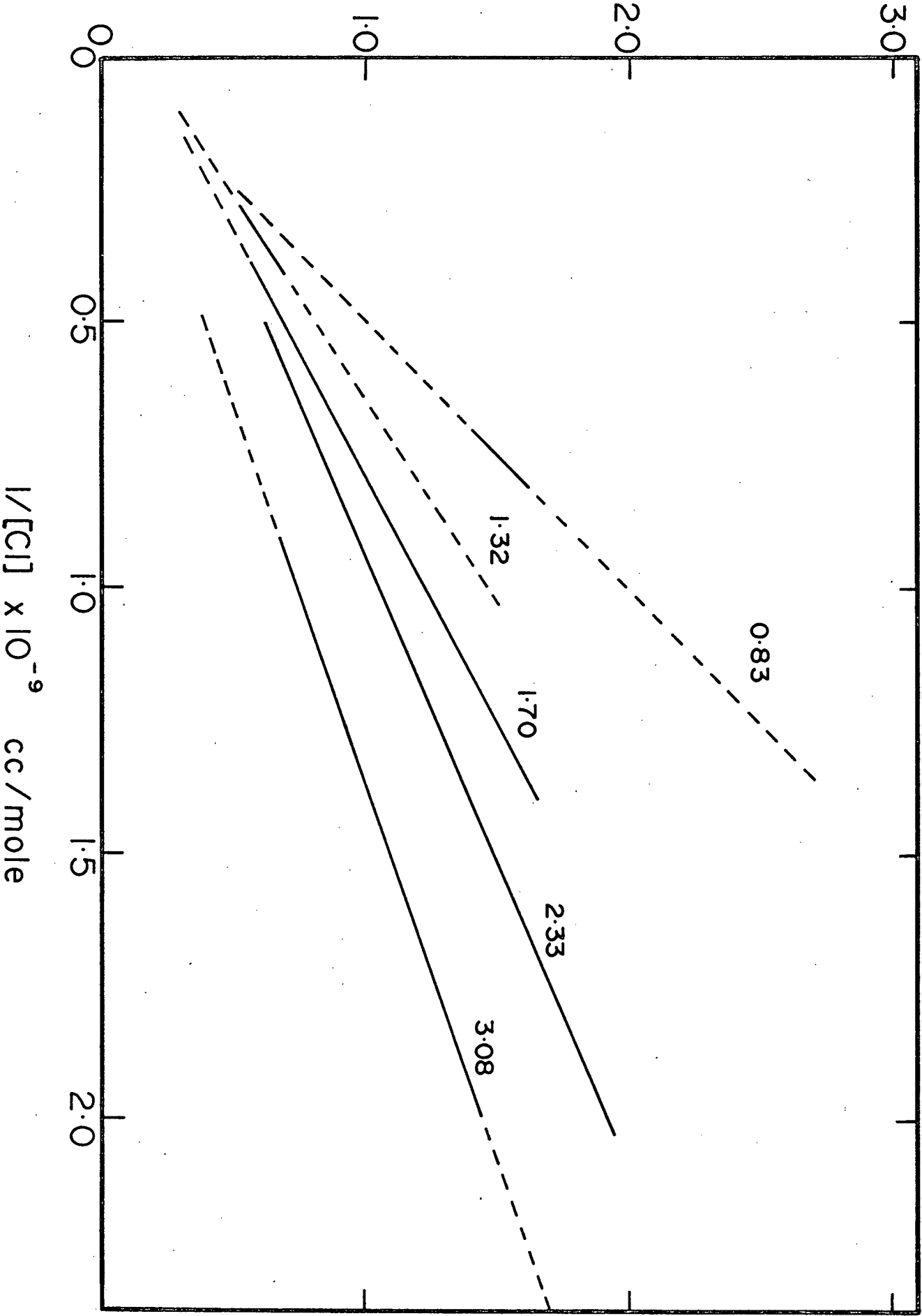


Figure 26. Plot of  $k_{app}^{TOTAL}$  vs.  $1/[Cl]$  for five pressures. Pressures are in torr.

$k_{app}^{TOTAL} \times 10^{-13}$  cc<sup>2</sup>/mole<sup>2</sup> sec



while the broken lines represent regions obtained by an extrapolation of either set of data. The error in the rate constants caused by neglecting the emission beyond  $12000\text{\AA}$  is less than 5%.

#### Estimation Of Error In The Rate Constants

In evaluating the emission rate constants for the chlorine and bromine afterglows, the largest source of error is in the value of  $k_s$ , the rate constant for the standard emission. Schiff et al (9) report this value within an accuracy of 30%. The error in the measurement of atom concentrations is 2% for chlorine atoms and around 5% for bromine atoms. Other errors such as those caused by changes in photomultiplier sensitivity are difficult to evaluate but probably do not contribute more than 5%. Therefore, we estimate that the values of  $k_{app}$  for the chlorine afterglow are accurate to within 40% while those for the bromine afterglow are within 50%.

## DISCUSSION

There were two major questions towards which this investigation of the emission from halogen atom recombination was directed: (1) what fraction of the total recombination occurs via electronically excited states, and (2) what part do elementary processes such as vibrational relaxation and electronic quenching play in the recombination luminescence. The former question can be answered from a knowledge of the absolute rate constants for the emission without making any assumptions about the mechanism of the reaction. The latter question demands a more detailed knowledge of the kinetics of the emission and of the energetically favourable states which are available for population.

The molecule for which the most detailed information about electronic states is available is iodine, but we were unable to make kinetic measurements on the iodine afterglow. On the other hand, our most accurate kinetic results were obtained for chlorine, but relatively little is known about its electronic states. Intermediate between these two cases is bromine, for which two electronically excited states are well known, and for which fairly complete kinetic data has been obtained.

Contribution Of Two Body Radiative Recombination  
To The Halogen Afterglows

Two body recombination into a repulsive state, or the repulsive portion of a bound state, may give rise to continuous emission. This process might be expected to be important if the radiative lifetime of such a state is short and emission from bound levels is prevented. The latter situation could arise because of slow termolecular recombination, rapid redissociation, quenching of the bound states or some combination of these conditions.

In atom recombination studies at high pressure and temperature such as are produced in shock tube experiments, continuous emission has been found to predominate over banded emission, the latter arising from three-body recombination. Although in the present work the predominant emission was banded, it was necessary to investigate the possibility that continuous emission could be making a sizable contribution to the total intensity.

Since no experimental technique of separating a continuum from the banded spectrum could be devised, it was necessary to calculate theoretically the contribution which might be expected. To do this, we have used the expressions derived by Palmer (52) for the population of the repulsive region of an excited state and applied these to the cases of two body radiative recombination in chlorine and bromine.

## (a) Chlorine

The two body process in chlorine may be represented in the following equations:



$$I = k_3 [\text{Cl}_2^*] = \frac{k_3 k_1}{k_2} [\text{Cl}]^2 = k_3 K^*(r) [\text{Cl}]^2. \quad (35)$$

The equilibrium constant  $K^*(r)$  relates the concentration of atoms to the concentration of  $\text{Cl}_2^*$  molecules having an internuclear separation from  $r$  to  $r + dr$ . For each accessible excited state there will be an equation 35, and the total intensity would then be the sum of the contributions from all of these states.

In the case of chlorine, population of the repulsive portion of the  ${}^3\Pi_{o+u}$  state and subsequent radiation would give rise to emission at wavelengths below  $4500\text{\AA}$ . Since the spectrum of discharged chlorine was not observed to extend below  $5000\text{\AA}$ , we conclude that this state cannot be a source of continuous emission. The only remaining state with a sufficiently short radiative lifetime is the  ${}^1\Pi_{1u}$ , for which the lower energy portion of the potential curve is not accurately known. However, based on the potential curve as drawn in figure 1, a rough calculation can be made. The equilibrium constant  $K^*(r)$ , for a homonuclear

diatomic molecule, has been given by Palmer:

$$K^*(r) = 2\pi r^2 (g^*/g_x g_y) e^{-U^*(r)/kT} dr.$$

In this equation,  $g^*$  is the statistical weight of the excited state,  $g_x$  and  $g_y$  are the statistical weights of the atomic states and  $U^*(r)$  is the energy of the state, at internuclear separation  $r$ , above the energy of the free atoms.  $dr$  is fixed by the spectral slit width of the monochromator and is determined from the potential energy diagram as is  $U^*(r)$ . To determine, for example, the rate of two body emission in a band at  $6500\text{\AA}$  and for a spectral slit width of  $120\text{\AA}$ , the following values are obtained:  $dr = 0.02\text{\AA}$ ,  $r = 2.41\text{\AA}$ ,  $U^*(r) = 2253 \text{ cm}^{-1}$ , and  $K^*(r) = 6.3 \times 10^{-6} \text{ cm}^3 \text{ mole}^{-1}$ . Taking Palmer's (19) value of  $\sim 2$  microseconds for the radiative lifetime of the  ${}^1\Pi_{1u}$  state of  $\text{Cl}_2$ , we calculate  $k_3 K^*(r) = 3.2 \text{ cc mole}^{-1} \text{ sec}^{-1}$ . This is equivalent to a termolecular reaction with  $k = 2.0 \times 10^7 \text{ cc}^2 \text{ mole}^{-2} \text{ sec}^{-1}$  at a pressure of 3.03 torr, and this is several orders of magnitude smaller than the rate constant for the experimentally observed process (typically around  $10^{10} \text{ cc}^2 \text{ mole}^{-2} \text{ sec}^{-1}$  in a  $120\text{\AA}$  band centred at  $6500\text{\AA}$ ). Similarly, for emission at  $7500\text{\AA}$ ,  $K^*(r)k_3/[\text{Cl}_2] = 7.4 \times 10^7 \text{ cc}^2 \text{ moles}^{-2} \text{ sec}^{-1}$ . From these calculations, we conclude that the contribution to the total emission intensity from two-body radiative processes is negligible. It should be

pointed out, however, that the values obtained for  $K^*(r)$  are very sensitive to changes in the shape and position of the  $\text{Cl}_2(^1\Pi_{1u})$  state. Since the low energy portion of this state has never been directly observed, its position and point of crossing of the  $^3\Pi_{0+u}$  state are the subject of some conjecture. We have drawn the  $^1\Pi_{1u}$  to cross the  $^3\Pi_{0+u}$  between the thirteenth and fourteenth vibrational levels, following Bader and Ogryzlo (34) who observed no emission originating in levels greater than  $v' = 13$  in the spectrum of discharged  $\text{Cl}_2$ . It was therefore postulated that the levels above the thirteenth were being predissociated by a crossing state, assumed to be the  $^1\Pi_{1u}$ . Bader and Ogryzlo's argument in favour of locating the  $^1\Pi_{1u}$ , based on a perturbation of the rotational levels at  $v' = 14$ , has largely been discounted (50) by the fact that such discontinuities in the Br values are probably experimental in origin. If the  $^1\Pi_{1u}$  were relocated to cross the  $^3\Pi_{0+u}$  at around  $v' = 8$ , the calculated contribution to the total intensity from the continuum becomes sizable. At  $7500\text{\AA}$  for example,  $I_{\text{cont}}/I_{\text{bands}} = 0.72$ . Although measuring an underlying continuum presents many experimental difficulties, it would be expected that a continuum of this intensity could be observed, especially at longer wavelengths where band overlap is minimal. For this reason we conclude that the  $^1\Pi_{1u}$  state must cross above the eighth vibrational level of the  $^3\Pi_{0+u}$  state.

## (b) Bromine

Similar considerations apply in the case of bromine. If continuous emission arises from molecules on the repulsive portions of the  $^3\Pi_{O+u}$  or the  $^3\Pi_{1u}$  states, such emission would be detected at wavelengths shorter than  $5100\text{\AA}$  and  $6350\text{\AA}$  respectively. Since the observed intensity is effectively zero at  $6000\text{\AA}$ , contributions from these sources must be negligible. Therefore, continuous emission is possible only from the repulsive  $^1\Pi_{1u}$  state. The radiative lifetime of this state has not been measured, but since we are concerned here with estimating the maximum possible radiation from two-body recombination, we will place a lower limit of  $10^{-6}$  sec. on its value. For a pressure of 0.92 torr, we calculate  $K^*(r)k_3/[\text{Br}_2] = 2 \times 10^{11} \text{cc}^2 \text{mole}^{-2} \text{sec}^{-1}$  for emission at  $8500\text{\AA}$ . This latter rate constant is less by a factor of 100 than the experimentally determined rate constant for a band centred at  $8500\text{\AA}$  ( $k_{\text{exp}} = 1.2 \times 10^{13} \text{cc}^2 \text{mole}^{-2} \text{sec}^{-1}$ ). Since the position of the  $^1\Pi_{1u}$  state is more firmly established in the case of bromine (53) than chlorine, and in view of the fact that we have taken a lower limit for the lifetime of the  $^1\Pi_{1u}$  state, we can be more confident here that any underlying continuum is contributing a negligible amount to the total intensity.

### The Iodine Afterglow

In view of the known and calculated potential energy curves shown in figure 3, the iodine afterglow most likely originates from the  $^3\Pi_{1u}$  state of  $I_2$ . The energy difference between the  $^2P_{1/2}$  and  $^2P_{3/2}$  states in iodine is  $7616\text{ cm}^{-1}$ . This splitting is far too large to allow for any population of the  $^3\Pi_{0+u}$  state, either by thermal excitation, or inverse predissociation via one of the repulsive states correlating with ground state  $^2P_{3/2}$  atoms. Also, the short radiative lifetime of the  $^3\Pi_{0+u}$  state ( $7 \times 10^{-7}\text{ sec}$ ) (54) precludes its origin in the discharge. Thus we would expect to see only the  $^3\Pi_{1u}$  state, and the fact that the afterglow extends from  $0.8\mu$  to beyond  $2.3\mu$  (figures 16 and 17) substantiates this assignment. The maximum of the emission appears to be at  $1.25\mu$  which corresponds to a vertical transition from  $v' = 3$  to  $v'' = 19$ .

### The Origin Of The Bromine Afterglow

Gibbs and Ogryzlo (49) have measured some of the band heads in the spectrum of discharged bromine between  $6200\text{Å}$  and  $8300\text{Å}$  in the pressure range of 0.5 to 2.5 torr. They identified four series of bands originating in the 0, 1, 2, 3 levels of the  $^3\Pi_{0+u}$  state and in addition, mentioned several bands appearing further into the red which they were unable to identify.

In the present study of the emission between  $6850\overset{\circ}{\text{Å}}$  and  $12000\overset{\circ}{\text{Å}}$  we have identified bands originating in the 0, 1, 2 levels of the  ${}^3\Pi_{\text{O}+\text{u}}$  states, but not from  $v' = 3$ . A large number of bands in this region, however, have been assigned to the  ${}^3\Pi_{1\text{u}} \longrightarrow {}^1\Sigma_{\text{g}}^+$  transition with most of the emission arising from  $v' = 5$  to  $v' = 14$  of the excited state.

Identification of the transitions giving rise to the bands beyond  $9000\overset{\circ}{\text{Å}}$  poses a special problem. It has already been mentioned that these bands are probably the result of the overlapping of a number of transitions. Since the resolution of the monochromator is quite low in this region, the contributing bands cannot be separated. In a recent study of the rotational fine structure of nine bands in the  ${}^1\Sigma_{\text{g}}^+ \longrightarrow {}^3\Pi_{1\text{u}}$  system of bromine (in absorption), Horsley (45) calculated the equilibrium internuclear distance for the  ${}^3\Pi_{1\text{u}}$  state to be  $2.55\overset{\circ}{\text{Å}}$ . This value is somewhat lower than has been predicted (44) and leads to a further complication in the identification of the infrared bands in the emission spectrum. The predicted Franck-Condon maximum for emission from the  $v' = 0$  level of the  ${}^3\Pi_{1\text{u}}$  state, based on this new value of the internuclear distance, is at  $10700 \text{ cm}^{-1}$  (0-12), while emission from the  $v' = 0$  level of the  ${}^3\Pi_{\text{O}+\text{u}}$  is expected to be a maximum at  $10400 \text{ cm}^{-1}$  (0-17). Spectra recorded at high pressure have a maximum intensity at around  $10,500\overset{\circ}{\text{Å}}$  as would be expected

if vibrational relaxation were populating the zero vibrational level of the excited states. However, because of the similarity of the Franck-Condon factors in this region, it is difficult to determine whether or not emission from one state is predominant. The fact that the vibrational level spacing of the  $^3\Pi_{1u}$  state below  $v' = 8$  is uncertain makes assignments in this region even more difficult.

Decreasing the total pressure and increasing the atom concentration shifts the maximum emission intensity to higher energy. This is consistent with a decrease in vibrational relaxation causing emission predominantly from higher vibrational levels. At the lowest pressure at which the afterglow spectrum was recorded (0.3 torr), the true spectral distribution (figure 13) shows the maximum intensity occurs at around  $13050 \text{ cm}^{-1}$ . In this region, emission from the  $^3\Pi_{0+u}$  state originates in the first and second vibrational levels. The most intense band from  $v' = 2$  is predicted to be the (2, 10) transition which occurs at  $13051 \text{ cm}^{-1}$ . It thus appears that at low pressures the population of the  $^3\Pi_{0+u}$  may be approaching an initial distribution, if as Gibbs and Ogryzlo (49) suggest, the recombination into this state occurs via the  $^1\Pi_{1u}$  state. This state is assumed to intersect the  $^3\Pi_{0+u}$  potential curve in the location of the third vibrational level (53), so that recombination into the repulsive  $^1\Pi_{1u}$  state, followed by a collision induced crossing to the bound

$^3\Pi_{o+u}$  state, would favour formation into the second and third vibrational levels. However, just how large a contribution to the total radiative recombination scheme is made by formation into the  $^3\Pi_{o+u}$  state is uncertain, since we cannot estimate the fraction of the total emission originating in this state.

In a study of the spectrum of discharged bromine carried out concurrently with the present work, Clyne and Coxon (48) identified a large number of bands, most of which they assigned to the  $^3\Pi_{1u} \rightarrow ^1\Sigma_g^+$  transition. We have observed many of the same bands reported by these authors. However, our results differ in the assignment of bands to the  $^3\Pi_{o+u}$  state. Clyne and Coxon have identified the following series:

$^3\Pi_{o+u}$	v' = 0	1	2
$^1\Sigma_g^+$	v'' = 1 to 4	v'' = 2 to 8	v'' = 2 to 8

Reference to figure 2 shows that these bands should be relatively weak since they occur at significantly higher energies than the predicted Franck-Condon maxima for each level. However, no assignments to these levels have been made in the spectral regions where the maximum intensity would be expected.

Clyne and Coxon found that many bands beyond  $8000\text{\AA}$  could not be reconciled with Darbyshire's (44) vibrational analysis of the "extreme red" ( $^3\Pi_{1u} \rightarrow ^1\Sigma_g^+$ ) system and its

infrared extension. Beyond  $8000\overset{\circ}{\text{A}}$  marked deviations between the observed and predicted wave numbers began to appear, and this forced them to conclude that either Darbyshire's vibrational assignments were in error, or a new band system was beginning to appear in this region. In earlier studies of the absorption spectrum of bromine, Darbyshire (44) and Brown (47) did not observe transitions below  $v' = 6$  and, thus, a rather long extrapolation was necessary to obtain the value of  $\omega'_e$ . Because reasonable doubt as to the position and spacing of the low vibrational levels of this state does exist, Clyne and Coxon (48) chose to interpret the bands beyond  $8000\overset{\circ}{\text{A}}$  as an extension of the  ${}^3\Pi_{1u} \rightarrow {}^1\Sigma_g^+$  system. This required a modification of Darbyshire's original analysis which involved reassigning three bands and dropping five others, allowing a smooth continuation from the bands observed in absorption to Clyne's new bands. The new spectroscopic constants were then calculated for the  ${}^3\Pi_{1u}$  state yielding  $\omega'_e = 153 \pm 2 \text{ cm}^{-1}$  which is much lower than the original  $170.7 \text{ cm}^{-1}$  calculated by Darbyshire.

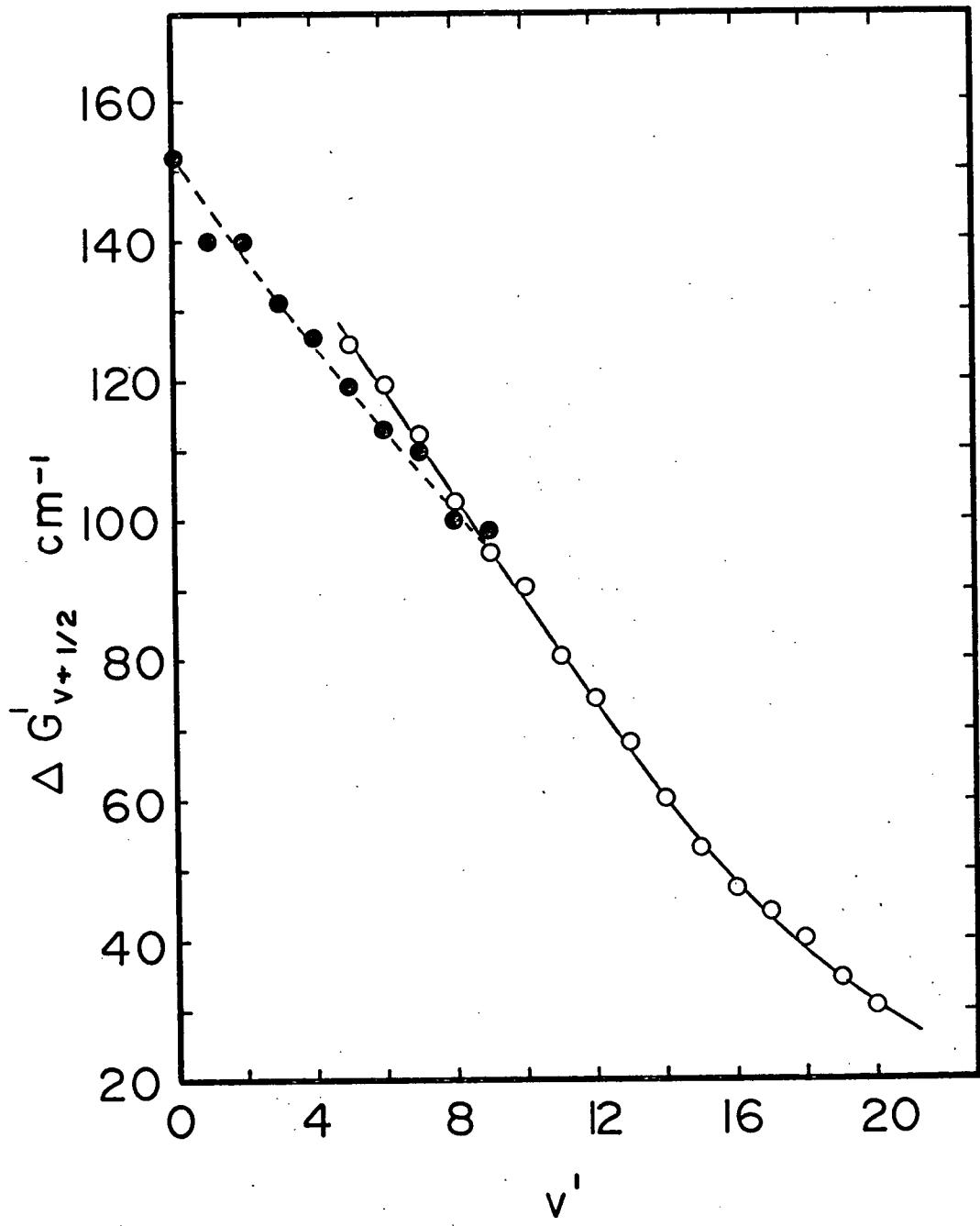
Our observations on the infrared bands suggest that this procedure is justified, but there are a number of inconsistencies in the work of Clyne and Coxon. Calculations of the vibrational energy levels using these new constants are in fair agreement with the observed transitions up to around the tenth vibrational level, but for higher levels deviations become quite large. The (17-3) transition, for

example, is calculated to appear at  $14635 \text{ cm}^{-1}$  while it actually is located (45) at  $14559 \text{ cm}^{-1}$ . The cause of this discrepancy can be understood by plotting the values of  $\Delta G'(v + 1/2)$  against  $(v' + 1/2)$  ie. the vibrational energy spacing vs. vibrational number (figure 27). Using Clyne's results together with those of Darbyshire (44) and Brown (47), this curve exhibits a region of positive curvature at high vibrational numbers, a sharp point of inflection at  $v' = 9$ , followed by a region of slight negative curvature to  $v' = 0$ . To obtain constants which would be consistent with this type of curve, the data would have to be fitted to an equation containing higher powers of  $(v' + 1/2)$ , ie.  $\omega_e x_e$  and  $\omega_e y_e$  should have been calculated. For this reason Clyne's spectroscopic constants are valid over the range  $v' = 0$  to  $v' = 8$  only.

In the spectral region observed photographically, the lowest level of the  $^3\Pi_{1u}$  observed was the fifth level, so we were unable to confirm Clyne's assignments for the low vibrational levels of this state. The bands which were assigned to the fifth and sixth levels however, did not agree well with either Darbyshire's or Clyne's scheme.

In summary, the emission spectrum of discharged bromine is very complex consisting of a large number of diffuse red-degraded bands. The spectrum does show the following features.

Figure 27. Plot of  $\Delta G'_{v+1/2}$  vs.  $v'$  for the  ${}^3\Pi_{1u}$  state of  $\text{Br}_2$ . Open circles are values of Darbyshire (44) and Brown (47) and closed circles are data of Clyne and Coxon (48).



- (a) Most of the bands identified arise from the  ${}^3\Pi_{1u} \rightarrow {}^1\Pi_g^+$  transition.
- (b) Emission from the 0, 1, 2 levels of the  ${}^3\Pi_{0+u}$  has been observed. High pressures favour emission from the zeroth level, low pressures the second vibrational level.

### Kinetics Of The Bromine Afterglow

Using a photographic technique to measure emission intensity, Gibbs and Ogryzlo (49) studied the dependence of the bromine afterglow intensity on atom concentration and pressure. Fitting their data to the equation

$$I = k[\text{Br}]^n[\text{Br}_2]^m,$$

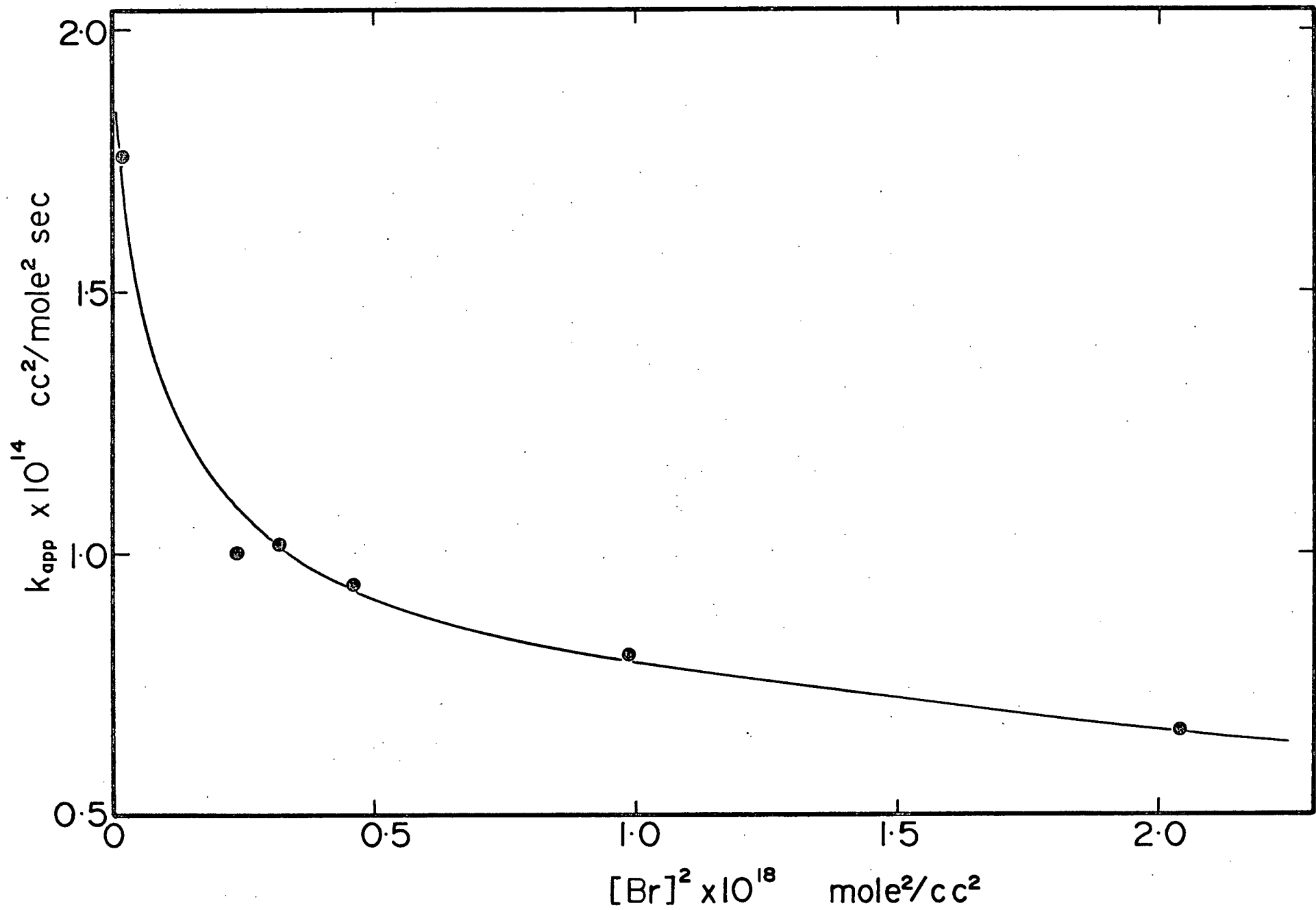
they obtained  $n = 1.9 \pm 0.2$  and  $m = 0.8 \pm 0.2$  and concluded that within experimental error,

$$I = k[\text{Br}]^2[\text{Br}_2].$$

We have determined the value of the light emission rate constant defined by  $k_{\text{app}} = I/[\text{Br}]^2[\text{Br}_2]$ , by measuring the absolute emission intensity of the bromine afterglow. If the kinetic order is that predicted by Gibbs and Ogryzlo, then  $k_{\text{app}}$  should be constant at all values of atom concentration and pressure. This has not been observed to be the case, as is illustrated in figure 28.

This variation of  $k_{\text{app}}$  can be understood by examining the dependence of  $\int I_\lambda d\lambda$  (6000Å to 12000Å) on atom con-

Figure 28. Plot of  $k_{\text{app}}$  vs.  $[\text{Br}]^2$  for a pressure of 0.92 torr.



centration, as shown in Table 8. The integrated emission intensity was found to vary as  $[\text{Br}]^{1.2 \pm 0.2}$  at 0.52 torr, and as  $[\text{Br}]^{1.8 \pm 0.1}$  at 1.82 torr, but was not found to depend on the square of the atom concentration under any of the experimental conditions used.

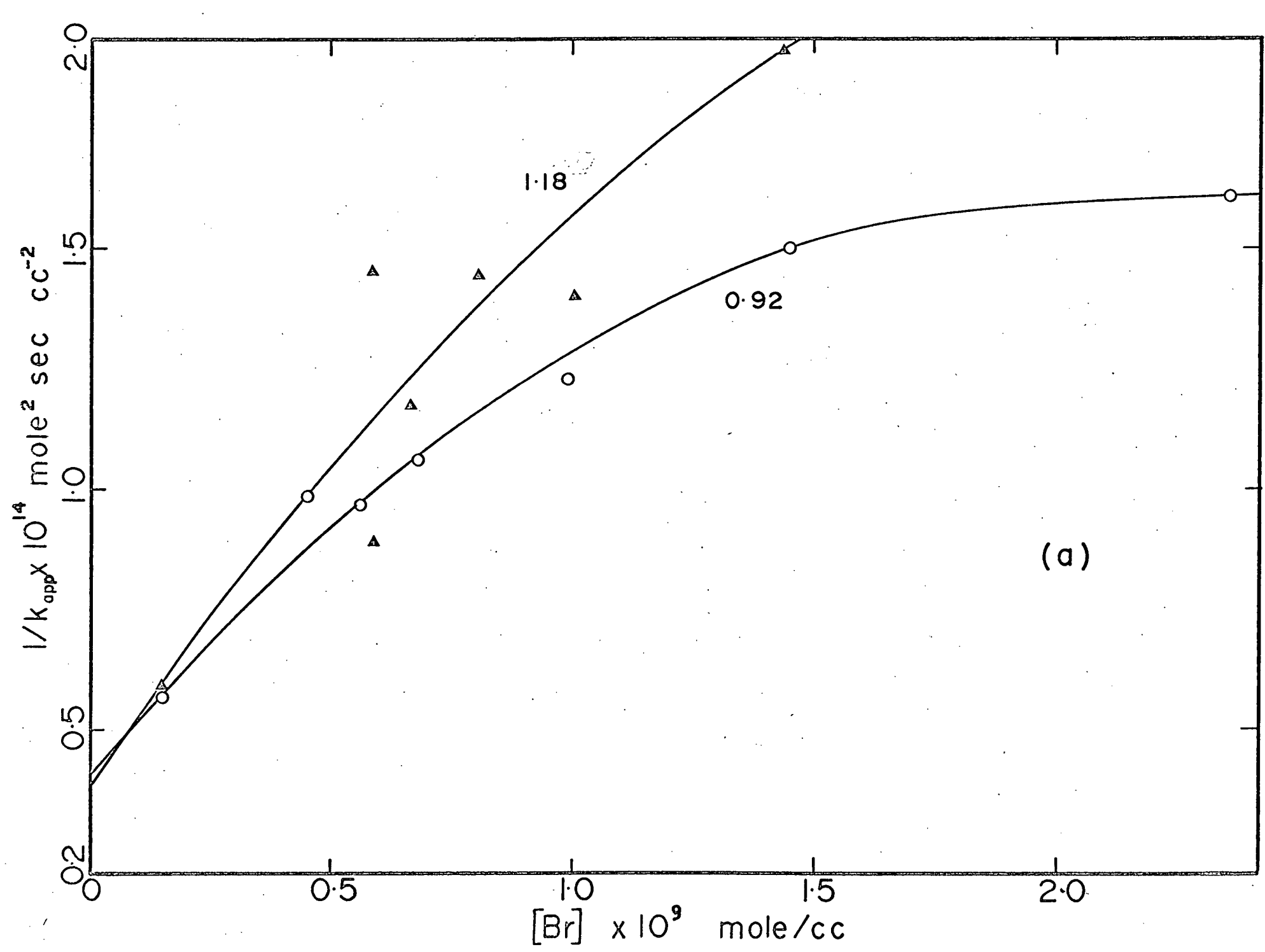
Assuming that the rate of formation of the excited states is second order in atom concentration, the fact that less than a second order dependence was observed for the overall emission process suggests that bromine atoms are involved in quenching the luminescence. Therefore, in order to obtain the rate of emission in the absence of atom quenching, we must evaluate  $k_{\text{app}}$  at very low  $[\text{Br}]$ . We have plotted  $1/k_{\text{app}}$  against  $[\text{Br}]$  in figure 29 and extrapolated to zero atom concentration. The most reliable intercepts will be obtained from figure 29(b) since the atom concentration range of these data is less by an order of magnitude than that of figure 29(a). The values of rate constants at zero  $[\text{Br}]$ , obtained at pressures of 0.53 and 1.50 torr, are  $k_{\text{app}} = 0.4 \times 10^{16} \text{cc}^2 \text{mole}^{-2} \text{sec}^{-1}$  and  $k_{\text{app}} = 2.0 \times 10^{16} \text{cc}^2 \text{mole}^{-2} \text{sec}^{-1}$  respectively. Comparing these rates with the value of  $13 \times 10^{16} \text{cc}^2 \text{mole}^{-2} \text{sec}^{-1}$  obtained for the overall rate of recombination using  $\text{Br}_2$  as a third body (37), we find that between 3 and 15% of the total recombination takes place into electronically excited states.

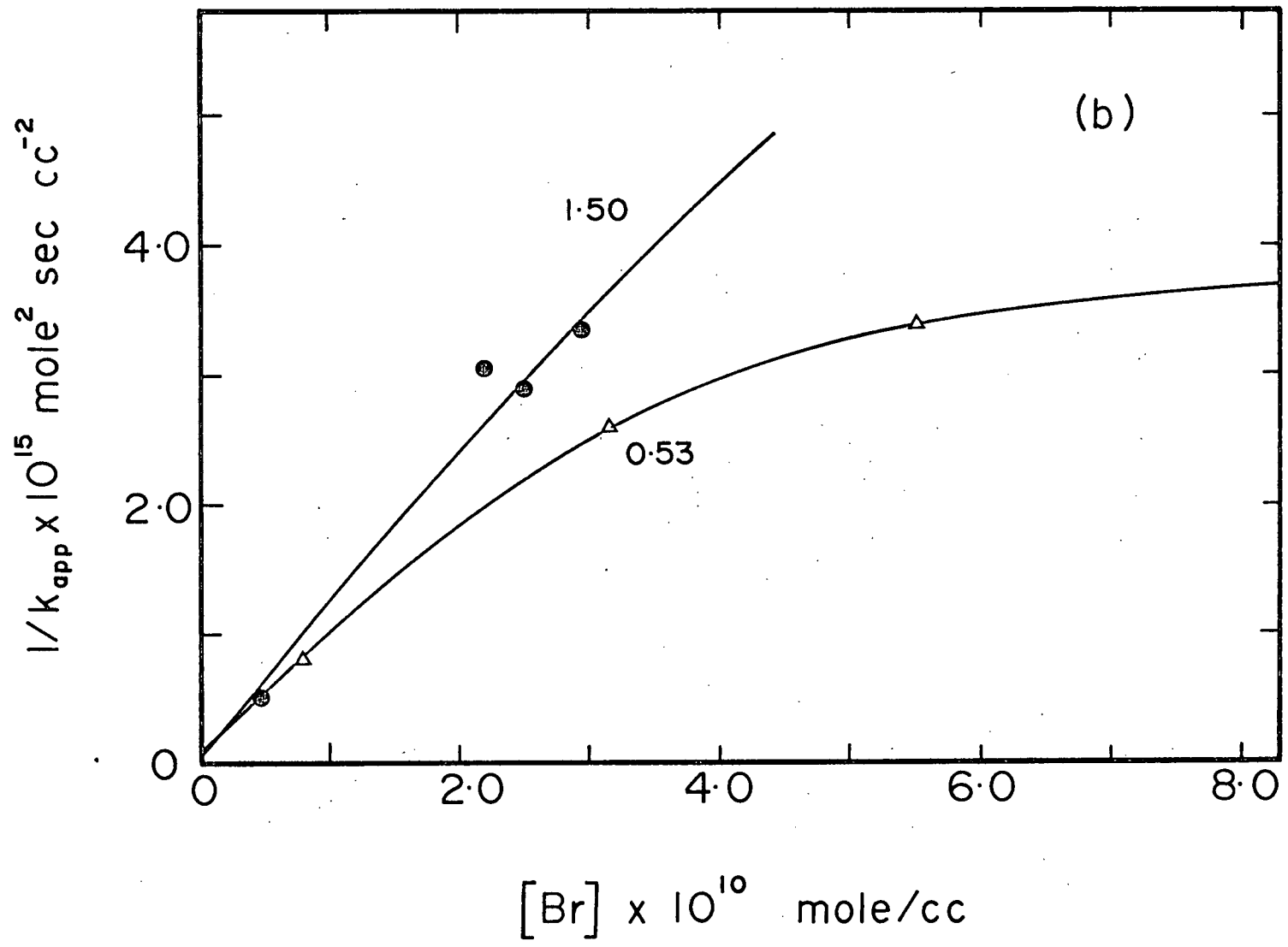
In view of our study of the emission intensity at various wavelengths as a function of atom concentration

Figure 29. Plots of  $1/k_{app}$  vs.  $[Br]$  for four values of pressure:

(a)  $\circ$  0.92 torr and  $\blacktriangle$  1.18 torr

(b)  $\triangle$  0.53 torr and  $\bullet$  1.50 torr.





(Table 5), we can now suggest a possible explanation for the results obtained by Gibbs and Ogryzlo. The technique used by these authors to measure emission intensity involved photographing the afterglow, and then relating the optical density of the film to intensity. The photographic film used was sensitive only to  $8800\text{\AA}$ , so that the long wavelength radiation was not recorded. Reference to Table 5 shows that it was at these shorter wavelengths that close to a second order dependence on [Br] was observed, and this led the authors to suggest that  $I \propto [\text{Br}]^2$ .

Our results on the pressure dependence of the integrated intensity indicate that some process involving bromine molecules is also quenching the luminescence. Although these data are subject to considerable error, they show a less than first order dependence of the rate of emission on the pressure.

#### Mechanism Of The Emission Reaction

##### (a) Formation Of Excited States In The $\text{Br}_2$ Afterglow

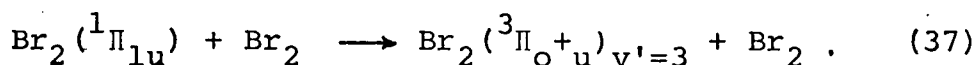
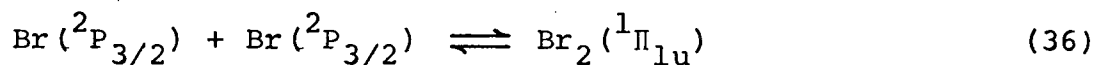
Unlike the iodine afterglow, in which all the emission originates in the  $^3\Pi_{1u}$  state, two electronically excited states are involved in the bromine emission. These states are the  $^3\Pi_{1u}$ , which correlates with two ground state  $^2P_{3/2}$  atoms, and the  $^3\Pi_{o+u}$ , which correlates with one ground state  $^2P_{3/2}$  and one excited  $^2P_{1/2}$  atom (figure 2).

The direct formation of the  $^3\Pi_{o+u}$  state from one excited and one ground state atom does not appear to be a

favourable process because of the low concentration of  ${}^2P_{1/2}$  atoms in the gas stream. The equilibrium concentration of the excited atom is expected to be very small (48)  $[I^2P_{1/2}]/[I^2P_{3/2}] \sim 1 \times 10^{-8}$  at  $300^\circ\text{K}$ ) due to the large energy difference between the  ${}^2P_{3/2}$  and  ${}^2P_{1/2}$  atomic states. Recent flash photolysis studies (55) have shown that molecular bromine is very efficient at causing spin-orbit relaxation of  ${}^2P_{1/2}$  atoms. For this reason, excited atoms formed in the discharge would be extremely short lived and could not be considered as a possible source of the  ${}^3\Pi_{O+u}$  state.

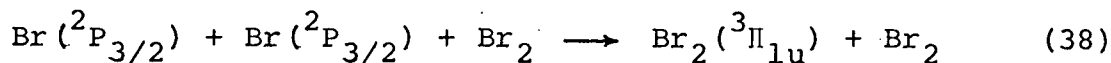
Gibbs and Ogryzlo (49) suggested an alternative mechanism by which the  ${}^3\Pi_{O+u}$  state could be populated. This involved the formation of an intermediate state, correlating with ground state atoms, which could then undergo a collision-induced transition into the emitting state. The two possible electronic states which could fulfill this role are the  ${}^3\Pi_{O-u}$  which is predicted to intersect the  ${}^3\Pi_{O+u}$  at small values of internuclear distance (34), and the  ${}^1\Pi_{1u}$ , which is assumed to cross at about the third vibrational level of the  ${}^3\Pi_{O+u}$  (53). Our observations on the afterglow spectrum indicate that the population of the  ${}^3\Pi_{O+u}$  state takes place into the second or third vibrational levels, since at low pressures the maximum emission originates from  $v' = 2$ . This evidence, together with the fact that emission from levels higher than  $v' = 3$  has never

been observed, suggests that the  ${}^1\Pi_{1u}$  is the intermediate state in the formation of the  ${}^3\Pi_{o+u}$ . The  ${}^3\Pi_{o-u}$  state, on the other hand, would be expected to populate a much wider range of vibrational levels at, or below, the dissociation limit. Therefore, we propose the following mechanism for the formation of the  ${}^3\Pi_{o+u}$  state:



Any alternative mechanism, such as one involving  $\text{Br}_3$  or a simple termolecular collision, would be expected to populate chiefly the zeroth vibrational level of the  ${}^3\Pi_{o+u}$  state, since this is the only level which lies below the dissociation limit of ground state atoms.

The formation of the  ${}^3\Pi_{o+u}$  state in the third vibrational level (equation 37) would involve a fairly large activation energy since this level lies  $430 \text{ cm}^{-1}$  above the energy of two ground state atoms. The formation of the  ${}^3\Pi_{1u}$  state, on the other hand, should involve no activation energy.

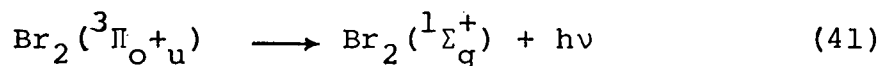
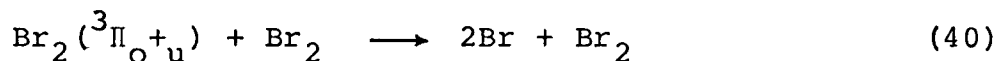
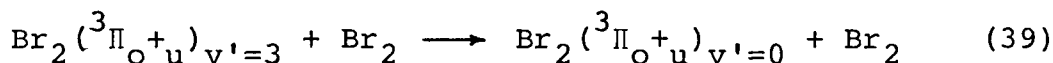


Since it has not been possible to separate the contributions to the total emission from each of these states, it is not possible to state unequivocally which is predominant. However, considering the activation energy required to form

the  ${}^3\Pi_{0^+u}$  state, and the large number of bands which we have assigned to the  ${}^3\Pi_{1u}$  state, it would appear that the latter is more important in the recombination process.

(b) Relaxation Processes In The Excited States

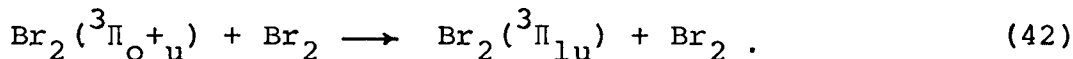
Following the formation of the  ${}^3\Pi_{0^+u}$  state, the molecule may radiate, redissociate, or be vibrationally relaxed to the zeroth and first vibrational levels:



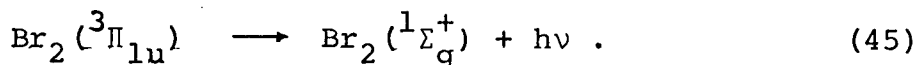
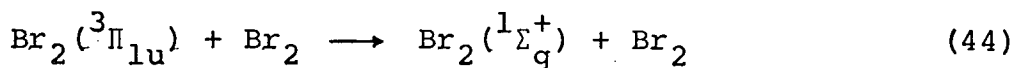
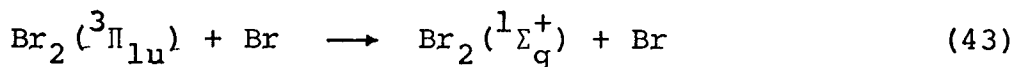
Vibrational relaxation would most probably occur one quantum at a time and thus equation (39) represents the results of a number of collisions. Since we observe a less than first order pressure dependence for the total emission, some process involving  $\text{Br}_2$  must be removing excited molecules. In the  ${}^3\Pi_{0^+u}$ , this would most probably occur through the dissociation shown in equation (40), this being the reverse of the formation process.

There may be another process by which the  ${}^3\Pi_{0^+u}$  state is relaxed and that is by a collision induced crossing to the  ${}^3\Pi_{1u}$ . If quenching by  $\text{Br}_2$  is effective in the upper state, there is no reason for assuming that deactivation directly to the ground state occurs. In fact, Franck-Condon factors and symmetry considerations (56) would

probably favour a conversion to another component of the  $^3\Pi$  state. Thus, we include the following reaction:



The radiative lifetimes of these two excited states of bromine have not been measured. We assume, however, that the radiative lifetime of the  $^3\Pi_{0+u}$  state of bromine lies between the lifetimes of the equivalent states in iodine and chlorine, or around  $10^{-6}$  sec. On the other hand, calculations based on the theoretical work of Mulliken (15) indicate a radiative lifetime of the  $^3\Pi_{1u}$  state of  $10^{-4}$  sec. It would be expected that processes leading to the deactivation of the excited states would be more effective for the  $^3\Pi_{1u}$  state, since these processes would be competing with spontaneous emission. We propose that the relaxation of the  $^3\Pi_{1u}$  state is the result of the following reactions:



Throughout the  $^3\Pi_{1u}$  electronic state, the energy interval between adjacent vibrational levels is less than  $kT$  at room temperature (44). It is known theoretically that when energy levels are this closely spaced, the probability of collision-induced transitions between them becomes very

high (57). Excited iodine molecules, which have vibrational spacings very similar to these excited bromine molecules, were found to undergo vibrational transitions at practically every collision (58). Thus, rapid vibrational relaxation of this state of bromine would be expected, and Tiffany (59) has suggested that no more than 100 collisions would be necessary to reach vibrational and rotation equilibrium. This is consistent with our observation that at high pressures, the maximum emission occurs at  $9400\overset{\circ}{\text{Å}}$ . Although we have assigned some of the bands in this region to the  $(0, v'')$  transitions of the  ${}^3\Pi_{o+u} \rightarrow {}^1\Sigma_g^+$  system, this wavelength also corresponds to the predicted Franck-Condon maximum from the zeroth level of the  ${}^3\Pi_{1u}$  state, which is undoubtedly contributing to the total intensity.

The measurement of the variation of  $1/k_{app}$  with atom concentration and pressure is consistent with the above mechanism. Although the data contain a large amount of scatter, they do show three trends. First of all, the value of  $k_{app}$ , the rate constant for the total emission, decreases with increasing atom concentration indicating that quenching by atoms does occur. Secondly, the slope of the  $1/k_{app}$  vs.  $[\text{Br}]$  plots (figure 29) increases with increasing pressure. This is explained qualitatively by a collision induced crossing from the  ${}^3\Pi_{o+u}$  to the  ${}^3\Pi_{1u}$  (equation 42), followed by a quenching by atoms which is expected to be more efficient in the latter state. The

third observation which we can make about these  $1/k_{app}$  vs. [Br] plots is that they are curved and that they appear to flatten out at high values of [Br]. This flattening out would correspond to a "steady state" being reached between the collision induced crossing to the  $^3\Pi_{1u}$  state and the removal from this state by atomic quenching.

#### Origin Of The Chlorine Emission

All of the emission arising from the recombination of chlorine atoms has been assigned to the  $^3\Pi_{o+u} \rightarrow ^1\Sigma_g^+$  transition. The fact that no bands in the emission spectrum could be attributed to the  $^3\Pi_{1u} \rightarrow ^1\Sigma_g^+$  transition, is consistent with Mulliken's (14) theoretical prediction, and also with recent absorption studies (60).

The observed change in spectral distribution with pressure can be attributed to vibrational relaxation in the emitting state caused by collisions with chlorine molecules. Thus, at low pressures, the emission maximum was observed at  $6700\overset{\circ}{\text{A}}$ , corresponding to radiation from the fourth and fifth vibrational levels of the  $^3\Pi_{o+u}$ . At higher pressures, this maximum was observed to shift until at 3 torr, emission from the zeroth and first vibrational levels predominated.

## Kinetics Of The Chlorine Afterglow

### (a) Order Of Emission Intensity With Respect To [Cl]

In previous investigations of chlorine afterglow (27, 34), the emission intensity was found to vary as the square of the atom concentration and the first power of the third body concentration. For Cl<sub>2</sub> as a third body, the rate equation then becomes

$$I = k[\text{Cl}]^2[\text{Cl}_2] \quad (46)$$

We have determined the value of the light emission rate constant, as defined in equation (46), for a number of values of [Cl<sub>2</sub>] and [Cl] over the range 5000Å to 12000Å. When this rate constant was plotted against [Cl]<sup>2</sup>, as in figure 30, its value was observed to increase sharply at low values of [Cl]<sup>2</sup>. Since the formation of the excited state must proceed via a termolecular reaction, this apparent change in order with respect to chlorine atom concentration indicates a quenching of the luminescence by atoms. Therefore, to find the rate of recombination into the <sup>3</sup>Π<sub>o</sub>+<sub>u</sub> state, we must determine the value of the emission rate constant at very low atom concentration. In figure 31 we have constructed plots of 1/k<sub>app</sub><sup>TOTAL</sup> against [Cl], using the data of figure 26. By extrapolating these curves to zero atom concentration, the average value of k<sub>app</sub><sup>TOTAL</sup> (at [Cl] = 0) was found to be 1.8 x 10<sup>14</sup> cm<sup>6</sup> mole<sup>-2</sup> sec<sup>-1</sup>. Compared to the total rate of recombination,

Figure 30. Plot of  $k_{\text{app}}$  vs.  $[\text{Cl}]^2$  for a pressure of 1.70 torr.

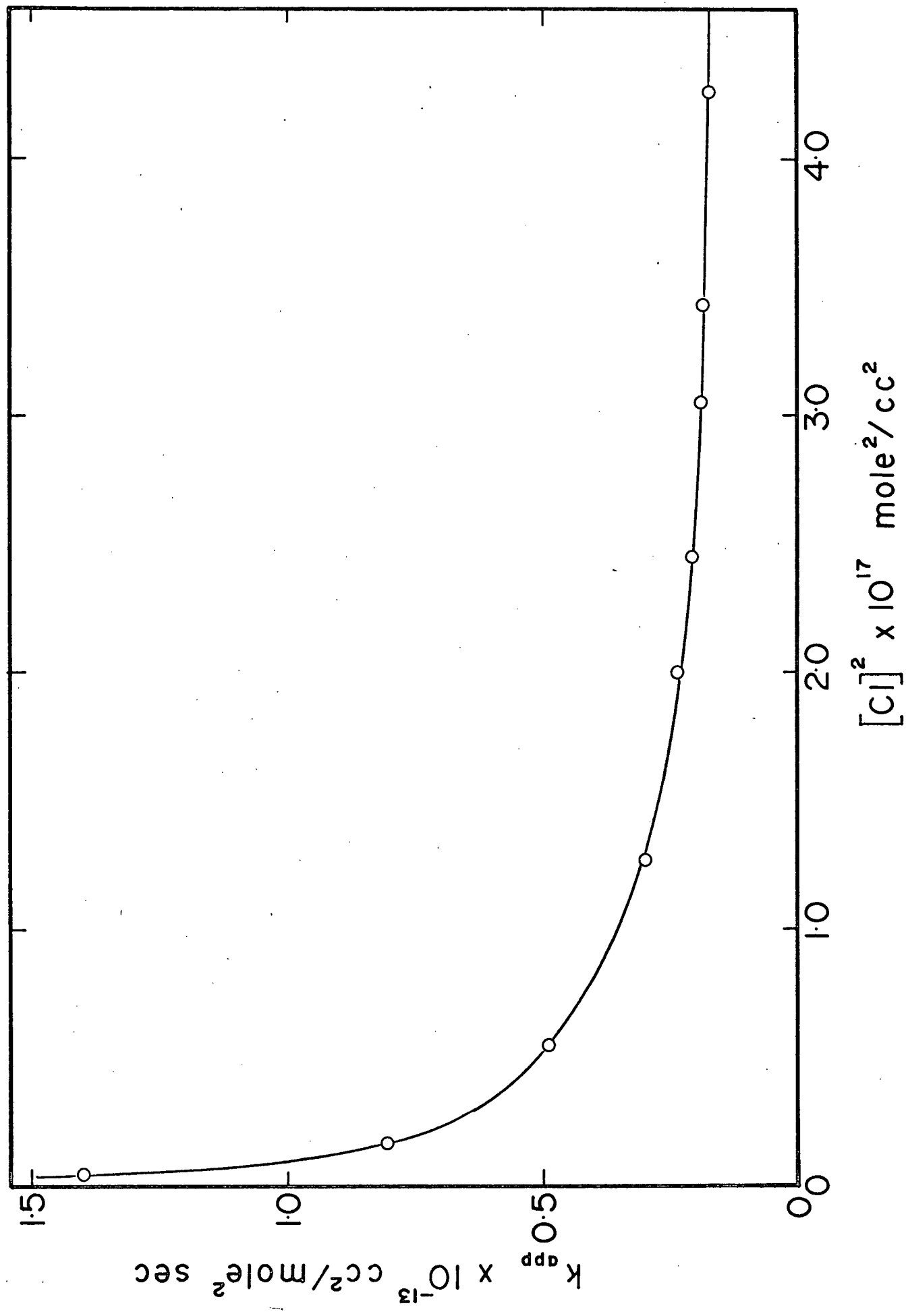
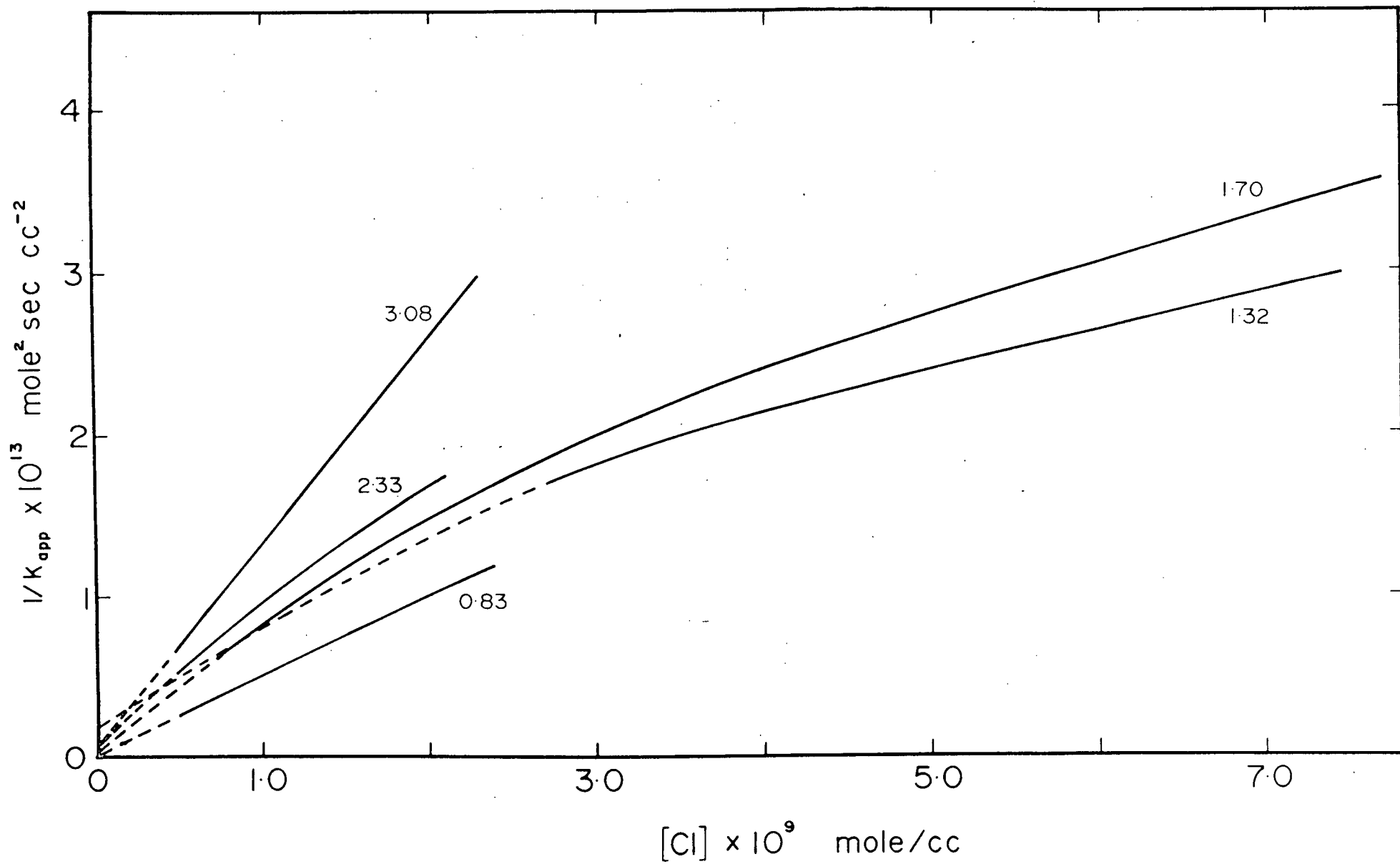


Figure 31. Plots of  $1/k_{app}^{TOTAL}$  vs. [Cl] in the pressure range 0.83 to 3.08 torr. Broken curves obtained by extrapolation.



$k = 2.0 \times 10^{16} \text{ cm}^6 \text{ mole}^{-2} \text{ sec}^{-1}$  (27), this value indicates that 1% of the total recombination takes place into the  $^3\Pi_{0+u}$  state.

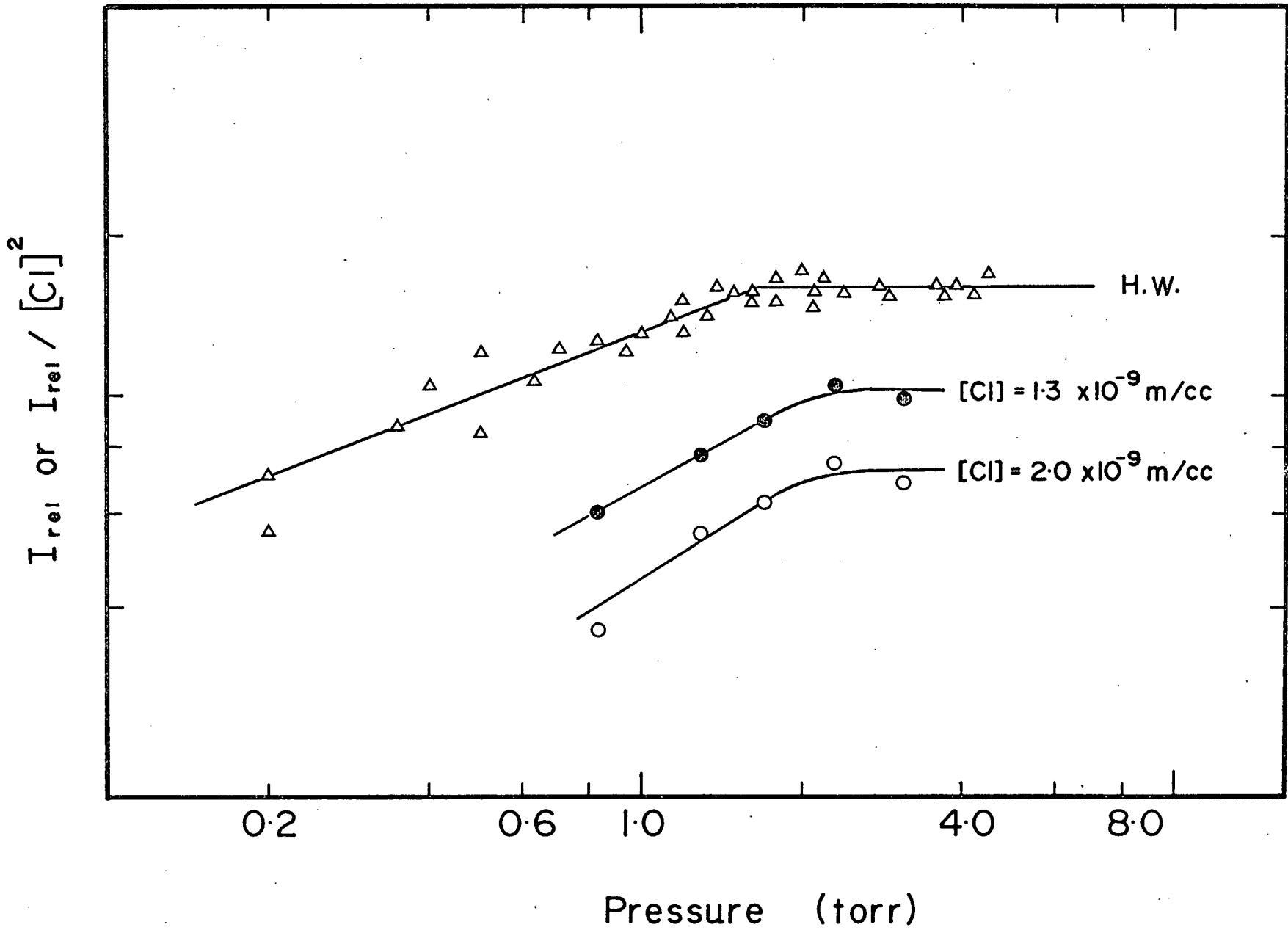
The error made by previous investigators in determining the order of the emission intensity with respect to [Cl] can be attributed to the fact that only the short wavelength region of the afterglow spectrum was studied. We have found a large variation in the dependence of emission intensity on atom concentration over the entire emitting region (see Table 9). At a pressure of 1.70 torr, for example, this dependence decreased from  $I \propto [\text{Cl}]^{2.0 \pm 0.1}$  at  $5500\text{\AA}$  to  $I \propto [\text{Cl}]^{0.9 \pm 0.1}$  at  $10600\text{\AA}$ . In their study of the chlorine afterglow, Bader and Ogryzlo (34) measured intensity using a photographic technique by relating the optical density of the film to emission intensity. Although infrared-sensitive film was used, and a filter eliminated radiation below  $6250\text{\AA}$ , it is possible that much of the emission recorded lay below  $7000\text{\AA}$ . In that case, the infrared portion would not have contributed to the intensity and a second order dependence would have been observed. Our calculation of the integrated emission intensity in the visible region ( $5000\text{\AA} - 6800\text{\AA}$ ) yielded  $I \propto [\text{Cl}]^{1.8 \pm 0.1}$  while Bader's (26) results indicated  $I \propto [\text{Cl}]^{1.9 \pm 0.1}$ . The same explanation could apply to the work of Hutton and Wright (27) who used a photomultiplier having its maximum sensitivity in the visible region.

## (b) Pressure Dependence Of The Emission Intensity

On the question of the dependence of I upon  $[Cl_2]$ , there appears to be a discrepancy between the results of Bader and Ogryzlo and Hutton and Wright. The former workers claim a first power dependence, but their determination was based on experiments performed at only two pressures and no results were obtained at pressures greater than 1.6 torr. Hutton and Wright concluded that the emission intensity was dependent on the molecular chlorine concentration below 2 torr, but above this pressure was independent of  $[Cl_2]$ .

If we assume that in the wavelength range over which Hutton and Wright's intensity measurements were made  $I \propto [Cl]_2^2$ , we can compare our values of intensity at fixed atom concentration with their values of  $I/[Cl]_2^2$ . This has been done in the logarithmic plot of figure 32, where the slope of these curves corresponds to m in the equation  $I = k[Cl]^n[Cl_2]^m$ . Our results are in essential agreement with those of Hutton and Wright, since they indicate a change in kinetic order around 2 torr and show a less than first order dependence below this pressure. The slope of our plots at  $[Cl_2] = 1$  torr gives  $I \propto [Cl_2]^{0.6 \pm 0.1}$ , while Hutton and Wright's results yield  $I \propto [Cl_2]^{0.4}$ . This discrepancy can be attributed to the fact that these workers measured the emission intensity below  $8000\text{\AA}$ , where we observed a lower order dependence on pressure (Table 10 and figure 23). Our measured

Figure 32. Pressure dependence of the chlorine afterglow emission intensity. Results of Hutton and Wright ( $\Delta$ ) plotted as  $I_{\text{rel}}/[\text{Cl}]^2$  vs. P; this work ( $\bullet$  and  $\circ$ ) plotted as  $I_{\text{rel}}$  vs. P.



intensity values include all the emission from 5000Å to 12000Å and are thus expected to indicate a higher overall order in molecular chlorine concentration.

In a preliminary study of the chlorine afterglow emission carried out at the same time as this work, Clyne and Steadman (61) observed a similar behaviour of the intensity with pressure. The intensity in a narrow wavelength band at 5800Å was found to be pressure independent above 1 torr while the intensity in a band at 7800Å was found to be dependent on  $[\text{Cl}_2]$ . These workers were not able to measure total intensities owing to the low sensitivity of their photomultiplier at long wavelengths, but they suggested that the total intensity could be proportional to  $[\text{M}]$  in the pressure range studied. This we have not found to be the case. Clyne and Steadman also examined the effect of using argon as a third body and found that while an overall decrease in intensity was observed, there was no significant difference in intensity distribution between argon and chlorine systems.

#### Mechanism Of The Emission Reaction In Chlorine

##### (a) Formation Of The Emitting State

The chlorine afterglow emission has been shown to originate in the  $^3\Pi_{0+u}$  electronic state of molecular chlorine. Since this state correlates with one ground state  $^2P_{3/2}$  atom and one excited  $^2P_{1/2}$  atom, we are faced

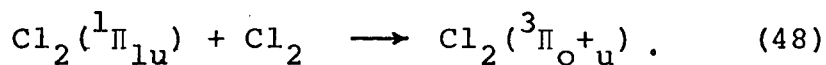
with the problem of how this state is formed in the recombination process.

Direct recombination into the  $^3\Pi_{O_u}$  state by one normal and one excited atom has been suggested by Hutton and Wright (27) on the basis that the small doublet separation of the atoms ( $881\text{ cm}^{-1}$ ) allows a sufficient thermal population of the excited  $^2P_{1/2}$  atomic state. At room temperature, however, only about 0.7% of the atoms are in the excited state.

In recent E.P.R. studies on the discharge products of  $CF_3Cl$  and mixtures of  $CF_3Cl$  and  $Cl_2$ , Carrington et al (62) detected signals corresponding to the excited  $Cl$  ( $^3P_{1/2}$ ) atoms. By comparing these signals to those from the more abundant ground state atoms, they were able to estimate the relative populations of the two states, and calculated  $N_{1/2}^{\circ}/N_{3/2}^{\circ} = 3.6 \times 10^{-2}$ . Since this represents a population distribution five times larger than that expected for a Boltzmann distribution, it may indicate that excited atoms are produced by some reaction subsequent to the discharge. However, the population of the  $^2P_{1/2}$  state is still too low to explain the large concentration of  $^3\Pi_{O_u}$  observed in the chlorine afterglow, if direct formation of this state from one normal and one excited atom is assumed.

The  $^3\Pi_{O_u}$  state must therefore be formed in some process involving ground state atoms. One mechanism by

which this might occur could involve two ground state atoms combining into an intermediate state, which can then undergo a radiationless transition into the  ${}^3\Pi_{O+u}$  emitting state. Such an intermediate is probably another electronically excited state of  $Cl_2$  such as the  ${}^1\Pi_{1u}$  repulsive state, or the  ${}^3\Pi_{O+u}$ . The process may be represented by the equations:



Since there is additional evidence (page 76) that the  ${}^1\Pi_{1u}$  is the precursor of the  ${}^3\Pi_{O+u}$  state in bromine, we have assumed that this is also the case for chlorine. However, unlike bromine, where a considerable activation energy was required to populate the  $v' = 3$  level of the  ${}^3\Pi_{O+u}$ , none is required to populate the highest observed vibrational level of the  $Cl_2({}^3\Pi_{O+u})$  state. The energy difference between two ground state atoms and the  $v' = 13$  level of the  ${}^3\Pi_{O+u}$  state is  $162 \text{ cm}^{-1}$ , and this can be made up by the mean kinetic energy of approach of the reactant particles ( $kT \sim 200 \text{ cm}^{-1}$  at  $300^\circ\text{K}$ ).

The Lewis-Rayleigh nitrogen afterglow exhibits many characteristics similar to the halogen afterglows. The recombination of nitrogen atoms leads to emission predominantly in the first positive ( $B {}^3\Pi_g \longrightarrow A {}^3\Sigma_u^+$ )

system of molecular nitrogen. The emitting B state, however, does not correlate with ground state atoms and hence must be populated via some intermediate state. Bayes and Kistiakowsky (63) suggested that a steady state population of the  $^5\Sigma_g^+$  state followed by a collision induced radiationless transition to the B  $^3\Pi_g$  state was responsible for the emission. However, in a recent study of the absolute emission from the nitrogen afterglow, Campbell and Thrush (64) determined that half of the total recombination was occurring via the B  $^3\Pi_g$  state. This high rate of formation of nitrogen molecules in the B state could not be accounted for by a steady state population of the  $^5\Sigma_g^+$  state since its binding energy is only of the order of 2 Kcal/mole. They thus concluded that atoms recombine into the A  $^3\Sigma_u^+$  state and population of the B state proceeds via a collision induced crossing from the A state.

Although such radiationless transitions as the  $^5\Sigma_g^+ \rightarrow ^3\Sigma_u^+$  of  $N_2$  and the  $^1\Pi_{1u} \rightarrow ^3\Pi_{o+u}$  of  $Cl_2$  are forbidden because of spin and symmetry requirements, Zener (65) has pointed out that the electric field of a colliding molecule can relax the "orbital" selection rules, and the spin change is probably unimportant for these states of chlorine (page 6).

(b) Relaxation Of The  $^3\Pi_{o+u}$  State

The experimental observations on the chlorine afterglow provide evidence for the following relaxation processes.

## (i) Vibrational Relaxation

The observation that the spectral distribution of the emission shifts to the red with increasing pressure, suggests that vibrational relaxation by collision with  $\text{Cl}_2$  is taking place. If, as was suggested in the previous section, formation into the  ${}^3\Pi_{0+u}$  takes place via the  ${}^1\Pi_{1u}$  state, vibrational relaxation would depopulate the levels close to the point of crossing of this intermediate state. Presumably, at very low pressures a spectral distribution corresponding to emission from these high vibrational levels would be observed.

For emission in narrow band widths, we find that  $I \propto [\text{Cl}_2]^0$  for emission from high vibrational levels while the pressure dependence approaches  $[\text{Cl}_2]^1$  for the  $v' = 0, 1$  levels. If formation into the high vibrational levels is a third order process, ( $d[\text{Cl}_2^*]/dt = k_f[\text{Cl}_2][\text{Cl}]^2$ ) and removal is first order in  $[\text{Cl}_2]$ , the overall process will be pressure independent. If the lower levels are formed exclusively by relaxation from higher vibrational levels, a first order dependence on  $[\text{Cl}_2]$  should be observed.

(ii) Quenching By  $[\text{Cl}_2]$ 

If vibrational relaxation were the only process involving chlorine molecules, the pressure dependence of the integrated emission intensity would be  $\int I_\lambda d\lambda \propto [\text{Cl}_2]$ . Our data indicate that  $\int I_\lambda d\lambda \propto [\text{Cl}_2]^{0.6 \pm 0.1}$  at 1 torr,

and this implies that quenching by  $[\text{Cl}_2]$  is taking place.

(iii) Quenching By Atoms

Although previous workers (27, 34) have overlooked the possibility of atom quenching of the emitting state in chlorine, our data provide conclusive evidence that this is an extremely important process. Furthermore, atoms are most efficient at quenching the  ${}^3\Pi_{\text{O}+\text{u}}$  state in low vibrational levels as is indicated by the fact that  $I_{\lambda} \propto [\text{Cl}]^{1.0 \pm 0.1}$  for emission at  $10600\text{\AA}$ . For high vibrational levels  $I_{\lambda} \propto [\text{Cl}]^{2.0 \pm 0.1}$ , implying that atom quenching does not play an important part. This latter observation is difficult to interpret unless the lifetime of the  ${}^3\Pi_{\text{O}+\text{u}}$  state is shorter at high vibrational levels than at low. Owing to a misinterpretation of the  $\nu^3$  term in the Einstein radiation law, Bayes and Kistiakowsky (63) stated that this was the case for the B  ${}^3\Pi_{\text{g}}$  state of nitrogen. However, Douglas (66) pointed out that the correct use of this term implies that high vibrational levels should actually have longer lifetimes.

The variation of the electric transition moment with internuclear distance is another effect which will cause a variation in the lifetime of an electronic state. During a vibration of large amplitude, in which the molecule approaches dissociation, the transition moment of chlorine must vary from that for the normal  ${}^3\Pi_{\text{O}+\text{u}} \longrightarrow {}^1\Sigma_{\text{g}}^+$  transition

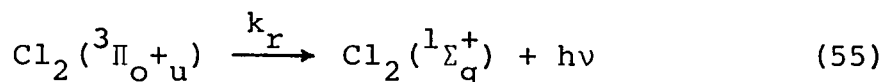
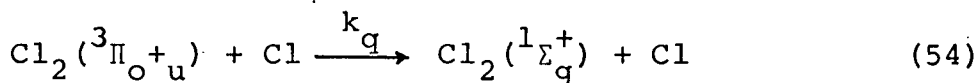
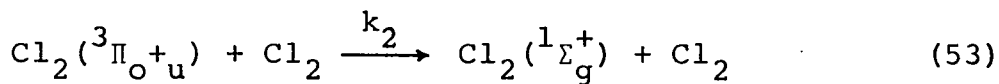
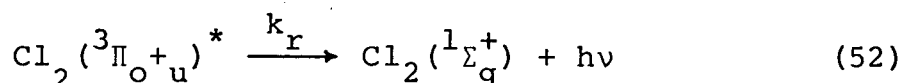
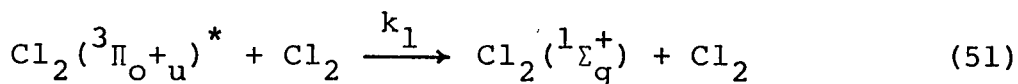
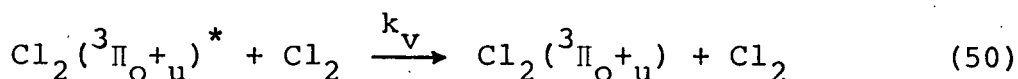
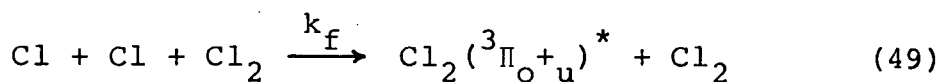
to a value approaching the  ${}^3P_{1/2} \longrightarrow {}^3P_{3/2}$  atomic transition. Since this latter transition is forbidden, the high vibrational levels would be expected to have a longer radiative lifetime than the lower lying levels. This has been found to be the case for the  ${}^3\Pi_{O+u}$  state of iodine (54) where a sevenfold increase in lifetime was observed between the  $v' = 10$  and  $v' = 50$  vibrational levels. Thus, the preferential quenching by atoms cannot be attributed to lifetime variation.

The  ${}^3\Pi_{O-u}$  state is predicted (15) to cross the  ${}^3\Pi_{O+u}$  near the bottom of the potential well. Bader and Ogryzlo (34) have drawn it to approach the  ${}^3\Pi_{O+u}$  state at the inside classical turning point at low vibrational levels. If the process by which the atoms quench the excited state involves an induced crossing to the  ${}^3\Pi_{O-u}$  state, the quenching would be most effective near the point of crossing, and therefore, at low vibrational levels. This mechanism can also explain another experimentally observed phenomenon which is that the atomic quenching efficiency increases with increasing pressure. At high pressure, vibrational relaxation forces the excited molecules into the low vibrational levels where, because of the proximity of the  ${}^3\Pi_{O-u}$  state, they are more easily quenched by atoms.

Without actually specifying how this low-level quenching occurs, let us see if the mechanism thus far described quantitatively explains the experimental results.

To do this, let us assume that the excited  ${}^3\Pi_{O+u}$  state consists of two levels, such that  ${}^3\Pi_{O+u}^*$  represents the high vibrational levels and  ${}^3\Pi_{O+u}$  represents the lowest vibrational levels (figure 33).

The following equations may be written:

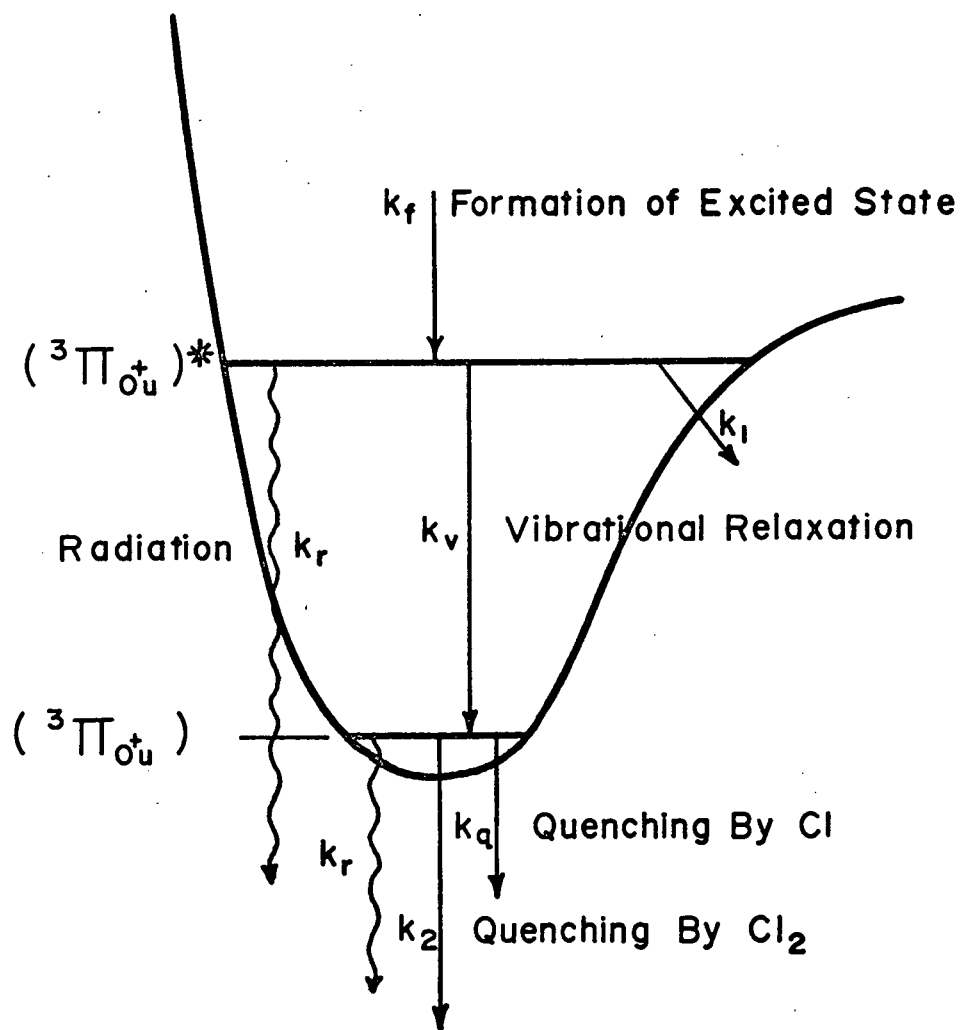


Making the usual steady state assumptions we calculate

$$\begin{aligned} I &= k_r \text{Cl}_2({}^3\Pi_{O+u})^* + k_r \text{Cl}_2({}^3\Pi_{O+u}) \\ &= \frac{k_r k_f [\text{Cl}]^2 [\text{Cl}_2]}{(k_r + k_v [\text{Cl}_2] + k_1 [\text{Cl}_2])} + \frac{k_r k_v k_f [\text{Cl}]^2 [\text{Cl}_2]^2}{(k_r + k_v [\text{Cl}_2] + k_1 [\text{Cl}_2]) (k_r + k_q [\text{Cl}] + k_2 [\text{Cl}_2])} \end{aligned} \quad (56)$$

and since  $k_{\text{app}} = I/[\text{Cl}]^2 [\text{Cl}_2]$ ,

Figure 33. Schematic diagram for proposed mechanism of Cl atom recombination. Non-radiative processes shown as straight arrows.



$$\frac{1}{k_{app}} = \frac{1}{k_f} \left\{ 1 + \frac{k_v k_2 [Cl_2] + k_1 k_r + k_1 k_2 [Cl_2]}{k_r (k_r + k_q [Cl] + k_v [Cl_2] + k_2 [Cl_2])} \right\} [Cl_2]$$

$$+ \left\{ \frac{k_2 (k_r + k_1) [Cl_2]}{k_r k_f (k_r + k_2 [Cl] + k_v [Cl_2] + k_2 [Cl_2])} \right\} [Cl] \quad (57)$$

These equations provide a qualitative description of the experimental results. The intercepts of the  $1/k_{app}$  vs.  $[Cl]$  plots are predicted to be a function of pressure and although their determination involved an extrapolation of the data, these are found to increase with pressure (figure 31). The second term predicts that the slopes of the  $1/k_{app}$  vs.  $[Cl]$  plots increase with pressure and that at large values of  $[Cl]$ , these should "flatten out" as the term  $k_2 [Cl]$  in the denominator becomes larger.

(c) Participation Of Other Electronic States In The  
 $Cl_2$  Afterglow

The  $^3\Pi_{o-u}$  has already been mentioned as a possible intermediate in the quenching of emission by atoms. There is, however, a possibility that the  $^3\Pi_{1u}$  may play an important part in atom recombination, since much of the recombination occurs into this state in the case of bromine. The radiative lifetime of the  $^3\Pi_{1u}$  state of chlorine is undoubtedly long, since absorption into this state has never been observed. Quenching by atoms would

be expected to be more efficient in this state than in the  $^3\Pi_{O+u}$  because of this longer lifetime. A collision-induced crossing between the two states, and a more rapid quenching of the  $^3\Pi_{1u}$  state by atoms would be entirely consistent with our observation that the quenching efficiency increases with increasing pressure.

#### Suggestions For Further Study Of Halogen Afterglows

##### (a) Bromine

The accurate measurement of bromine atom concentrations remains one of the largest barriers in obtaining quantitative kinetic results. A quantitative chemical titration for Br atoms equivalent to the  $\text{NOCl} + \text{Cl}$  reaction has not been found, and the isothermal detector has not proven to be reliable. Bromine atoms, however, do give a good ESR signal, and this method of detection may warrant further study.

The spectrum of the bromine afterglow in the region  $9000\text{\AA}$  to  $12000\text{\AA}$  should be accurately measured on a high resolution spectrophotometer. The use of a time averaging computer could be used, in this application, to accumulate sufficient signal to be measured. A study of the bromine afterglow at a number of temperatures might provide the final answer to the question of the origin of the  $^3\Pi_{O+u}$  state. At very low temperatures, very little emission would be seen from this state if formation proceeds via the  $^1\Pi_{1u}$ .

(b) Chlorine

To understand the quenching processes which are operative in the  $\text{Cl}_2$  afterglow, studies of individual transitions could be undertaken. It might be possible to discover whether atom quenching occurs in certain specific levels near the bottom of the  $^3\Pi_{0_u}$  state providing evidence for a crossing by another state in that region.

P A R T   T W O

STUDIES ON EXCITED MOLECULAR OXYGEN

## INTRODUCTION

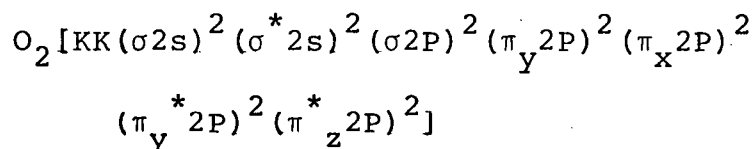
During the course of this research, the very interesting problem of simultaneous electronic transitions in two oxygen molecules in the gas phase arose. Two features of our apparatus (as described in Section 1) made it ideally suited to a study of these transitions. Firstly, our equipment was designed for detecting emission in the near infrared region of the spectrum and many of these "double molecule" transitions appear between  $6000\text{\AA}$  and  $13000\text{\AA}$ . Secondly, the calibration of the detectors for absolute emission intensity made possible the study of transition probabilities. Considering these facts, we hoped to make absolute intensity measurements on the  $(\text{O}_2)_2$  bands and extend this study to excited oxygen produced in solution.

### Electronic States Of Molecular Oxygen

The literature on the subject of oxygen spectroscopy is extensive and no attempt will be made here to give a detailed review. However, a brief discussion of the lower electronic states and some of the transitions in which these are involved will be presented.

There are, as yet, only comparatively few diatomic molecules for which a large number of electronic states have been established on the basis of their observed band spectra. However, in the case of oxygen, seven bound states have been identified. Six of these states correlate with ground state  $^3P$  atoms, and one correlates with one normal  $^3P$  atom and one excited  $^1D$  atom. These states are shown in the potential diagram of figure 34 as drawn by Gilmore (67).

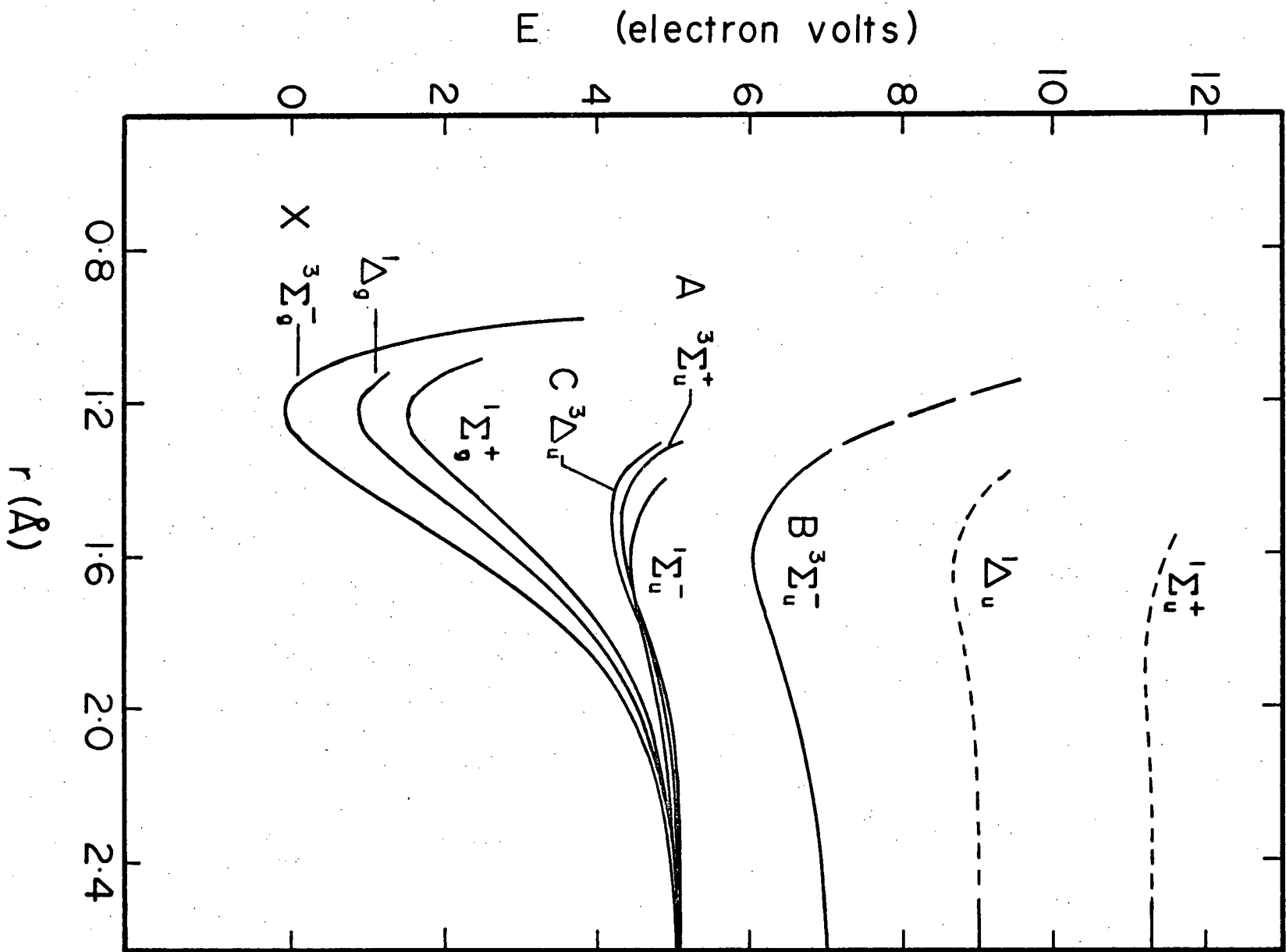
The lowest electronic configuration of  $O_2$ , as predicted by molecular orbital theory (68), is



and this gives rise to the states  $^3\Sigma_g^-$ ,  $^1\Delta_g$  and  $^1\Sigma_g^+$ . The ground state is the  $^3\Sigma_g^-$  state, and the fact that it is a triplet accounts for the observed paramagnetic properties of oxygen.

The  $^1\Delta_g$  state of  $O_2$  is the lowest excited state, lying 0.98 eV above the ground  $^3\Sigma_g^-$  state (69). The half life for spontaneous radiative emission has been found to be of the order of 45 minutes (70). In the isolated molecule, transitions between the ground level and the two upper levels ( $^1\Delta_g$  and  $^1\Sigma_g^+$ ) are of the magnetic dipole type since the selection rules for this radiation include the rotational level combination  $+ \leftrightarrow +$  which is strictly

Figure 34. Potential energy curves for the oxygen molecule.



forbidden for electric dipole radiation. These transitions are weak, even for magnetic dipole transitions, because they involve singlet-triplet intercombinations. Furthermore, the  ${}^3\Sigma_g^- \leftrightarrow {}^1\Delta_g$  transition is doubly forbidden because it also violates the  $\Delta\Lambda = 0 \pm 1$  rule. This would explain the exceptionally long radiative lifetime of the  ${}^1\Delta_g$  species.

The transitions between  ${}^1\Delta_g$  and  ${}^3\Sigma_g^-$  form the infrared atmospheric absorption system which lies in the range of  $13000\overset{\circ}{\text{A}}$  to  $7300\overset{\circ}{\text{A}}$ . The (0-0) transition lies at  $1.27\mu$  and as predicted, has an intensity of about 1/400 that of the  ${}^1\Sigma_g^+ \leftrightarrow {}^3\Sigma_g^-$  system.

The (0-0) and (0-1) emission bands have also been recorded in the twilight and airglow spectrum of the atmosphere (71).

The  ${}^1\Sigma_g^+$  state of oxygen lies 1.626 eV above the ground state and has an estimated radiative lifetime of 7 seconds (72). The  ${}^1\Sigma_g^+ \leftrightarrow {}^3\Sigma_g^-$  transition is known as the red atmospheric system and has its (0-0) band at  $7619\overset{\circ}{\text{A}}$ . The intensity of this system is low since this transition involves a singlet-triplet intercombination and is also symmetry forbidden. Bands of the red atmospheric system are found in absorption in liquid (72) and gaseous (73) oxygen, and in emission in the airglow (74) and aurora (75).

The other bound states of oxygen which have been observed spectroscopically are the  ${}^3\Delta_u$ ,  ${}^1\Sigma_u^-$  and A  ${}^3\Sigma_u$

which correlate with ground state atoms, and the  $B \ ^3\Sigma_u^-$  which correlates with one  $^1D$  and one  $^3P$  atom.

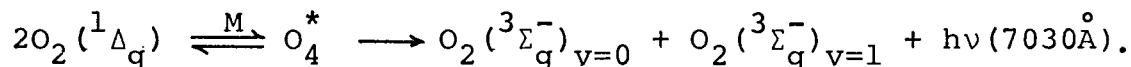
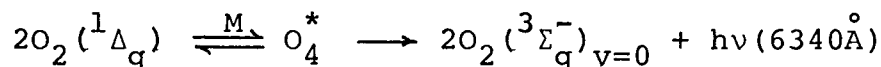
The strongest band system in oxygen is the Schuman-Runge system ( $B \ ^3\Sigma_u^+ \leftrightarrow X \ ^3\Sigma_g^-$ ), which is a fully allowed electric dipole transition with an oscillator strength of  $f = 0.16$  (76). These bands are found in the ultraviolet and converge to a very clear limit (at  $1759\overset{\circ}{\text{A}}$ ) which corresponds to the dissociation limit of  $O_2(^3\Sigma_u^-)$ .

### Studies On Excited Molecular Oxygen

For many years discharge-flow techniques have been used to produce high concentrations of oxygen atoms in a flow system. Ogryzlo (7) found that if the atoms are removed from a stream of discharged oxygen by distilling mercury into the discharge region, the gas stream still contained an excited species. Mass spectrometric (77) and calorimetric (78) measurements have shown that the predominant excited state of  $O_2$  in such a system is  $^1\Delta_g$ , and it has been found that up to 10% of the total stream can be produced in the discharge products.

In a spectroscopic study of a stream of excited oxygen molecules, Bader and Ogryzlo (7) found two unique emission bands, one at  $6340\overset{\circ}{\text{A}}$  and the other at  $7030\overset{\circ}{\text{A}}$ . The intensity of the  $6340\overset{\circ}{\text{A}}$  band was found to be proportional to the square of the  $O_2(^1\Delta_g)$  concentration as measured by a calorimetric detector, and both bands were observed to

be broad and structureless. Noting that the energy of the 6340Å band is equivalent to twice the excitation energy of  $O_2(^1\Delta_g)$ , Bader and Ogryzlo proposed that the bands arose as a result of the following processes:



Although Bader and Ogryzlo stated that the binding energy of the  $O_4$  double molecule was 600 calories, a remeasurement of the temperature dependence of the 6340Å band by Arnold (79) led to the conclusion that the  $O_4$  double molecule was actually a collision complex, and hence could more correctly be represented as  $O_2 - O_2$ .

Simultaneous electronic transitions in two molecules were first suggested by Ellis and Kneser (80) in 1933 to explain bands appearing in the absorption spectrum of liquid oxygen. They suggested a dissociation limit of 142 cal/mole from a study of the line shapes of the absorption bands. In 1936, Salow and Steiner (81) found these bands in the absorption spectrum of the compressed gas and determined that the intensity was dependent on the square of the oxygen pressure but independent of the pressure of added gases. More recently Dianov-Klovov (82) studied the temperature dependence of the band intensities and concluded that the absorption was due to an  $O_2 - O_2$  collision complex.

Excited oxygen molecules have also been observed in the products of some chemiluminescent reactions in solution. The extremely interesting observation that a red chemiluminescence is produced during the reaction of hydrogen peroxide and sodium hypochlorite in aqueous solution was reported by Seliger (83). Using a low resolution apparatus, he recorded one emission band and gave its peak wavelength as  $6348\overset{\circ}{\text{A}}$ . The work was extended by Khan and Kasha (84) who found a second band at  $7032\overset{\circ}{\text{A}}$  having the same half width as the first. They attributed these bands to the (0-0) and (0-1) bands of the  ${}^1\Sigma_g^+ \rightarrow {}^3\Sigma_g^-$  transition of molecular oxygen. This assignment was based on the fact that the band separation of  $1567\text{ cm}^{-1}$  coincides, within experimental error, to the ground state vibrational frequency ( $1580\text{ cm}^{-1}$ ) of molecular oxygen. The authors concluded that the discrepancy between the position of these bands in solution and in the gas phase was caused by a solvent shift of the bands of  $2593\text{ cm}^{-1}$ . Subsequent crystal field calculations on hydrated oxygen (85) suggested that such a high frequency shift was theoretically possible. However, in a study of discharged oxygen in the gas phase, Ogryzlo et al (86, 7) found these same bands, thereby ruling out this interpretation. These authors suggested that the emission arose from simultaneous electronic transitions in two oxygen molecules.

### Purpose Of This Investigation

The determination of the absolute rate of emission in three bands of the spectrum of discharged molecular oxygen was undertaken. From the rate constant of the emission from the 7619Å band arising from the  $O_2(^1\Sigma_g^+ \rightarrow ^3\Sigma_g^-)$  transition, we hoped to be able to estimate the concentration of  $O_2(^1\Sigma_g^+)$  in the gas stream. We also undertook a measurement of the absolute intensities of the 6340Å  $(^1\Delta_g)_2 \rightarrow (^3\Sigma_g^-)_2$  and 7030Å  $(^1\Delta_g)_2(0,0) \rightarrow (^3\Sigma_g^-)_2(0,1)$  bands in order to determine the radiative lifetime of the  $(O_2(^1\Delta_g))_2$  complex.

We hoped to extend the foregoing investigation to a study of the chemiluminescence from the reaction of  $H_2O_2$  and  $Cl_2$  in solution and to identify the excited species giving rise to this emission.

EXPERIMENTALProduction Of  $O_2(^1\Delta_g)$  And  $O_2(^1\Sigma_g^+)$  Molecules

When commercially available tank oxygen is discharged, the products are oxygen atoms, excited oxygen molecules ( $^1\Delta_g$  and  $^1\Sigma_g^+$ ), and small amounts of nitrogen atoms which subsequently react to produce NO and NO<sub>2</sub>. By using Matheson medical grade oxygen, the amount of NO<sub>2</sub> in the discharge products was minimized, as indicated by the low intensity of the O + NO afterglow.

To obtain a pure stream of excited oxygen molecules, removal of the oxygen atoms produced in the discharge was necessary. This was accomplished by distilling a small amount of mercury into the discharge region. The mercuric oxide ring which forms immediately after the discharge is very effective at removing atoms while it does not deactivate the excited molecules. A drop of mercury was placed 3 cm. upstream from the microwave cavity and the temperature of the mercury was controlled by means of a heating tape wrapped around the reservoir. After the discharge was initiated and allowed to warm up, the temperature of the mercury was raised to a point at which just enough mercury was distilled into the discharge to cause an

extinction of the residual O + NO glow.

The control and calibration of gas flowrates has been described in Part 1 and will not be discussed here. The reaction tube used in the oxygen work, however, differed from those described in connection with the halogens in that the monochromator viewed the emission down the length of a 10 cm. section of the tube. The detector and water jacket were placed at the end of this section around a 90° bend. The discharge region was jacketed, allowing cooling air to be blown through it, and a standard C type microwave antenna was used.

The flow of  $O_2(^1\Delta_g)$  was measured with the isothermal calorimetric detector described previously. However, since cobalt has been found to be more efficient than nickel in deactivating the  $O_2(^1\Delta_g)$  molecules, the platinum coil was electro-plated with cobalt. This electro-plating was found to give best results when done at a current of 10 ma. and a voltage of 6 volts for about one hour. The electro-plating solution was a dilute solution of cobalt chloride and ammonium chloride.

#### Measurement Of Emission From The $Cl_2 - H_2O_2$ System

A very simple procedure was employed in making measurements on the  $Cl_2 - H_2O_2$  system. Approximately 10 ml. of a dilute solution of ammonium hydroxide was cooled in an ice bath and then 1 ml. of 90%  $H_2O_2$  was added. Chlorine was

bubbled into the solution through a small glass jet placed in such a way that a fine stream of bubbles was directed against the wall of the glass vessel. The small reaction zone so produced was found to be an advantage in increasing the length of time the reaction could be viewed, since reactants were used up more slowly and the temperature of the solution did not rise too rapidly. The red emission from the bubbles was focused on the slit of the monochromator by means of a lens system, and the wall of the glass vessel viewed by the monochromator was kept free of condensation by blowing dry nitrogen over it. The reaction normally proceeded for four to five minutes after which time the solution heated up quite rapidly and the emission terminated.

## RESULTS

### Estimation Of $[O_2(^1\Sigma_g^+)]$ From Absolute Emission

In using the isothermal calorimetric detector to estimate  $O_2(^1\Delta_g)$  concentration in a stream of excited oxygen molecules, the assumption is made that there are no other excited species in the gas stream capable of releasing heat to the detector. The only excited state of  $O_2$  with low enough energy to be formed in the discharge, or in subsequent reactions, is the  $^1\Sigma_g^+$  state. Most of the emission from this state appears in the (0-0) band of the  $O_2(^1\Sigma_g^+ \rightarrow ^3\Sigma_g^-)$  transition at  $7619\text{\AA}$ , so that by finding the absolute emission from this band, an estimation of the concentration of  $O_2(^1\Sigma_g^+)$  should be possible. The peak was scanned using the cooled RCA 7102 photomultiplier and the calculations were performed as described in the experimental section of Part 1. In this case, however, the rate of emission follows from the equation

$$I = k[O_2(^1\Sigma_g^+)]$$

and the rate constant for spontaneous emission  $k$  is known to be  $0.14 \text{ sec}^{-1}$  (72). Rearranging equation (28) we have

$$[\text{O}_2(^1\Sigma_g^+)] = k_s [\text{O}] [\text{NO}] A_o \int_{7500}^{7700} \frac{F_s(\lambda) i_o(\lambda) d\lambda}{i_s(\lambda)} \bigg/ (0.14) A_s \int_{7500}^{7700} F_s(\lambda) d\lambda$$

Under the following experimental conditions

$$P = 2 \text{ torr}$$

$$[\text{O}_2] = 1.08 \times 10^{-4} \text{ moles/l.}$$

$$[\text{O}] = 3.81 \times 10^{-6} \text{ gm.atoms/l.}$$

$$[\text{NO}] = 5.43 \times 10^{-6} \text{ moles/l.}$$

the integrals were calculated to be

$$A_o \int_{7500}^{7700} \frac{F_s(\lambda) i_o(\lambda) d\lambda}{i_s(\lambda)} = 0.101$$

$$A_s \int_{7500}^{7700} F_s(\lambda) d\lambda = 11.24$$

from which a value of the concentration of  $\text{O}_2(^1\Sigma_g^+)$  is calculated to be

$$[\text{O}_2(^1\Sigma_g^+)] = 1.77 \times 10^{-9} \text{ moles/l.}$$

Under similar experimental conditions, the concentration of  $\text{O}_2(^1\Delta_g)$  is usually of the order of  $10^{-6}$  moles/l. This measurement, therefore, confirms the previous suggestions (7, 79) that  $\text{O}_2(^1\Sigma_g^+)$  is a minor constituent in the products of discharged oxygen in flow systems. Consequently, the

error introduced by the assumption that the excited  $O_2$  stream is entirely  $^1\Delta_g$ , is negligible.

### Absolute Emission Intensity Of The 6340Å Band

The 6340Å peak of molecular oxygen was observed using the monochromator and the cooled RCA 7102 photomultiplier and the concentration of the excited  $O_2(^1\Delta_g)$  species was measured using the cobalt-plated isothermal calorimetric detector. A number of measurements were taken under conditions of varied total pressure and excited molecule concentration and an average value of the rate constant for emission in this band was found. Bader and Ogryzlo (7) showed that the intensity of the 6340Å band is proportional to the square of the  $^1\Delta_g$  concentration; thus we define the rate constant for the emission to be

$$I = k' [O_2(^1\Delta_g)]^2. \quad (58)$$

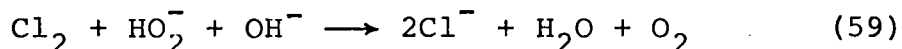
Using equation 28 as outlined in the experimental section and the O + NO calibration procedure, an average value of  $k'$  was calculated to be  $k' = 0.090 \text{ l.mole}^{-1}\text{sec}^{-1}$ . A typical set of values used in equation (28) to obtain this value of  $k'$  was

$$\begin{aligned} [O] &= 3.20 \times 10^{-6} \text{ moles/l.} \\ [NO] &= 2.96 \times 10^{-6} \text{ moles/l.} \\ [O_2(^1\Delta_g)] &= 8.14 \times 10^{-6} \text{ moles/l.} \\ A_o/A_s &= 3.2 \times 10^{-4} \end{aligned}$$

$$\int_{6000}^{7000} \frac{F(\lambda) i_o(\lambda) d\lambda}{i_s(\lambda)} \bigg/ \int_{6000}^{7000} F_s(\lambda) d\lambda = 0.242$$

### The Chlorine-Hydrogen Peroxide System

When chlorine is bubbled into an alkaline solution of hydrogen peroxide in water, the chlorine is consumed and molecular oxygen is formed. The equation for the overall reaction can be written as



The bubbles formed in the reaction emit a red light of quite high intensity. Making the solution more basic had the effect of reducing the size of the bubbles formed and also of extending the length of time the reaction lasted. Typical proportions of reactants which were found to produce the best emission were 5 ml. of  $\text{NH}_4\text{OH}$ , 5 ml. of water and 10 drops of 90%  $\text{H}_2\text{O}_2$ .

The spectrum of the emission originating in the bubbles was recorded using the f/4.5 Hilger and Watts monochromator and a cooled RCA 7102 photomultiplier and is shown in figure 35. All the bands in the spectrum can be assigned to known transitions involving  $\text{O}_2(^1\Sigma_g^+)$ ,  $\text{O}_2(^1\Delta_g)$  and the collisional pair  $(\text{O}_2(^1\Delta_g))_2$ . These are listed in Table 12.

Figure 35. Emission spectrum from the reaction of chlorine with hydrogen peroxide. Solid line is from the aqueous-ammonia system. Broken line is emission from the chloroform-pyridine system.

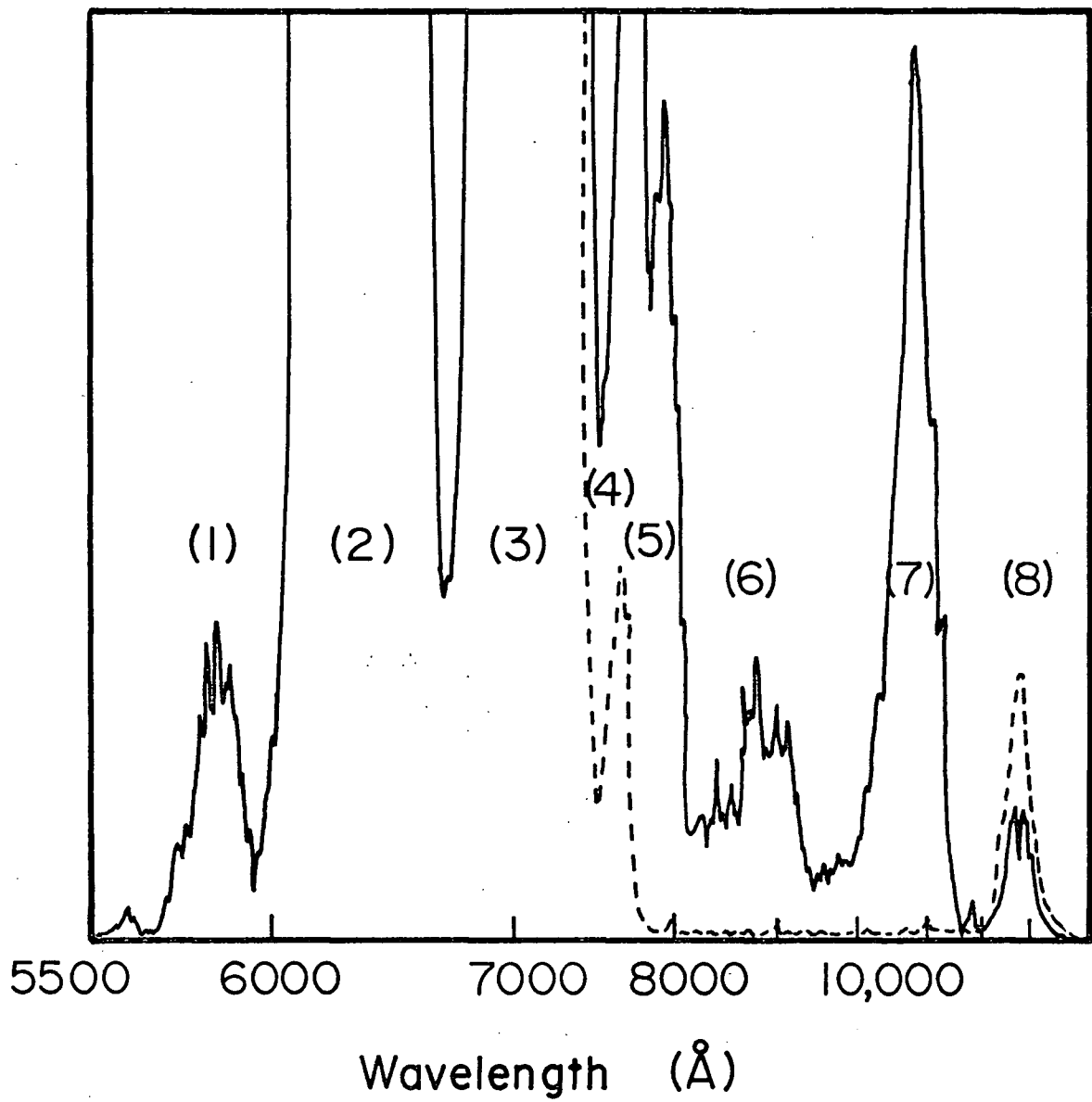


TABLE 12  
BANDS OBSERVED IN THE SPECTRUM OF THE Cl<sub>2</sub>-H<sub>2</sub>O<sub>2</sub> SYSTEM

Peak Number	Wavelength (Å)	Electronic States	Vibrational Levels
1	5800	$(^1\Delta_g)_2 \longrightarrow (^3\Sigma_g^-)_2$	(0,1 $\longrightarrow$ 0,0)
2	6340	$(^1\Delta_g)_2 \longrightarrow (^3\Sigma_g^-)_2$	(0,0 $\longrightarrow$ 0,0)
3	7030	$(^1\Delta_g)_2 \longrightarrow (^3\Sigma_g^-)_2$	(0,0 $\longrightarrow$ 0,1)
4	7619	$^1\Sigma_g^+ \longrightarrow ^3\Sigma_g^-$	(0,0)
5	7700	$^1\Sigma_g^+ \longrightarrow ^3\Sigma_g^-$	(1,1)
6	8645	$^1\Sigma_g^+ \longrightarrow ^3\Sigma_g^-$	(0,1)
		$^1\Delta_g \longrightarrow ^3\Sigma_g^-$	(2,0)
7	10,700	$^1\Delta_g \longrightarrow ^3\Sigma_g^-$	(1,0)
8	12,700	$^1\Delta_g \longrightarrow ^3\Sigma_g^-$	(0,0)

Because water is known to be an extremely efficient deactivator for both  $O_2(^1\Sigma_g^+)$  and for vibrationally excited oxygen (87), experiments were performed to see if reducing the water vapour content of the bubbles had any effect on the spectrum. First, all solutions were cooled to  $5^\circ\text{C}$  before being used and during the experiment, a cold finger helped to maintain the low temperature. This resulted in higher intensities in peaks (5) and (6) as might be expected.

A second set of experiments were conducted using a non-aqueous system to produce the chemiluminescence. A 50% solution of chloroform and pyridine was cooled and then a layer of 90%  $H_2O_2$  was added. The mixture was shaken to extract some hydrogen peroxide into the chloroform layer. The chlorine was then bubbled into this layer. Figure 35 shows the resulting spectrum in which bands due to vibrationally excited oxygen are noticeably absent. The small intensity of the  $7619\text{\AA}$  ( $^1\Sigma_g^+ \rightarrow ^3\Sigma_g^-$ ) band indicates the lower concentration of  $O_2(^1\Sigma_g^+)$  in this system.

An estimate of the yield of  $O_2(^1\Delta_g)$  can be obtained by comparing the intensities of bands found in the solution work with those found in the study of discharged gaseous oxygen. As was mentioned previously, the emission intensity of the  $6340\text{\AA}$  band has been found to be proportional to the square of the  $^1\Delta_g$  concentration (7, 79):

$$I_{6340} = k' [O_2(^1\Delta_g)]^2. \quad (58)$$

Since the band at  $12700\text{\AA}$  arises from one  $\text{O}_2(^1\Delta_g)$  molecule, we can write

$$I_{12700} = k'' [\text{O}_2(^1\Delta_g)] . \quad (60)$$

The ratio of the emission intensities in these two bands is given by

$$R = \frac{I_{6340}}{I_{12700}} = \frac{k'}{k''} [\text{O}_2(^1\Delta_g)] . \quad (61)$$

When  $\text{O}_2(^1\Delta_g)$  is obtained from an electrical discharge, the concentration of the excited species can be found using the cobalt detector previously described. A value for  $k'/k''$  in equation 61 can then be found by measuring the ratio of the intensities of the two emission lines. With this value of  $k'/k''$  it is possible to estimate the  $\text{O}_2(^1\Delta_g)$  concentration in any system simply by measuring  $R$  for that system. In contrast to other methods of determining chemiluminescence yields, geometric factors and collisional quenching rates need not be accounted for when equation 61 is used.

Using the  $f/4.5$  monochromator and the RCA 7102 photomultiplier and with a slit width of  $500\mu$ , the following results were obtained when  $\text{O}_2(^1\Delta_g)$  was measured in the products of an electrical discharge:

$$[\text{O}_2(^1\Delta_g)] = 1.5 \times 10^{-5} \text{ mole l.}^{-1}$$

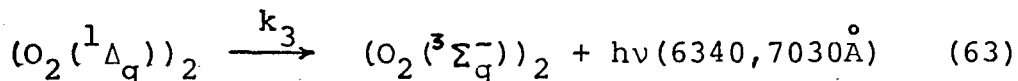
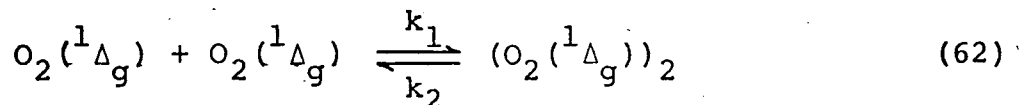
$$R = 36$$

$$k'/k'' = 2.4 \times 10^6 \text{ l. mole}^{-1}$$

Using the same optical system to measure the emission from the  $\text{Cl}_2 - \text{H}_2\text{O}_2$  system, R was found to be  $1.8 \times 10^3$ . However, Badger, Wright and Whitlock (70) have shown that 1/5 of the intensity in the  $12700\text{\AA}$  band is due to spontaneous emission, the remaining intensity arising from collision induced transitions. Thus, in calculating the concentration of  $\text{O}_2(^1\Delta_g)$ , a value of R five times greater than the measured value should be used, ie.  $R = 9.0 \times 10^3$ . Using this corrected intensity ratio in equation 61, we calculate  $[\text{O}_2(^1\Delta_g)] = 3.75 \times 10^{-3} \text{ mole l.}^{-1}$ . If we assume that the bubble temperature is  $300^\circ\text{K}$ , this corresponds to a partial pressure of 70 torr. Since the total oxygen pressure in the bubbles is about 750 torr, this corresponds to a yield of 10%  $\text{O}_2(^1\Delta_g)$  in the reaction.

DISCUSSIONRadiative Lifetime Of The  $(O_2)_2$  Complex

Bader and Ogryzlo (7) have proposed the following mechanism to explain the emission at  $6340\overset{\circ}{\text{Å}}$  and  $7030\overset{\circ}{\text{Å}}$  in the spectrum of discharged oxygen:



$$I = (k_1/k_2)k_3 [O_2(^1\Delta_g)]^2 \quad (64)$$

The value of the rate constant for emission in the  $6340\overset{\circ}{\text{Å}}$  band can be used to estimate the radiative lifetime of the  $(O_2)_2$  collisional complex. If we assume that the probabilities of the transitions giving rise to the  $6340\overset{\circ}{\text{Å}}$  and  $7030\overset{\circ}{\text{Å}}$  bands are equal, since the intensities of these bands are almost equal, we can calculate the value of the total light emission rate in equation 64:

$$(k_1/k_2)k_3 = 2(k') = 2(0.090) = 0.18 \text{ l. mole}^{-1}\text{sec}^{-1}.$$

The rate constants  $k_1$  and  $k_2$  can be estimated on a basis of simple collision theory, assuming that dissociation

of the complex occurs within one vibration. Thus  $k_1 = 10^{11}$  l. mole<sup>-1</sup>sec<sup>-1</sup>,  $k_2 = 10^{13}$ sec<sup>-1</sup> and  $k_3$  is then calculated to be 18. Expressed as the radiative half-life of  $(O_2(^1\Delta_g))_2$ :  $t^{1/2} = 0.693/k_3 = 37.5$  msec.

Obviously this estimate could be considerably low depending upon how strong are the attractive forces between two  $O_2(^1\Delta_g)$  molecules.

The problem, then, is one of finding an accurate equilibrium constant for equation 62 ( $K = k_1/k_2$ ).

In an attempt to estimate the contribution of bound species to the second virial coefficient, Stogryn and Hirschfelder (88) derived an equation enabling this equilibrium constant to be calculated. The authors divided the second virial coefficient into three parts:

$$B(T) = B_f(T) + B_b(T) + B_m(T) . \quad (65)$$

In this equation,  $B_f(T)$  arises from collisions between free molecules,  $B_b(T)$  is related to the equilibrium constant for the formation of bound double molecules in the gas and  $B_m(T)$  is related to the equilibrium constant for the formation of "metastable" double molecules. The difference between these species can be understood if an effective potential energy of interaction between molecules is defined as

$$\phi_{\text{eff}}(r,L) = \phi(r) + L/r^2 \quad (66)$$

where  $L/r^2$  is called the centrifugal potential and

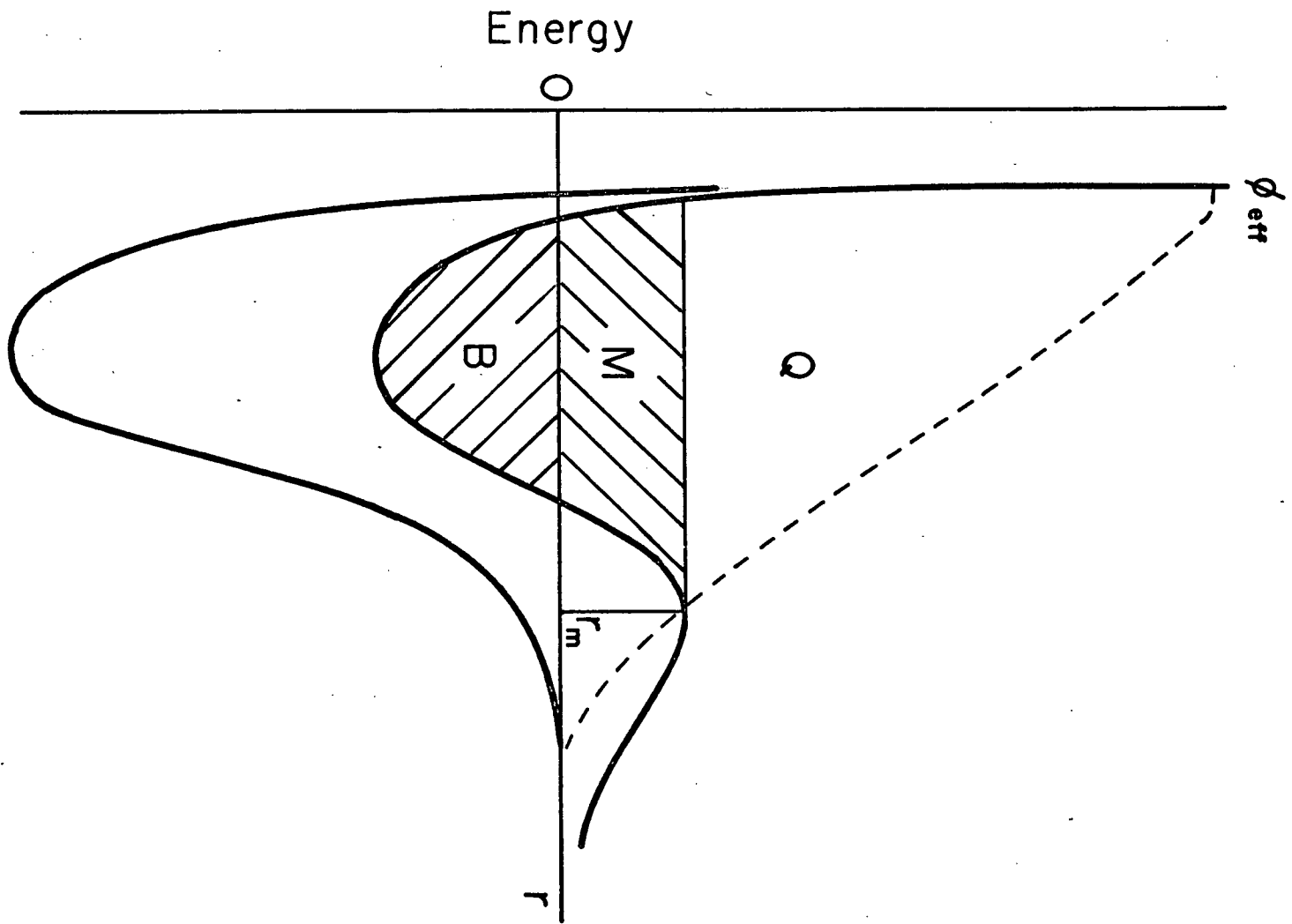
represents the energy of rotational motion.  $\phi(r)$  can be approximated by a Lennard-Jones (6-12) potential

$$\phi(r) = 4\epsilon[(\sigma/r)^{12} - (\sigma/r)^6] \quad (67)$$

where  $(-\epsilon)$  is the maximum energy of attraction between two molecules and  $\sigma$  is the low-velocity collision diameter. When the centrifugal potential term has a finite value, the effective potential energy curve contains a "hump" or rotational barrier. In figure 36 one such potential energy curve is shown for a small value of  $L$ . Region B in this figure corresponds to the region of phase space occupied by those two-molecule systems where the total energy is less than the energy of the separated molecules. These are termed bound dimers and can only be freed by a collision with another molecule. Region M contains the metastable species which have greater energy than the separated molecules. Although classically, these can only be freed by a collision with another molecule, quantum mechanically they can dissociate by leakage through the energy barrier. Depending on whether the half-life of dissociation is greater or less than the average time between collisions, this species can behave like a bound or free molecule.

Using a statistical mechanical argument, Stogryn and Hirschfelder derived an expression for the equilibrium constant for the formation of both the bound and

Figure 36. Effective potential energy curves for the Lennard-Jones (6-12) potential.



metastable species. For  $O_2$  gas at  $294^\circ C$ , their expression yields  $K = 0.0254 \text{ l. mole}^{-1}$ . Since  $Kk_3 = 0.18 \text{ l. mole}^{-1} \text{ sec}^{-1}$ , substitution of this value of  $K$  yields  $k_3 = 7.1 \text{ sec}^{-1}$ . Expressing this as a radiative halflife gives  $t^{1/2} = 0.69/7.1 \sim 0.1 \text{ seconds}$ .

In a theoretical treatment of gas viscosity, Kim and Ross (89) extended the work of Stogryn and Hirschfelder to include the effect of "quasidimers" in addition to the bound and metastable dimers. Kim and Ross defined a dimer complex by assigning it a phase space bounded by  $L \leq L_c, \frac{\phi_{\text{eff}}}{\epsilon} \leq 0.8, R \leq R_m(q)$  where  $L_c =$  largest value of angular momentum for which there appears an inflection point in the  $\phi_{\text{eff}}$  curve, and  $R_m(q)$  is the locus of the maximum in this curve. Thus, in addition to the dimers considered by Stogryn and Hirschfelder which arise as a result of three-or-more-body collisions, Kim and Ross consider the quasidimer which arises from two-body collisions. This takes into account molecules which approach each other with small relative kinetic energy so that orbiting occurs in the vicinity of the maximum of the effective potential. In the case of atomic recombination, Bunker (30) considers this the most important type of collision leading to reaction. The equilibrium constant calculated for all three regions of phase space (bound, metastable and quasidimers) for the case of  $O_2$ , is  $K = 0.079 \text{ l. mole}^{-1}$ . Comparing this value with the  $K$

obtained from the theory of Stogryn and Hirschfelder, we see that the addition of quasidimers increases the equilibrium constant considerably.  $k_3$  is now calculated to be  $2.3 \text{ sec}^{-1}$  and  $t^{1/2} = 0.3$  seconds for the radiative half-life of the  $(\text{O}_2(^1\Delta_g))_2$  species.

Since relatively little is known about the mechanism of double transitions in molecules, no decision can be made as to which regions of phase space should be considered in calculating the equilibrium constant for the  $(\text{O}_2)_2$  complex.

#### Chemiluminescence From The $\text{Cl}_2\text{-H}_2\text{O}_2$ System

We have assumed that the chemiluminescence observed in the reaction of chlorine and hydrogen peroxide originates from excited gaseous oxygen in the bubbles. This assumption is reinforced by the observation that the intensities of the (0-0) and (1-0) bands of the  $^1\Sigma_g^+ \rightarrow ^3\Sigma_g^-$  transition are in the same ratio as those observed in atmospheric absorption studies (73). The intensities of the (1-0) and (0-0) transitions of the main chemiluminescence bands, however, are roughly equal, as is the case in compressed  $\text{O}_2$  (90). This fact supports the interpretation of these bands as collision induced  $\text{O}_2 - \text{O}_2$  pair transitions.

Water is known to have a high efficiency in deactivating vibrationally excited oxygen (87), and for this

reason the high intensity of the (1,0)  $O_2(^1\Delta_g \rightarrow ^3\Sigma_g^-)$  band is surprising. It has not, however, been clearly established whether water maintains this high efficiency of vibrational quenching in excited oxygen molecules. It is quite likely that the efficiency of water in this respect may be due to the similarity of the vibrational frequency of  $O_2(^3\Sigma_g^-)$  ( $1580\text{ cm}^{-1}$ ) and the frequency of the "wagging mode" in  $H_2O$  ( $1595\text{ cm}^{-1}$ ). In that case, since the vibrational frequency of  $O_2(^1\Delta_g)$  is  $1509\text{ cm}^{-1}$  and of  $O_2(^1\Sigma_g^+)$  is  $1433\text{ cm}^{-1}$ , the efficiency with which vibrational energy transfer occurs may be considerably decreased for these excited molecules.

There are a number of reasons for believing that the yield of  $O_2(^1\Delta_g)$  is actually larger than the 10% found experimentally. Since the reaction is 62 kcal exothermic, the temperature of the gas in the bubbles is probably somewhat above room temperature. Direct measurement of the bubble temperature was found to be impossible. However, the "vibrational temperature" (69, page 203) of the emitting gas can be estimated from the relative intensity of the emission from vibrationally excited states. From the intensity of the  $(^1\Delta_g)_{v=1} \rightarrow (^3\Sigma_g^-)_{v=0}$  transition at  $10670\overset{\circ}{\text{A}}$ , an estimated vibrational temperature of about  $600^\circ\text{K}$  can be calculated. Assuming that the true temperature of the gas is somewhat less than this value, the reported yield can, at most, be low by a factor of 2.

A second effect contributing to the low value for the yield could be the dilution of the  $O_2(^1\Delta_g)$  by  $Cl_2$  and  $H_2O$  vapor, since the reaction is not infinitely fast. Both these effects, however, have been minimized by working with cooled solutions where the vapor pressure of water is low and the bubble temperature is nearer to  $25^\circ C$ . Also, by using a very basic solution the reaction rate was maximized.

Badger, Wright and Whitlock (70) have measured the absolute intensities of the discrete-line absorption band and the underlying continuous absorption at  $12600\text{\AA}$  in oxygen gas at pressures up to 4.3 atmospheres. They concluded that the discrete absorption is a measure of the intrinsic transition probability in isolated molecules, and the continuum arises from an enhancement of the transition probability in collision complexes. By studying the pressure dependence of the integrated absorption coefficients of each of these absorptions, they derived an equation for the reciprocal mean lifetime of  $^1\Delta_g$  oxygen molecules subject to decay only by radiative processes:

$$(1/\tau_m) = \bar{A} = (2.6 \times 10^{-4}) (1 + 3.8P_{O_2} + 3.0P_{CO_2} + 0.7P_{N_2}) \quad (68)$$

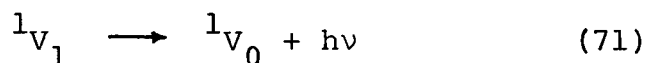
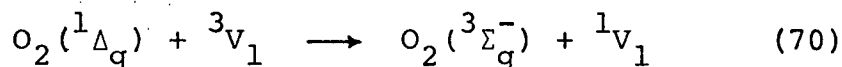
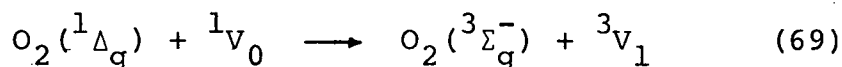
where  $P$  is partial pressures in atmospheres. The halflife of an isolated  $^1\Delta_g$  molecule is then about 45 minutes, which in pure oxygen is reduced to 9.2 minutes at one atmosphere.

This means that only 1/5 of the 12600Å band intensity is due to the spontaneous emission process, the remaining intensity arising from collision induced transitions. For this reason, in calculating the yield of  $O_2(^1\Delta_g)$ , R in equation (61) has been increased by a factor of five.

From the observed intensity sequence in absorption, Badger et al predicted that the (0-1) transition probability in the  $(^1\Delta_g)_2$  collision complex would be relatively large while the intensity of the (0-2) and higher levels would be negligible. The fact that we have not observed the (0-2) transition confirms this prediction.

The importance of this reaction is in its applicability to the interpretation of many oxidation reactions where there is organic molecule chemiluminescence. The extreme prohibition of the singlet  $\leftrightarrow$  triplet ( $g \leftrightarrow g$ ) transition results in a relatively high stability of singlet excited oxygen. For this reason, energy transfer processes between excited oxygen and acceptor molecules having suitable energy levels occur quite readily. If, for example, a small amount of dibenzanthrone is added to the solution in which the chlorine-peroxide reaction is proceeding, an extremely bright red chemiluminescence is seen. Examination of the spectrum shows that it is identical to the fluorescence band of dibenzanthrone. Many other substances are capable of being excited in this reaction as was shown by Mallet (91), and this is a manifestation

of the many energy levels in the oxygen system available for transferring energy. Khan and Kasha (92) have recently found a band at  $4780\overset{\circ}{\text{A}}$  in this system, which is undoubtedly due to the ( $^1\Delta_g$ ,  $^1\Sigma_g$ ) collision complex, and this confirms the presence of levels of sufficiently high energy to excite many large aromatic compounds. It is probable, therefore, as Khan and Kasha have suggested, that in any reaction producing singlet oxygen, chemiluminescence may occur if there exists a species capable of accepting the energy from the oxygen. Recently, Ogryzlo and Pearson (93) have studied the excitation of violanthrone by singlet oxygen confirming this hypothesis. These authors have attributed the luminescence of the violanthrone to the following reactions:



where  $^1V_0$  is the singlet ground state of violanthrone,  $^3V_1$  is the lowest triplet excited state and  $^1V_1$  is the lowest singlet excited state.

A P P E N D I X

### Calculation Of Potential Energy Curves

Accurate potential energy diagrams were drawn for each of the halogens to assist in the interpretation of the emission spectra. When rotational data were available for an electronic state, the potential function used to calculate the shape of the curve was the Hulburt-Hirschfelder potential (94):

$$V = D[(1 - e^{-x})^2 + cx^3 e^{-2x} (1 + bx)] \quad (72)$$

$$x = \frac{\omega_e}{2(B_e D)^{1/2}} \left[ \frac{r - r_e}{r_e} \right]$$

where b and c are constants calculated from spectroscopic data, and the remaining symbols have their usual spectroscopic meaning. When the rotational constants of a state were not known, a Morse (95) function was used in the calculation. Computations were carried out on the IBM 7044 computer and the output was plotted from each molecule. Large scale drawings were also made and these were used in the actual interpretational work.

#### (a) Chlorine

The ground state  $^1\Sigma_g^+$  curve for chlorine was calculated using the Hulburt-Hirschfelder potential and the data of Douglas, Møller and Stoicheff (60). The  $^3\Pi_{0+u}$  curve was taken directly from the paper of Todd, Richards and Byrne (96) who used the more accurate R.K.R. method

of finding the classical turning points. Very little is known about the low energy portion of the  ${}^1\Pi_{1u}$  state and its position and point of crossing of the  ${}^3\Pi_{o+u}$  curve is indefinite. Following Bader and Ogryzlo (34) we have drawn it to cross the  ${}^3\Pi_{o+u}$  state between the thirteenth and fourteenth vibrational levels. The high energy portion of this state has been drawn from the data of Palmer (19).

Recently Clyne and Coxon (50) have studied the spectrum of discharged chlorine and have observed transitions to all the low lying vibrational levels of the  ${}^3\Pi_{o+u}$  state. Since their calculation of  $\omega_e'$  avoids the long extrapolation from  $v' = 6$  made by Douglas et al (60), their value for this constant has been used in calculating the position of the vibrational levels.

(b) Bromine

Horsley and Barrow (46) have recently done a careful study of the absorption spectrum of bromine and have recalculated the spectroscopic constants for the ground  ${}^1\Sigma_g^+$  and  ${}^3\Pi_{o+u}$  states. The ground state potential curve was drawn using their data and the Hulbert-Hirschfelder potential. The  ${}^3\Pi_{o+u}$  curve was taken directly from the paper by Todd, Richards and Byrne (96) who used the more accurate Rydberg-Klein-Rees method (97) to locate the turning points. The lower portion of the  ${}^1\Pi_{1u}$  curve has been drawn to cross the  ${}^3\Pi_{o+u}$  state between the third and fourth vibrational levels as suggested by Bayliss and Rees (53). The

shape of the  ${}^3\Pi_{1u}$  state is less accurately known because of the difficulties involved in analyzing the spectrum. The vibrational assignment of this state was first made by Brown (47) and later revised by Darbyshire (44). The numbering of this state suggested by Darbyshire has been used, but could be in error by  $\pm 2$  units. The potential energy curve of this state was calculated using the spectroscopic constants given by Horsley (45) who has studied the rotational fine structure of a number of the  ${}^3\Pi_{1u} \longleftrightarrow {}^1\Sigma_g^+$  bands. The upper portions of the curves were extrapolated from the diagram in the paper of Kistiakowsky and Sternberg (98).

(c) Iodine

Much more accurate spectroscopic data are available for iodine than the other halogens, so that the potential energy diagram is much more precisely known. The ground state function for  $I_2$  was calculated using the data of Rank and Rao (99) while the  ${}^3\Pi_{0+u}$  curve was taken from the paper of Steinfeld, Zare, Jones, Lesk and Klemperer (100). The  ${}^3\Pi_{1u}$  state was calculated using a Morse potential, and the data of Mathieson and Rees (101). Since only qualitative data were obtained for the iodine afterglow in this work, the location of repulsive curves was not necessary and are therefore not shown.

## BIBLIOGRAPHY

1. E. Becquerel, Ann. Chim. Phys. 57, 40 (1859).
2. R. W. Wood, Proc. Roy. Soc. A97, 455 (1920);  
A102, 1 (1923).
3. K. F. Bonhoeffer, Z. Physik 113, 199, 492 (1924).
4. Chemical Reactions in the Lower and Upper Atmosphere, Ed. H. I. Schiff, (Interscience Publishers Inc., New York (1961)).
5. I. W. Hastings, Q. H. Gibson and C. Greenwood, Photochem. and Photobiol. 4, 1227 (1965).
6. E. A. Ogryzlo, Can. J. Chem. 39, 2556 (1961).
7. L. W. Bader and E. A. Ogryzlo, Disc. Faraday Soc. 37, 46 (1964).
8. F. Kaufman, Proc. Roy. Soc. A247, 123 (1958).
9. A. Fontijn, C. B. Meyer and H. I. Schiff, J. Chem. Phys. 40, 64 (1964).
10. E. Wigner and E. E. Witmer, Z. Physik 51, 883 (1928).
11. R. S. Mulliken, Phys. Rev. 36, 1440 (1930).
12. R. S. Mulliken, Rev. Mod. Phys. 4, 1 (1932).
13. R. S. Mulliken, Phys. Rev. 36, 699 (1930).
14. R. S. Mulliken, Phys. Rev. 46, 549 (1934).
15. R. S. Mulliken, Phys. Rev. 57, 500 (1940).
16. V. Kondratjew and A. Leipunsky, Z. Physik 50, 366 (1928).
17. Y. Uchida, Sci. Pap. Inst. of Phys. and Chem. Res. 30, 71 (1936).
18. H. B. Palmer, J. Chem. Phys. 26, 648 (1957).

19. R. A. Carabetta and H. B. Palmer, J. Chem. Phys. 46, 1325 (1967); 49, 2466 (1968).
20. H. B. Palmer and D. F. Hornig, J. Chem. Phys. 26, 98 (1957).
21. D. Britton, J. Phys. Chem. 64, 742 (1960).
22. G. Burns and D. F. Hornig, Can. J. Chem. 38, 1702 (1960).
23. E. Rabinowitch and W. C. Wood, Trans. Faraday Soc. 32, 907 (1936).
24. G. Porter and J. A. Smith, Proc. Roy. Soc. A261, 28 (1961).
25. G. M. Schwab, Z. Physik B27, 452 (1934).
26. L. W. Bader, M.Sc. Thesis (University of British Columbia, (1964)).
27. E. Hutton and M. Wright, Trans. Faraday Soc. 61, 78 (1965).
28. J. W. Linnett and M. H. Booth, Nature 199, 1181 (1963).
29. E. Rabinowitch, Trans. Faraday Soc. 33, 283 (1937).
30. D. L. Bunker, J. Chem. Phys. 32, 1001 (1960).
31. D. L. Bunker and N. Davidson, J. Am. Chem. Soc. 80, 5085, 5090 (1958).
32. S. K. Kim, J. Chem. Phys. 46, 123 (1967).
33. G. Burns, private communication.
34. L. W. Bader and E. A. Ogryzlo, J. Chem. Phys. 40, 64 (1964).
35. D. B. Gibbs, B.Sc. Thesis (University of British Columbia (1964)).
36. R. L. Strong, J. C. W. Chien, P. E. Graf and J. E. Willard, J. Chem. Phys. 26, 1287 (1957).
37. W. G. Givens and J. E. Willard, J. Am. Chem. Soc. 81, 4773 (1959).

38. R. A. Young, *J. Opt. Soc. Am.* 50, 627 (1960).
39. F. C. Fehsenfeld, K. M. Evenson and H. P. Broida, *Rev. Sci. Inst.* 36, 294 (1965).
40. M. L. Spealman and W. H. Rodebush, *J. Am. Chem. Soc.* 57, 1474 (1935).
41. W. G. Burns and F. S. Dainton, *Trans. Faraday Soc.* 48, 39 (1952).
42. E. A. Ogryzlo, Ph.D. Thesis (McGill University (1958)).
43. P. Harteck and R. R. Reeves, *Disc. Faraday Soc.* 37, 82 (1964).
44. O. Darbyshire, *Proc. Roy. Soc.* 159, 93 (1937).
45. J. A. Horsley, *J. Molec. Spect.* 22, 469 (1967).
46. J. A. Horsley and R. F. Barrow, *Trans. Faraday Soc.* 63, 32 (1967).
47. W. G. Brown, *Phys. Rev.* 39, 777 (1932); 38, 1179 (1931).
48. M. A. A. Clyne and J. A. Coxon, *J. Molec. Spect.* 23, 258 (1967).
49. D. B. Gibbs and E. A. Ogryzlo, *Can. J. Chem.* 43, 1905 (1965).
50. M. A. A. Clyne and J. A. Coxon, *Proc. Roy. Soc.* A298, 424 (1967).
51. *Progress in Reaction Kinetics*, Edited by F. Kaufman (Pergamon Press 1961), Volume 1, p. 11.
52. H. B. Palmer, *J. Chem. Phys.* 47, 2116 (1967).
53. N. S. Bayliss and A. L. G. Rees, *J. Chem. Phys.* 7, 854 (1939).
54. A. Chutjian, J. K. Link and L. Brewer, *J. Chem. Phys.* 46, 2666 (1967).
55. R. J. Donovan and D. Husain, *Trans. Faraday Soc.* 62, 2643 (1966).

56. J. H. Van Vleck, *Phys. Rev.* 40, 544 (1932).
57. T. L. Cottrell and J. C. McCoubrey, *Molecular Energy Transfer in Gases* (Butterworths Scientific Publications Ltd., London, (1961)), pp. 147-148.
58. J. I. Steinfeld and W. Klemperer, *J. Chem. Phys.* 42, 3475 (1965).
59. W. B. Tiffany, *J. Chem. Phys.* 48, 3019 (1968).
60. A. E. Douglas, Chr. Kn. Møller and B. P. Stoicheff, *Can. J. Phys.* 41, 1174 (1963).
61. M. A. A. Clyne and D. H. Stedman, *Chem. Phys. Letters* 1, 36 (1967).
62. A. Carrington, D. H. Levy, and T. A. Miller, *J. Chem. Phys.* 45, 4093 (1966).
63. K. D. Bayes and G. B. Kistiakowsky, *J. Chem. Phys.* 32, 992 (1960).
64. I. M. Campbell and B. A. Thrush, *Proc. Roy. Soc.* 296, 201 (1967).
65. C. Zener, *Proc. Roy. Soc.* 140, 660 (1933).
66. A. E. Douglas, *J. Chem. Phys.* 45, 1007 (1966).
67. R. F. J. Gilmore, *Quant. Spect. Radiative Transfer* 5, 369 (1965).
68. C. A. Coulson, *Valence* (Oxford University Press, (1961) p. 104.
69. G. Herzberg, *Spectra of Diatomic Molecules* (D. Van Nostrand Company Inc., (1950)) p. 203.
70. R. M. Badger, A. C. Wright and R. F. Whitlock, *J. Chem. Phys.* 43, 4345 (1965).
71. A. Vallance Jones and A. W. Harrison, *J. Atm. Terr. Phys.* 13, 45 (1958).
72. W. H. J. Childs and R. Mecke, *Z. Physik* 68, 344 (1931).

73. H. D. Babcock and G. Herzberg, *Astrophys. J.* 108, 167 (1948).
74. A. B. Meinel, *Astrophys. J.* 112, 464 (1950).
75. A. B. Meinel, *Astrophys. J.* 113, 583 (1951).
76. K. Watanabe, E. C. Y. Inn and M. Zelinkoff, *J. Chem. Phys.* 21, 1026 (1953).
77. S. N. Foner and R. L. Hudson, *J. Chem. Phys.* 25, 601 (1956).
78. L. Elias, E. A. Ogryzlo and H. I. Schiff, *Can. J. Chem.* 37, 1690 (1959).
79. S. J. Arnold, Ph.D. Thesis (University of British Columbia (1966)).
80. J. W. Ellis and H. O. Kneser, *Z. Physik* 86, 583 (1933).
81. H. Salow and W. Steiner, *Z. Physik* 99, 137 (1936).
82. V. I. Dianov-Klokov, *Optics and Spectroscopy* 7, 377 (1959).
83. H. Seliger, *Anal. Biochem.* 1, 60 (1960).
84. A. U. Khan and M. Kasha, *J. Chem. Phys.* 39, 2105 (1963).
85. J. S. Griffith, *J. Chem. Phys.* 40, 2899 (1964).
86. S. J. Arnold, E. A. Ogryzlo and H. Witzke, *J. Chem. Phys.* 40, 1769 (1964).
87. H. Knotzel and L. Knotzel, *Ann. Physik* 2, 383 (1948).
88. D. E. Stogryn and J. O. Hirschfelder, *J. Chem. Phys.* 31, 1531 (1959); 33, 942 (1960).
89. S. K. Kim and J. Ross, *J. Chem. Phys.* 42, 263 (1965).
90. C. W. Cho, E. J. Allin and H. L. Welsh, *Can. J. Phys.* 41, 1991 (1963).
91. L. Mallet, *Compt. Rend.* 185, 352 (1927).
92. A. U. Khan and M. Kasha, *J. Am. Chem. Soc.* 88, 1574 (1966).

93. E. A. Ogryzlo and A. E. Pearson, *J. Phys. Chem.* 72, 2913 (1968).
94. H. M. Hulburt and J. O. Hirschfelder, *J. Chem. Phys.* 9, 61 (1941); 35, 1901 (1961).
95. P. M. Morse, *Phys. Rev.* 34, 57 (1929).
96. J. A. C. Todd, W. G. Richards and M. A. Byrne, *Trans. Faraday Soc.* 63, 2081 (1967).
97. W. G. Richards and R. F. Barrow, *Proc. Phys. Soc.* 83, 1045 (1964).
98. G. B. Kistiakowsky and J. C. Sternberg, *J. Chem. Phys.* 21, 2218 (1953).
99. D. H. Rank and B. S. Rao, *J. Mol. Spect.* 13, 34 (1964).
100. J. I. Steinfeld, R. N. Zare, L. Jones, M. Lesk and W. K. Klemperer, *J. Chem. Phys.* 42, 25 (1965).
101. L. Mathieson and A. L. G. Rees, *J. Chem. Phys.* 25, 753 (1956).